Louisiana State University
LSU Digital Commons

LSU Doctoral Dissertations | Graduate School

2010

Modulation of Cholinergic Signaling in Embryonic Zebrafish: Anatomical and Behavioral Consequences

Evdokia Menelaou
Louisiana State University and Agricultural and Mechanical College, emenel1@tigers.lsu.edu

Follow this and additional works at: https://digitalcommons.lsu.edu/gradschool_dissertations

Recommended Citation
Menelaou, Evdokia, "Modulation of Cholinergic Signaling in Embryonic Zebrafish: Anatomical and Behavioral Consequences" (2010). *LSU Doctoral Dissertations*. 3584.
https://digitalcommons.lsu.edu/gradschool_dissertations/3584

This Dissertation is brought to you for free and open access by the Graduate School at LSU Digital Commons. It has been accepted for inclusion in LSU Doctoral Dissertations by an authorized graduate school editor of LSU Digital Commons. For more information, please contactgradetd@lsu.edu.

MODULATION OF CHOLINERGIC SIGNALING IN EMBRYONIC ZEBRAFISH: ANATOMICAL AND BEHAVIORAL CONSEQUENCES

A Dissertation

Submitted to the Graduate Faculty of the
Louisiana State University and
Agricultural and Mechanical College
in partial fulfillment of the
requirements for the degree of
Doctor of Philosophy

in

The Department of Biological Sciences

by
Evdokia Menelaou
B.S., University of Louisiana at Monroe, 2002
M.S., Louisiana State University, 2004
August 2010

ACKNOWLEDGEMENTS

This has been a challenging but yet amazing journey for me that I will always remember. First I want to thank my wonderful husband for his love and tremendous support throughout the years. I thank him for being on my side every step of the way, for his patience for all the long hours and weekends that I spent in the lab and especially for just letting me be myself. No questions asked! I thank him for that. Great appreciation and respect goes to my parents that have been so patient and supportive even though I have been so far away from home for so many years. I would not have been in the United States pursuing my goals if it wasn't for them.

Next, I would like to thank my major professor, Kurt Svoboda, for being such an excellent mentor and a good friend for the past 4 years. I have great respect for him and I admire his dedication and hard work. Thank you for believing in me when I needed it the most, giving me the opportunity to explore my own potential and providing me with skills necessary to explore my research interests in the future. I have been very fortunate to have worked with you.

To my committee members, Dr. John Lynn, Dr. Nao Kato and Dr. Anne Grove, thank you for your time, help, support and most of all your advice throughout my dissertation work.

For the small neuroscience community here at LSU, I give out my appreciation for Dr. Evanna Gleason for organizing our weekly journal club which has made a tremendous impact on how I read scientific papers and allowed us to stay on top of current neuroscience topics. Journal club has definitely made it less cumbersome working in a neurobiology lab. I also want to give many thanks to the Belanger Lab; Jim, Richard and Andres. Andres, your help in performing and troubleshooting EMG recordings has been tremendous! Without you, I would have never accomplished the experiments described in Chapter 4 of this dissertation.

Special thanks go out to Prissy, who has been very helpful and friendly and providing great advice on so many other non-research related issues. I also want to thank everyone in the

Department of Biological Sciences that has helped me in any way in the past 4 years. To Dr. Geaghan and Dr. Southern, thank you for all your help and advice on statistical analysis for Chapter 4. To the Tanguay lab (Robert, Mike and Tamara) at Oregon State University, their expertise in molecular biology have provided me with the tools I needed to accomplish experiments under Chapter 5.

Lastly, I want to thank my friend Karen for making teaching here at LSU fun and for the good times we had together in Baton Rouge. To all my friends from Cyprus, your friendship has been remarkable and is greatly appreciated. To my lab mates, Latoya, Robin and Madelyn for all your help and friendship. Special thanks to Madelyn, for helping with the injections. You have helped me tremendously.

TABLE OF CONTENTS

LIST OF TABLES

LIST OF FIGURES

ABBREVIATIONS

α2	nAChR α2 subunit
ACh	acetylcholine
α-btx	α-bungarotoxin
CaP	caudal primary
CNS	central nervous system
CiA	circumferential ascending
CiD	circumferential descending
CEN	commissural excitatory interneuron
CIN	commissural inhibitory interneuron
CoPA	commissural primary ascending
CoBL	commissural bifurcating longitudinal
CPG	central pattern generator
dpf	days post fertilization
EIN	excitatory interneuron
EMG	electromyogram
GFP	green fluorescent protein
hpf	hours post fertilization
nAChR	nicotinic acetylcholine receptor
MO	morpholino
MiP	middle primary
MCoD	multipolar commissural ascending
MN	motoneuron
NMJ	neuromuscular junction
SMN	secondary motoneuron
PNS	peripheral nervous system

PMN	primary motoneuron
RB	Rohon-Beard
RoP	rostral primary

ABSTRACT

Smoking during pregnancy remains a major health concern in the United States. Nicotine is one of the main ingredients of cigarettes and a neurotoxicant which has been purported to affect many aspects of nervous system development causing long-term abnormalities in the offspring. We took advantage of the zebrafish model to investigate the effects of nicotine in nervous system anatomy and function. It was previously reported that embryonic nicotine exposure causes pathfinding errors in secondary motoneuron (SMN) axons through the activation of nicotine acetylcholine receptors (nAChRs). However, the nicotine-induced effects on SMN pathfinding coincided with muscle degeneration. We hypothesized that nicotine exposure could directly affect spinal neurons bypassing muscle degeneration effects.

Focusing on the neural specific effects of nicotine exposure, we identified four unique, abnormal axonal pathfinding errors which were caused by the exposure. We then demonstrated that the nicotine-induced motoneuron and muscle effects uncoupled in a dose-dependent manner. Showing that embryonic nicotine exposure could directly alter SMN axon pathfinding, we hypothesized that these nicotine-induced effects would persist into later stages of life. To test this hypothesis, we developed a live imaging method where transgenic zebrafish expressing green fluorescent protein in SMNs and their axons could be visualized over the course of several weeks. We demonstrated that embryonic nicotine exposure caused axonal pathfinding errors that persisted into adulthood. We then hypothesized that these anatomical changes would potentially coincide with physiological changes that would ultimately result in altered behavior of the adult. To test this hypothesis, we developed a method in which the swimming behavior in freely swimming adult zebrafish was examined using electromyographic recordings from the axial muscles of adult zebrafish exposed to nicotine as embryos. Our analyses revealed that several distinct features indicative of swimming behavior in zebrafish were altered by transient nicotine

exposure during embryogenesis. Changes in the overall swimming frequency, the relationship between burst duration and cycle time, and the alternating pattern of activity were all altered in adult fish. These may be related to alterations in the physiological properties of interneurons within the spinal circuitry that govern locomotor output.

The actions of nicotine are thought to be mediated through the activation of nAChRs. We investigated the expression pattern of the α2 nAChR subunit as evidence form others suggested it would be expressed by motoneurons and/or interneurons. Using a zebrafish-specific antibody, we showed that the α2 nAChR subunit exhibited a diverse and developmentally regulated pattern of expression. In order to examine the role of the α2 nAChR subunit during embryonic development, we blocked its expression using antisense modified oligonucleotides. Blocking the expression of α2 nAChR subunit altered the embryonic nicotine-induced swim-like behavior without affecting neuronal and muscle elements associated with this motor output. Since Rohon-Beard neurons and other spinal neurons expressed the α2 subunit during embryonic development, we propose that these spinal neurons express α2-containing nAChRs and are most likely involved in initiating and maintaining nicotine-induced motor output.

CHAPTER 1

INTRODUCTION

Maternal smoking represents a major health concern to the developing fetus. In the United States, approximately 12-25% of pregnant women (depending on the state) smoke during their pregnancy (Martin et al., 2007). Tobacco smoke is a complex mixture of chemicals associated with a wide range of health defects and disease. Nicotine, a plant alkaloid, is one of the main ingredients of cigarettes and has been purported to affect the developing nervous system. In the past century, nicotine has gained significant attention especially since it was first discovered to produce receptor-mediated responses in the autonomic nervous system (Langley, 1905).

In more recent studies, exposure of the developing fetus to nicotine through maternal serum has been shown to increase the incidence of spontaneous abortions, low birth weight, and sudden infant death syndrome (SIDS) (DiFranza and Lew, 1995; Thomson et al., 2009). The harmful effects of nicotine can also affect the offspring at later stages of life and lead to significant intellectual/cognitive impairments, behavioral problems, and learning disabilities including attention deficit disorders (Thapar et al., 2003; Potter et al., 2006; Levin et al., 2006). The actions of nicotine are mediated via the activation of nicotinic acetylcholine receptors (nAChRs) (Cohen et al., 2005), which lead to the hypothesis that any neuron that expresses nAChRs during development can potentially be altered by embryonic nicotine exposure. Although much is known about the repertoire and structure of nAChRs across species, the mechanisms by which nicotine and nAChRs interact with each other to disrupt normal vertebrate nervous system development is much less understood. In this study, we will take advantage of the zebrafish model to investigate the effects of embryonic nicotine exposure in a developing system. Using molecular, physiological and behavioral approaches, we can gain critical information on how nicotine exposure perturbs normal vertebrate development and also help identify potential roles for cholinergic signaling during important developmental process.

This introduction is focused towards background information and research studies from the past few years about nicotinic acetylcholine receptors and the importance of cholinergic signaling in a developing nervous system. Then the zebrafish model will be introduced by describing some basic topics associated with spinal neuron organization and morphology as well as simple behaviors associated with the embryo and adult fish. These will provide adequate information in understanding receptor-mediated effects of embryonic nicotine exposure in zebrafish.

Cholinergic Signaling via Nicotinic Acetylcholine Receptors

Nicotinic acetylcholine receptors (nAChRs) are ligand-gated ion channels and are pentameric in nature. Five transmembrane subunits are assembled in the plasma membrane and are arranged around a central pore to form functional receptors (Miyazawa et al., 2003). Each nAChR subunit contains a large N-terminal, crosses the membrane four times, and has an extracellular C-terminus (Fig. 1.1). In the vertebrate nervous system, acetylcholine (ACh) is the endogenous neurotransmitter that binds and activates nAChRs. Exogenous agonists such as nicotine, can also activate these receptors; hence their name "nicotinic". Upon agonist binding, a conformational change causes the channel to stabilize in an open state and transiently permeate cations before closing back to a resting state (Karlin, 2002). While open, nAChRs conduct cations (sodium, potassium and calcium), which causes local membrane depolarization and produces an intracellular ionic signal. Conversely, when agonist concentrations are high and agonist remains bound to the channel, nAChRs then undergo a conformational change, known as desensitization and the receptor becomes unresponsive to agonists (Katz and Thesleff, 1957).

In vertebrates, there are currently 17 types of nAChR subunits which can produce different nAChRs subtypes and are classified in two functional classes based on their pharmacological and physiological properties. First, the muscle-type subunits ($\alpha 1$, $\beta 1$, γ, δ, and ε) are among the most

well understood and are located in the postsynaptic membrane of skeletal muscle and mediate fast excitatory synaptic transmission at the neuromuscular junction (NMJ). They are organized in the membrane in the stoichiometry of two α subunits and one of each β, δ, and γ/ε. During development, the γ subunit of the embryonic muscle-type receptors is replaced by the adult ε subunit (Missias et al., 1996). Second, the neuronal-type subunits are widely expressed within the central (CNS) and peripheral nervous system (PNS) and are divided into subclasses based on nAChR subunit composition. One subclass includes α2–α6 and β2–β4 subunits and form heteromeric nAChRs with αβ combinations whereas, the second class includes α7–α9, and α10 which all form homomeric nAChRs (Kalamida et al., 2007). Different combinations of the α and β-type subunits contribute to the functional diversity of neuronal nAChRs. Among the homomeric subunits, the nAChRs containing the α7 subunit are among the most widely distributed receptor type in the central and peripheral nervous systems and their function can also

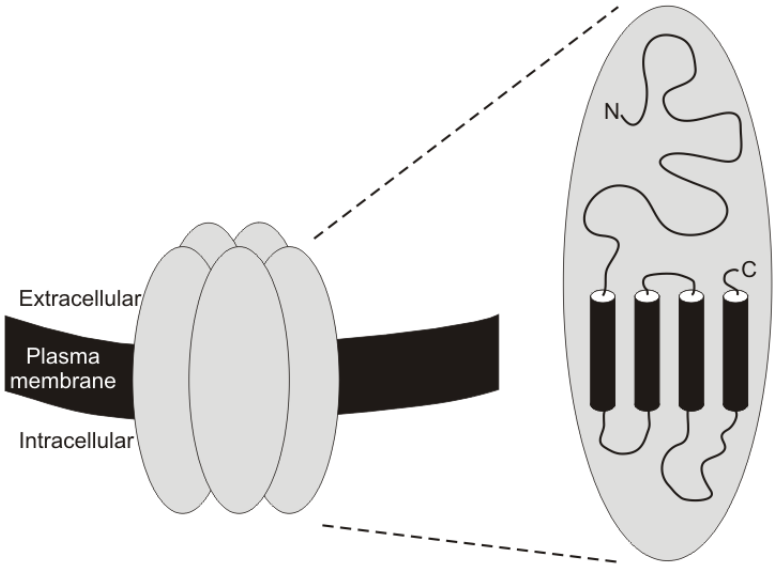

Figure 1.1. Schematic representation of nicotinic acetylcholine receptors. Assembled nAChRs contain five subunits arranged around a central ion channel. Each nAChR subunit contains a large N-terminal domain, four transmembrane domains and a small extracellular C-terminus.

be blocked by methyllycaconitine (MLA) (Zarei et al., 1999). Also, the function of muscle-type and some neuronal nAChRs (homomeric α7, homomeric α9 and heteromeric α9α10) can be blocked by the snake venom toxin, α-bungarotoxin (α-btx) (Baker et al., 2004; Kalamida et al., 2007).

The widespread subunit diversity confers distinct functional and structural properties of nAChRs and can produce many different responses to endogenous and exogenous agonists. Although the major function of nAChRs is to mediate fast synaptic transmission, their presynaptic localizations also support the idea for regulating neurotransmitter release by promoting exocytosis (Dajas-Bailador and Wonnacott, 2004). For example, nicotinic activity in the hippocampus, the center for learning and memory, influences the overall circuit by acting on pyramidal neurons and interneurons by modulating the release of glutamate (Ge and Dani, 2005). While nAChRs have been mainly associated with neurotransmitter release and regulation of synaptic transmission in the CNS and PNS, they have also been linked to regulating long-term changes in the cellular properties of postsynaptic cells and gene expression. In PC12 cells, activation of nAChRs by nicotine application triggered membrane depolarization which was followed by calcium influx into the cells through voltage-gated calcium channels. This receptor mediated nicotinic activation resulted in the induction of specific gene transcription (Greenberg et al., 1986).

The ability of nAChRs to govern this wide range of responses is due to their diverse roles in mediating intracellular processes. Nicotinic AChRs mediate intracellular calcium (Ca^{2+}) in two ways. Firstly, Ca^{2+} ions are permeable through nAChRs and their ionic conduction through the channel is highly dependent on nAChR subunit composition. For example, heteromeric receptors are less permeable to Ca^{2+}, whereas homomeric α7 nAChRs have the highest intrinsic Ca^{2+}permeability. Secondly, upon nicotinic receptor activation, Ca^{2+} signals can be

intracellularly augmented either by influx of extracellular Ca^{2+} through voltage-gated Ca^{2+} channels or release from intracellular stores. Essentially, the conversion of nAChR stimulation into sustained cellular events is largely governed by Ca^{2+} signals which link the nAChRs to downstream processes critical for many neuronal functions (Dajas-Bailador and Wonnacott, 2004).

The diversity of nAChR subtypes and their dendritic, somal, axonal, presynaptic, and postsynaptic locations contribute to the varied roles of cholinergic signaling play in the CNS (Lena et al., 1993; Zarei et al., 1999). In order for the cholinergic system to be active, an agonist must be present. The synthetic enzyme for ACh, choline acetyltransferase, has been detected as early as the neural plate stages in presumptive crest cells (Smith et al., 1979). Also, specific neuronal nAChRs transcripts were detected in premigratory neural crest cells in culture (Howard et al., 1995) and in the mouse CNS as early as embryonic day 2 (Zoli et al., 1995). Another requirement for cholinergic signaling is the presence of functional nAChRs. Even though the assembly of functional nAChRs has been extensively studied using heterologous expression systems such as *Xenopus* oocytes, analysis of functional nAChRs *in vivo* has been more of a challenge. However, in the recent years with the advances in electrophysiological and pharmacological approaches, it has been shown that functional nAChRs are present in early neural tube stages in the mouse cerebral cortex (Atluri et al., 2001).

Activation of nAChRs by acetylcholine has been implicated in regulating axon pathfinding and guidance of nerve growth cones in isolated *Xenopus* spinal neurons (Zheng et al., 1994). In the developing chick, nAChR activation has also been linked to motoneuron survival (Hory-Lee and Frank, 1995). In the chick developing tectum, activation of nAChRs resulted in significant developmental deficits in the nAChR-containing neurons such as neuritic outgrowth disruption and neuronal differentiation (Torrao et al., 2003). In zebrafish, a mutation in the *ache* gene

completely abolished the enzymatic activity of acetylcholinesterase, the enzyme responsible for catalyzing ACh released in the synaptic cleft. The *ache* mutants had excess ACh which resulted in severe motility impairments and accelerated cell death of primary sensory neurons (Behra et al., 2002).

Taken together, the role of cholinergic signaling in modulating critical developmental processes has been widely accepted. This suggests that modifying the function of cholinergic receptors, especially during vulnerable developmental stages, can lead to embryonic abnormalities with potentially subsequent consequences at later stages of development.

The Zebrafish Model

Zebrafish (*Danio rerio)* are tropical fresh-water fish and has served in the past 30 years as a vertebrate animal model to study neurobehavioral development, behavioral regulation, and vulnerability to chemical insult. Zebrafish possess many advantages when compared to other vertebrate animal models including the production of large number of embryos and the ease of fish maintenance. Also, their embryos develop outside of the mother, allowing for easy accessibility and experimental manipulations. Also, the early stages of zebrafish development are similar with other higher vertebrates, including humans (Moore and Persaud, 2003). Zebrafish have a short generation time (2-3 months) and their embryos develop fast in a matter of hours. For example, zebrafish embryos initiate neurulation within 10 hours of fertilization, whereas it takes 10 and 22 days in mice and humans, respectively, to reach neurulation (Westerfield, 1995; Moore and Persaud, 2003; Gilbert, 2003).

Among the greatest advantages of zebrafish as a model to study anatomy/morphology is the transparency of the embryos. This feature, in combination with recent advances in optical imaging and transgenic techniques, make this organism ideal for expressing green fluorescent protein (GFP) in specific classes of neurons which is important for studying development and for

investigating the physiological and functional roles of neurons in the nervous system (Higashijima, 2008).

Also, the zebrafish genome has been recently sequenced conferring this animal model its popularity for investigating the role of gene products in biological processes. Some of the genetic and molecular approaches used in zebrafish are reverse and forward genetic methods following mutagenesis (Skromme and Prince, 2008; Petzold et al., 2009) and gene silencing using antisense modified oligonucleotides, called morpholinos (Nasevicius and Ekker, 2000; Summerton, 2007). Several large-scale mutagenesis screens in zebrafish performed by the laboratory of Christine Nusslein-Volhard identified several mutants, including approximately 166 motility mutants (Granato et al., 1996; van Eeden et al., 1999). Mutants were screened based on behavioral defects and the genes were subsequently identified associated with the control of various locomotor behaviors, which were of particular interest for this study. Among the identified mutants relevant to our work were the paralytic *sofa potato* mutant which lacks muscle acetylcholine receptors and fails to cluster nAChR onto postsynaptic muscle fibers (Ono et al., 2001) and the *twister* mutant (van Eeden et al., 1999) which exhibits prolonged neuromuscular transmission due to a gain-of-function mutation in the α subunit of the muscle-specific AChR (chrna1) (Lefebvre et al., 2004).

The combination of readily accessible transgenic lines, optical imaging techniques, molecular manipulations that affect protein expression, and information from mutant zebrafish are highly advantageous allowing for a multidisciplinary approach for investigating spinal neuron development and function.

Zebrafish Spinal Cord Organization

The simple architecture of the zebrafish spinal cord has served as a foundation for studying the function of spinal neurons that produce simple locomotor behaviors. The zebrafish

trunk is segmented into ~30 myotomes and every trunk segment has two sides, called hemisegments. The zebrafish spinal cord is divided in three regions along the dorsal-ventral (DV) axis and is schematically illustrated in Figure 1.2. At the most dorsal region resides a population of mechanosensory neurons, namely Rohon-Beard (RB) neurons, along with some interneurons. The middle spinal cord consists primarily of interneurons, whereas the ventral-most part is mainly comprised of motoneurons (Myers et al., 1986; Bernhardt et a., 1990; Hale et al., 2001). This cellular diversity is mainly regulated by the expression of transcription factors, including members of the homeodomain protein and basic helix-loop-helix families. This results in spatially distinct progenitor domains along the DV axis of the neural tube and each domain generates one or more distinct neuronal types (Dessaud et al., 2008). In zebrafish, these different types of spinal neurons have been characterized based on their distinct morphological features (cell and axon size, axonal trajectory, dendritic morphology, extend of axonal projections and timing of axogenesis) (Bernhardt et al., 1990; Hale et al., 2001), transmitter phenotypes (Higashijima et al., 2004a), and molecular profiles (Appel et al., 1995; Higashijima et al., 2004b; Kimura et al, 2006).

RB cells are among the earliest born neurons and are located in dorsal spinal cord. They have large somas and each cell has an axon which projects rostrally in the hindbrain and caudally within the spinal cord. These central projections lie within the dorsal longitudinal fasciculus and make contacts with other interneurons in spinal cord and Mauthner cells in the hindbrain. A peripheral process exits spinal cord to innervate the skin (Clarke et l., 1984). At later stages of development, RB neurons are replaced by dorsal root ganglia (An et al., 2002).

Spinal interneurons are located along the DV axis of spinal cord and their position has been shown to reflect their functional properties (McLean et al, 2007). These neurons were classified based on which direction their axons run from the soma; ascending, descending, and

bifurcating (with rostral and caudal branches). Their axonal trajectories were also classified into three main types, commissural (Co), circumferential (Ci) and longitudinal (L). Commissural neurons have axons that cross the midline and ran longitudinally on the contralateral side. Circumferential neurons have axons that run longitudinally on ipsilateral side. Longitudinal neurons have axons that run along their cell body, essentially longitudinally (Bernhardt et al., 1990; Hale et al., 2001).

There are two classes of motoneurons in zebrafish, primary and secondary motoneurons. A combinatorial repertoire of transcription factors is critical for specifying motoneuron identity (Lewis and Eisen, 2003). Motoneurons are derived from the spinal cord motoneuron progenitor domain (ventral region) and express the LIM homeodomain transcription factors, *islet1* and *islet2* (Hutchinson and Eisen, 2006). Even though both primary and secondary motoneurons express the ventral domain nkx6.1 gene, it was shown that nkx6.1 was required for SMN formation, but not for PMNs (Cheesman et al., 2004). PMNs and SMNs are all positioned ventrally in each spinal hemisegment where they exit spinal cord from the same mid-segmental roots (Fig. 1.2) Primary motoneurons (PMN) are among the earliest born neurons in zebrafish and are characterized by a large soma and a single thick axon which begins axogenesis at ~16-17 hpf (Myers et al., 1986; Eisen et al., 1986). There are three distinct subtypes of PMNs which are defined by their axonal projection and which muscle fibers they innervate. The CaP (caudal primary) and MiP (middle primary) motoneurons extend their axons within the ventral and dorsal myotome, respectively, and eventually their axons grow along the lateral myosepta (Fig. 1.2). RoP (Rostral Primary) motoneurons reach the choice point and then project rostrally and medially (Figure 1.2). A fourth PMN subtype, VaP (variable primary), is short lived and exhibits variability in the typical features associated with the other three PMNs (Eisen et l., 1990). Secondary motoneurons (SMN) are born later than PMNs during neurogenesis and have smaller

somata and thinner axons and begin axogenesis at ~27 hpf (Bernhardt et al., 1990). Each hemisegment consists of ~20 SMNs and their axons form a fasciculated nerve bundle before they extend into the periphery (Fig. 1.2).

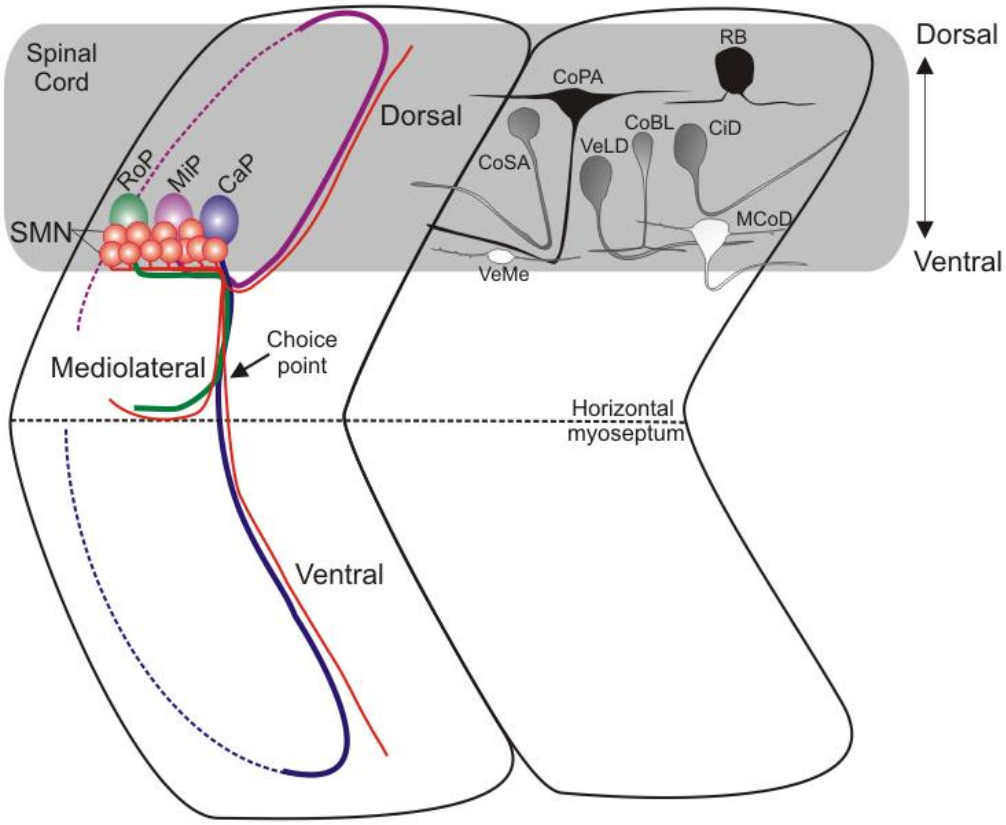

Figure 1.2. Zebrafish spinal neurons. Cartoon depicts spinal neurons (lateral view) within the embryonic/larval zebrafish spinal cord. Classes of spinal neurons are shown in two segments for simplification. The left hemisegment shows the two motoneuron classes, primary and secondary motoneurons. Primary motoneurons (CaP, MiP, and RoP) are larger than SMNs and are located in ventral spinal cord. Their axons exit spinal cord from a mid-segmental root, reach the choice point and then project in the myotome dorsally (MiP axon), ventrally (CaP) and mediolaterally (RoP). The dotted lines indicate axonal trajectories in the lateral myotome. SMNs are smaller and their axons fasciculate to form a nerve bundle that project dorsally, ventrally, and mediolaterally. The right hemisegment shows RB mechanosensory neurons and interneurons and their relative position along the dorsal-ventral axis as indicated by different color (black: dorsal, grey: middle, white: ventral). Abbreviations: CiD: circumferential descending; CoPA: commissural primary ascending; CoSA: commissural secondary ascending; MCoD: multipolar commissural ascending; VeLD: ventral longitudinal descending; VeME: ventral medial; CoB: commissural bifurcating longitudinal; RB: Rohon-Beard neuron; CaP: caudal primary; MiP: middle primary; RoP: rostral primary; SMN: secondary motoneuron. Rostral (head) is to the left. Cartoon is not drawn to scale.

Both, primary and secondary motoneurons extend their axons in a stereotypical manner to reach their appropriate target muscles. Primary and secondary motoneurons can also be distinguished based on their muscle innervation pattern. One PMN and two or more SMNs innervate one fast muscle fiber, which occupy the majority of axial musculature. On the other hand, slow muscle fibers, which are localized in the lateral periphery are innervated only by SMNs (Westerfield et al., 1986). The ability of motoneuron axons to navigate into the periphery and reach their muscle targets with such precision involves diffusible or membrane bound cues (Bernhardt and Schachner, 2000; Schweitzer et al., 2005) and multiple myotome-derived cues (Zeller et al., 2002). A cell surface adhesion molecule (DM-GRASP), unique to SMNs, was shown to play a role not only in axon fasciculation (Fashena and Westerfield, 1999) but also in axonal pathfinding (Ott et al., 2001). Another factor that plays a role in axonal pathfinding in zebrafish, is the path already established by PMN axons, which serves as a guide for SMN axons (Pike et al., 1992). Lastly, the proper expression of neuropilin-1 and plexin A3, two receptors that recognize axon-repelling semaphorins within the local environment, is required for spinal motor nerves to properly exit spinal cord at mid-segmental points (Feldner et al., 2005; Palaisa and Granato, 2007).

Zebrafish Locomotor Behaviors

The distinct classes of spinal neurons described above have specialized roles in producing diverse functions and control locomotor behaviors in both zebrafish embryos and adults. Spinal neurons form a repeated series of small, segmented spinal neural circuits, known as the central pattern generator (CPG) (Grillner et al., 1998). This spinal circuitry is necessary for the generation of rhythmic movements, whether walking or swimming. This rhythmic motor activity is governed by an input/output system. Input sources include descending brainstem inputs, sensory neurons (i.e. RB neurons) and interneurons (excitatory interneurons: EIN), whereas the

output side is associated with motoneurons (MN) and muscle (Figure 1.3). In short, these rhythmic locomotor behaviors result in alternating muscle contractions, and in most cases, this involves an excitatory and an inhibitory source. The excitatory source mainly drives a target neuron which generates the rhythm. In order to sustain the alternating cyclic action during rhythm generation, a modulatory factor is needed which is usually associated with other CPG cells such as commissural interneurons (Fig. 1.3, CENs and CINs). In zebrafish, CiD neurons are rhythmically active and provide the main source of on-cycle excitation to the swimming CPG (McLean et al., 2007).

The first locomotor behavior observed in the zebrafish embryo is the spontaneous activity of the trunk musculature. This activity begins at ~17 hours post fertilization (hpf) when primary motoneurons axons make their initial contacts with muscle fibers (Melancon et al., 1997; Saint-Amant and Drapeau, 1998). This spontaneous motor activity peaks at around 19 hpf and gradually decreases by 27-28 hpf (Saint-Amant and Drapeau, 1998; Thomas et al., 2009). In chick, spontaneously firing motoneurons release acetylcholine which then provides excitatory drive onto other interneurons (Hanson and Landmesser, 2003). In zebrafish, muscle fibers respond directly to ACh to produce muscle twitches as early as 17 hpf (Melancon et al., 1997).

By 27 hpf, zebrafish embryos exhibit a robust response to touch stimuli with touch-evoked tail coiling/swimming, resulting in the forward movement of the embryo (Saint-Amant and Drapeau, 1998). Touch-evoked responses are governed by the mechanosensory Rohon-Beard neurons which relay excitation from the skin to the contralateral spinal cord to generate contralateral muscle contraction (Ribera and Nusslein- Vollhard, 1998). This is achieved through activation of CoPA (commissural primary ascending) interneurons (Gleason et al., 2003) via glutamatergic synapses (Higashijima et al., 2004a). Upon activation of CoPA interneurons, the contralateral CPG cells on the opposite site of spinal cord are activated which results in a left-

right touch-evoked coiling (before 27 hpf) and swimming (following 27 hpf) (Downes and Granato, 2006).

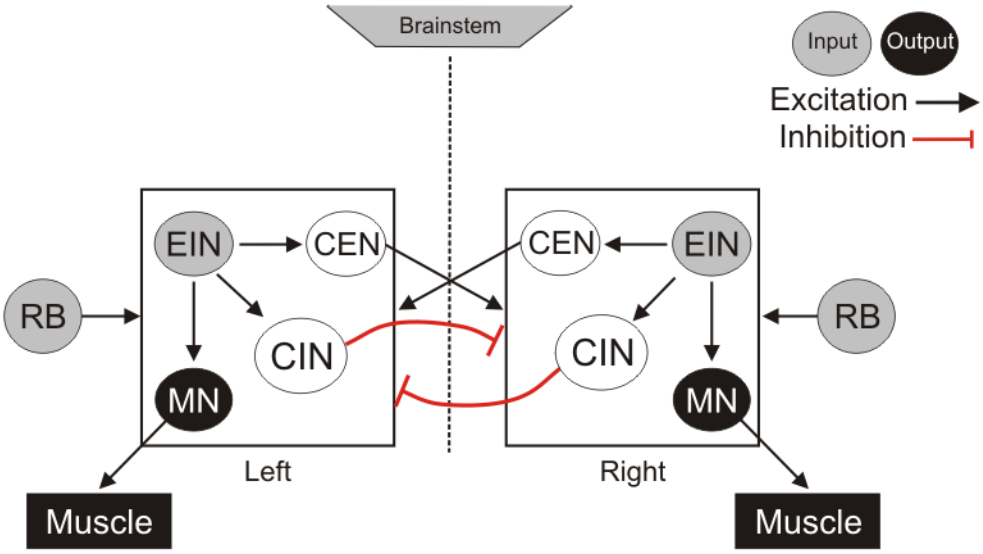

Figure 1.3. The major cell types associated with the swimming central pattern generator. Diagram illustrates the neural network within spinal cord known to generate rhythmic motor output based on studies from zebrafish, lamprey and *Xenopus*. Input excitatory drive into the CPG originates from descending brainstem inputs, RB neurons and excitatory interneurons (EINs). CPG units (black boxes) in each half of the spinal cord (left and right) drives rhythmic activity in a motor pool and maintains alternation by reciprocal inhibition through integrator cells (CINs). CINs fire in phase with ipsilateral MNs once per swimming cycle. Motoneurons are segmentally organized and innervate adjacent muscle fibers which produce the locomotor output. Abbreviations: RB: Rohon-Beard neuron; EIN: excitatory interneuron; CEN: commissural excitatory interneuron; CIN: commissural inhibitory interneuron; MN: motoneuron. Dashed line indicates the midline of spinal cord.

The neural circuits that govern these swim-like behaviors in embryos have similar functions in generating larval and adult locomotor swimming patterns. The different types of muscle fibers in the axial musculature exhibit distinct physiological properties. Slow muscle fibers are activated during long sustained swimming and are more resistant to fatigue, whereas fast muscle fibers are less resistant to fatigue and primarily responsible for fast swimming as well as startle responses. Intermediate fibers share characteristics of both slow and fast muscle fibers (Fetcho and O'Malley, 1995; te Kronnie, 2000). At different swimming speeds, there are

different patterns of recruitment for spinal interneurons and motoneurons (Bhatt et al., 2007; McLean et al., 2007). For example, excitatory interneurons activated during slow swimming are silent during fast swimming. Also, PMNs produce large amplitude endplate potentials and they synchronously activate whole regions of muscle during high amplitude body movements associated with fast swimming and escapes. On the other hand, SMNs produce small amplitude endplate potentials which provide more localized muscle control associated with finer movements such as slow swimming (Westerfield et al., 1986; Liu and Westerfield, 1988).

Studying the Effects of Embryonic Nicotine Exposure in Zebrafish

It is widely accepted by now that normal nervous system development can be disrupted by nicotine, a major ingredient of cigarettes. According to the most updated reports from the Centers for Disease and Control Prevention (CDC), at least 1 out of 8 (~13%) women smoke cigarettes during their pregnancy. Cigarette smoking leads to 94,000 infant deaths related to mothers smoking during pregnancy and more than 400,000 premature deaths in the United States each year (~1 in every 5 U.S. deaths). The most compelling evidence that nicotine has substantial negative neurodevelopment effects has come from animal studies. It has been demonstrated that nicotine is a neuroteratogen even at concentrations when no growth retardation occurs (Slotkin, 1998, Svoboda et al., 2002). Nicotine can also induce changes in neuronal replication and differentiation and inhibit DNA synthesis in the brain (Slotkin et al., 1987b; Slotkin, 2004). Nicotine exposure during vulnerable developmental stages can lead to programmed cell death (apoptosis) in hippocampal progenitor cells (Berger et al., 1998; Roy et al., 1998). When the fetus was exposed to smoking during the first trimester, the expression pattern of nAChRs exhibited some significant regional differences in the brainstem and cerebellum (Falk et al. 2005). Changes in nAChR density and distribution along with alterations in cellular replication and differentiation can lead to long lasting effects in the offspring at later stages in life. Children

of women who smoke are more likely to smoke and become nicotine-dependent later in life (Abreu-Villaca et al., 2004). Maternal smoking has also been linked with learning and memory deficits in adolescents (Levin and Chen, 2004; Levin et al., 2006). A high prevalence of attention deficit and hyperactivity disorder (ADHD) has been reported in children prenatally exposed to nicotine. This has been attributed to behavioral teratogenic effects of intrauterine brain exposure (Paz et al., 2007; Slotkin, 2004).

Nicotinic receptors are widespread in the nervous system, especially in the brain. As discussed above, they have many diverse yet important physiological functions. Nicotinic systems interact with a variety of neurotransmitter systems in the brain. With regard to regulating cognitive function, activation of nAChRs promotes release of several neurotransmitters such as acetylcholine, dopamine, serotonin, gamma-aminobutyric acid (GABA) and glutamate (Dani and Bertrand, 2007). Any alteration in cholinergic pathways during critical developmental stages, especially when functional nAChRs are present, can potentially have long lasting behavioral effects. Therefore, understanding the actions of nicotine on the developing nervous system would be of great clinical significance.

In the following chapters, we take advantage of zebrafish as a model vertebrate to investigate the effects of nicotine exposure during embryonic development. Chapter 2 is focused on spinal neuron development, specifically the process of spinal motoneuron axon pathfinding. We provide an extensive description of the main axonal trajectories and how they are affected when the embryo is exposed to varying concentrations of nicotine and also at different exposure windows. Within this chapter, the short-term nicotine-induced effects are examined since we focused on early stages of development. In Chapter 3, we investigate the effect of embryonic nicotine exposure on motoneuron axon pathfinding at later stages of life. In order to address this, a transgenic line of zebrafish, Tg(*isl1*:GPF) which expresses GPF in a subpopulation of

secondary motoneurons was initially characterized. This was essential to allow for live imaging *in vivo* and track individual fish as they transitioned into adulthood. Within this chapter, we demonstrate that nicotine-induced motoneuron pathfinding errors that arose during embryonic stages persisted into adult stages of development.

We then set out to address whether long-term anatomical effects following embryonic nicotine exposure would also manifest long-term physiological alterations in the form of behavior. In Chapter 4, we use the simple behavior of swimming in adult zebrafish to assess functional deficits. We first describe the basic features that characterize locomotor patterns in freely swimming zebrafish. Then the properties of the swimming behavior in zebrafish exposed to nicotine as embryos are investigated. This has helped identify elements associated with the spinal CPG for swimming that could be potentially affected resulting in altered swimming behavior.

Lastly, we investigate the role of specific nAChR subunits on embryonic locomotor behaviors and spinal neuron development. We focus on the α2 nAChR subunit because it was previously reported to localize to a distinct population of spinal neurons in intermediate spinal cord (Zirger et al, 2003). In Chapter 5, we first show the spatial and temporal expression profiles of the nAChR α2 subunit using a zebrafish-specific polyclonal antibody. We then blocked the expression of the nAChR α2 subunit using morpholino antisense oligonucleotides to investigate the role of α2-containing nAChRs in mediating nicotine-induced responses and other basic developmental process in zebrafish embryos. This helped identify potential cellular substrates within the CNS, which are potentially associated with exerting the nicotine-induced effects.

CHAPTER 2

CHOLINERGIC MODULATION OF SECONDARY MOTONEURON AXON PATHFINDING IN ZEBRAFISH

Introduction

Exposure to nicotine, a potent cholinergic agonist, during embryonic stages of development causes paralysis in zebrafish embryos. The nicotine-induced paralysis coincides with pronounced alterations in motoneuron (Svoboda et al., 2002; Menelaou and Svoboda, 2009) and muscle development (Welsh et al., 2009). In embryonic zebrafish, motoneuron axon growth and muscle development occur simultaneously and involves activity-dependent mechanisms (Hanson and Landmesser, 2004), calcium signaling (Brennan et al., 2005), and multiple myotome-derived cues (Zeller et al., 2002; Schweitzer et al. 2005; Schneider and Granato, 2006; Palaisa and Granato, 2007). In the presence of nicotine, neuronal and muscle substrates can be severely affected by activation of nAChRs. In zebrafish embryos, acetylcholine-generated calcium transients regulate muscle fiber development (Brennan et al., 2005). Following prolonged activation of skeletal muscle through AChR over-activation, motor axon defects and muscle degeneration occur (Lefebvre et al., 2004, Behra et al., 2002), possibly via excitotoxic mechanisms due to increases in calcium levels in the muscle (Leonard and Salpeter, 1979; Engel et al., 1982; Gomez et al., 2002). This evidence supports a direct action of nicotine on muscle fiber development via the activation of muscle-specific AChRs.

Sofa potato zebrafish mutants, which lack functional AChRs at the skeletal muscle (Ono et al., 2001), exhibited secondary motoneuron (SMN) pathfinding errors without any effects on muscle development following embryonic nicotine exposure (Welsh et al., 2009). This suggested that nicotine-induced neuronal and muscle effects occurred independently and that muscle fibers were not the sole substrate that nicotine acted upon to alter SMN anatomy. These results strongly indicated that nicotine can directly affect the cells within the nervous system.

The nicotine concentration levels for all previous embryonic zebrafish exposures were between 15μM and 33μM (Svoboda et al., 2002; Welsh et al., 2009). In mammalian embryonic

explants nicotine concentrations between 0.6μM and 6μM lead to malformations, and embryonic lethality occurs at 6μM (Zhao and Reece, 2005). In zebrafish, nicotine concentrations appeared rather high when compared to their mammalian counterparts. However, it was previously shown that only a fraction of the 30μM waterborne nicotine was incorporated into the embryos (Thomas et al., 2009), which suggested that nicotine concentration levels and potentially the length of the exposure would be critical factors when addressing cell-type specific effects.

The above evidence lead us to the hypothesis that embryonic exposure to nicotine can directly affect motoneuron axon pathfinding if one can bypass the muscle degeneration. In this chapter, wildtype zebrafish were used to test the above hypothesis by manipulating the nicotine concentration and length of exposure to nicotine. The results demonstrated that the motoneuron and muscle effects uncoupled in a dose-dependent manner following short and long nicotine exposure windows. Lastly, we identified 4 unique, abnormal axonal pathfinding errors that were caused by the exposure. We refer to these phenotypically unique errors as (1) trajectory errors, (2) forked axons, (3) stalled axons, and (4) duplicated axons. Describing these errors then allowed us to identify potential mechanisms that likely underlie nicotine-induced SMN axonal pathfinding errors.

Materials and Methods

Zebrafish Maintenance

Animal protocols were approved by the Institutional Animal Care and Use Committee at Louisiana State University. Adult fish were maintained at 28^{o}C with a lighting schedule of 14 h light and 10 h dark. Fertilized eggs were obtained from natural spawnings of wildtype lines according to the Zebrafish Book (Westerfield, 1995). Embryos were collected within 3 hours of spawning, rinsed, and placed into 100 mm Petri dishes containing embryo medium.

Nicotine Exposures

(-)-Nicotine was purchased from Sigma (St. Louis, Missouri, USA, catalog # N3876-5ml) and stock solutions were made fresh daily as needed in distilled water. The stock solution was then diluted in embryo medium (pH 7.2) to obtain the desired final concentrations. Zebrafish embryos while in their chorions were exposed to nicotine (1, 5, 15, and 30µM made in embryo medium) from 12-30 and 22-72 hours post fertilization (hpf). At 48 hpf, all nicotine-exposed and stage matched control embryos were manually dechorionated and at 72 hpf were fixed in 4% paraformaldehyde.

Immunohistochemistry

Whole mount immunohistochemistry was carried out in 72-hpf zebrafish that were first fixed in 4% paraformaldehyde overnight at 2-4^{o}C and then stored in PBST (PBS containing 0.1% Tween 20). After permeabilization, they were incubated in primary antibody overnight at 2-4^{o}C. The monoclonal antibodies zn8 (also known as zn5) (dilution 1:500) and F59 (dilution 1:250) were obtained from the Developmental Studies Hybridoma Bank (The University of Iowa, Iowa) and were used to reveal secondary motoneuron somata and their axons (Fashena and Westerfield, 1999) and slow muscle fibers (Devoto et al., 1996), respectively. The following day, the embryos were washed for 90 minutes and then incubated for another 90 minutes in an anti-mouse fluorescent secondary antibody conjugated to Alexa 546 or Alexa 488 (1:1000 dilution in PBST; Molecular Probes, Eugene, OR). They were then rinsed in PBST for another 60 minutes and prepared for image analysis.

Image Acquisition and Analysis of Morphological Data

Zebrafish processed via immunohistochemistry were laterally mounted on a slide in PBST, lightly cover slipped and sealed. Single focal plane images (zn8) and image stacks (zn8 and F59) were obtained using 20x dry and 40x oil (N.A: 1.3) objectives, respectively, mounted

on a Zeiss Axiovert 200M inverted microscope with epifluorescence and equipped with a Zeiss ApoTome (Carl Zeiss). Single focal plane images were used to analyze and score the motoneuron axon morphology based on their phenotypes. Image stacks were used to reveal motoneuron axon morphology (zn8) using volume-rendering software (Imaris 5.7.2, Bitplane Inc., Saint Paul, MN) and to measure muscle fiber widths (F59) using Axiovision 4.7 (Carl Zeiss). Images were cropped using Photoshop 7.0 (Adobe, San Jose, CA) and CorelDraw Graphics Suite 12 (Ottawa, Ontario, CA) was used to organize the figures. All the images are presented with rostral to the left and caudal to the right. The cartoons were created using CorelDraw by tracing motor axon phenotypes from photomicrographs.

Statistics

All values are reported as means ± standard error of the means (SEM). For multiple comparisons, one way analysis of variance (ANOVA coupled to a Holm-Sidak post-test) was applied on normally distributed values. Otherwise, Kruskal-Wallis analysis of variance was applied (Dunn's post-test) (SigmaStat3.5, Systat Software Inc., San Jose, USA). Significance was assigned if the p value was <0.05.

Results

The primary focus of the experiments in this chapter was geared towards nicotine exposure and its effect on SMN axonal pathfinding. Normal development of axons and the potential abnormal phenotypes following nicotine perturbations are described in this chapter.

Subpopulations of secondary motoneurons positioned in ventral spinal cord, extend their axons to form a fasciculated nerve bundle, which then exits at mid-segmental roots to innervate the dorsal and ventral myotome. As their axons exit ventral roots, they take specific paths into the myotome to target dorsally (Fig. 2.1A, red), ventrally (Fig. 2.1A, green) and mediolaterally (Fig. 2.1A, orange). These spatially distinct axonal trajectories are clearly visualized using zn5,

which allows for easy identification of nicotine-induced effects on dorsal, ventral and mediolateral SMN axonal trajectories (Fig. 2.1B) when compared to their control counterparts (Fig. 2.1A, black).

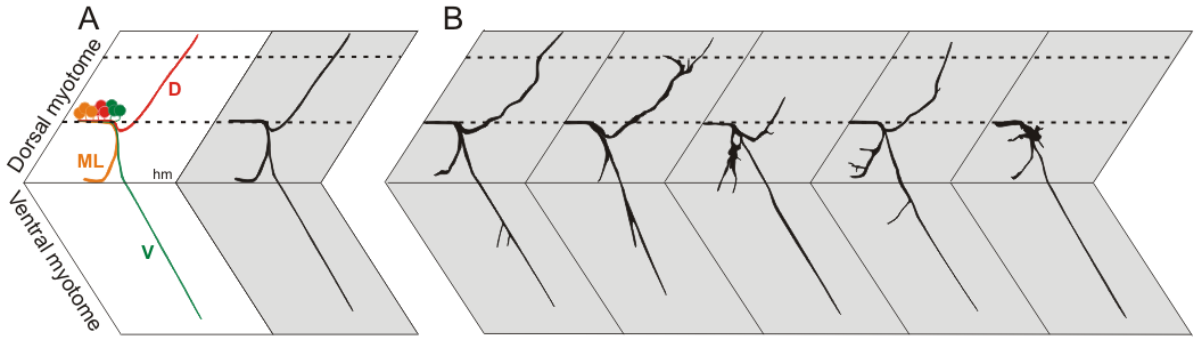

Figure 2.1. **Diagrammatic illustration of secondary motoneuron axons.** A) Left segment shows a lateral view of different subpopulations of secondary motoneurons (shown in orange, red and green) located in ventral spinal cord (indicated by dotted line). Axons exit a mid-segmental root and extend dorsally (D, red), ventrally (V, green), and mediolaterally (ML, orange). Right, normal pathfinding of secondary motoneuron axon trajectories. B) Examples of abnormal axonal pathfinding are shown in each segment in the dorsal and ventral myotome. Note that abnormal phenotypes occur in dorsal, ventral, and mediolateral projecting axons. Horizontal myoseptum: hm. Illustration is not drawn to scale.

Uncoupling Axonal Pathfinding Errors from Muscle Degeneration: 22-72 hpf Exposure

Embryonic nicotine exposure in zebrafish between 22-72 hpf is known to cause SMN axonal pathfinding errors and muscle degeneration at concentrations between 15 and 30μM nicotine (Svoboda et al., 2002; Welsh et al., 2009). Every time such an exposure paradigm was performed at these high nicotine concentrations, muscle degeneration and motoneuron errors coincided. Zebrafish embryos exposed to 1μM, 5μM, 15μM and 30μM (Fig. 2.2B-E) nicotine from 22-72 hpf exhibited SMN axonal pathfinding errors with varying phenotypes when compared to controls (Fig. 2.2A). The dorsal projecting axons of zebrafish embryos exposed to 1μM nicotine exhibited trajectory errors as they extended to their targets at the distal part of the myotome (Fig. 2.2B, filled arrow).

Figure 2.2. Nicotine exposure between 22-72 hpf and SMN axon anatomy. Zn5 immunoreactivity reveals secondary motoneuron axons and their somata in ventral spinal cord in 72 hpf control zebrafish (A). Zebrafish embryos exposed to varying concentrations of nicotine, 1μM (B), 5μM (C), 15μM (D) and 30μM (E) from 22-72 hpf. Note the abnormal motoneuron axon trajectories in the nicotine-exposed zebrafish when compared to their control counterparts. F) At 72 hpf, the percent (%) of hemisegments that possess normal dorsal, ventral, and mediolateral projecting motoneuron axons was quantified. Zebrafish exposed to 1μM (49.77±2.96 %, 516 segments from 18 fish), 5μM (29.04±5.03%, 355 segments from 14 fish), 15μM (14.02±2.85 %, 436 segments from 16 fish), and 30μM nicotine (9.50±2.36 %, 359 segments from 14 fish) possess less hemisegments with normal motoneuron axons when compared to their stage-matched controls (77.44±2.74 %, 455 segments from 17 fish). Filled arrows indicate errors in dorsal projecting axons. Open arrows indicate errors in ventral projecting axons. Arrowheads indicate errors in ventromedial projecting axons. Asterisks denotes significance with a p value <0.001. Scale bars, 20 μm.

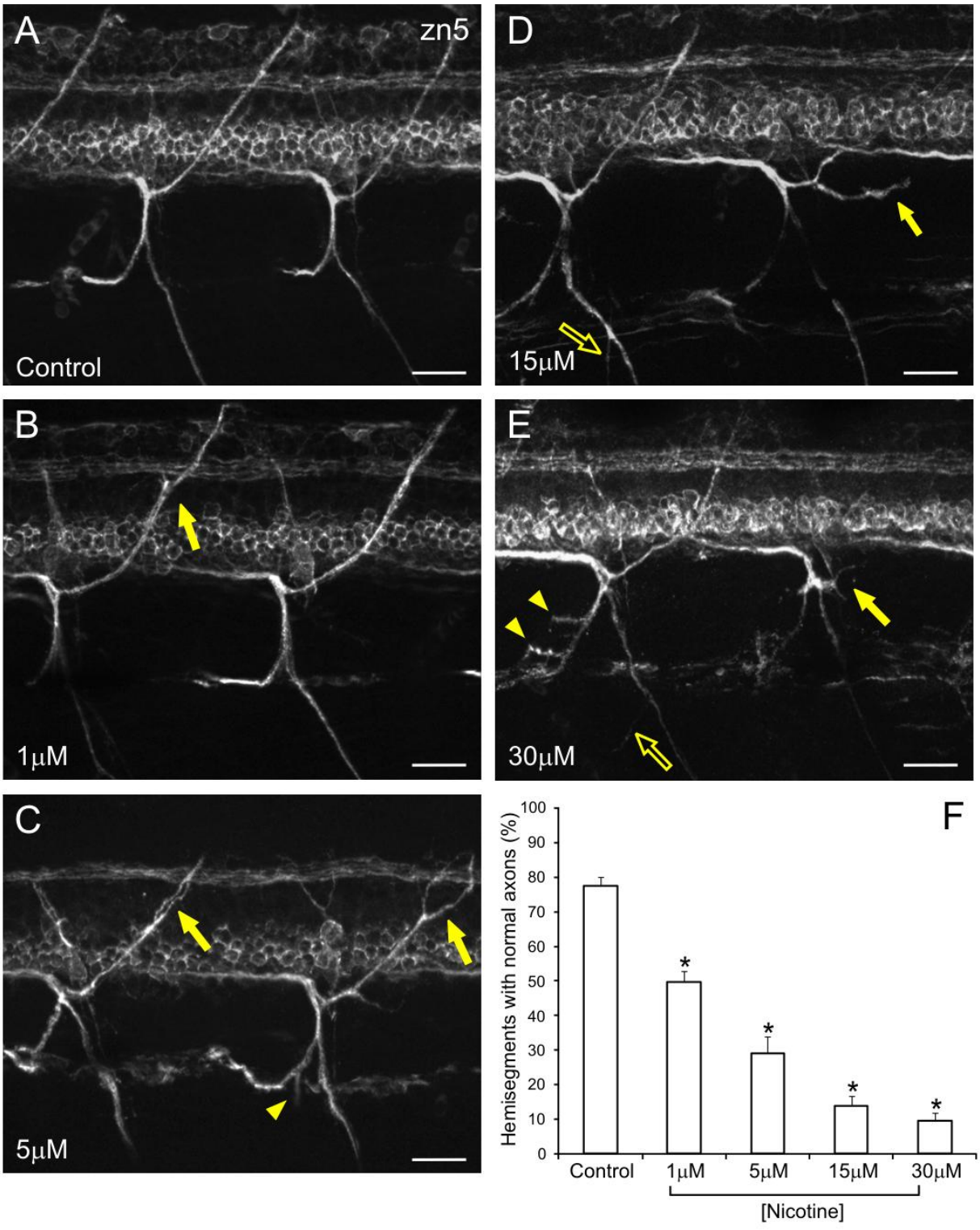
A
zn5
Control
D
15μM
B
1μM
E
30μM
C
5μM
F
Hemisegments with normal axons (%)
100
90
80
70
60
50
40
30
20
10
0
*
*
*
*
Control
1μM
5μM
15μM
30μM
[Nicotine]

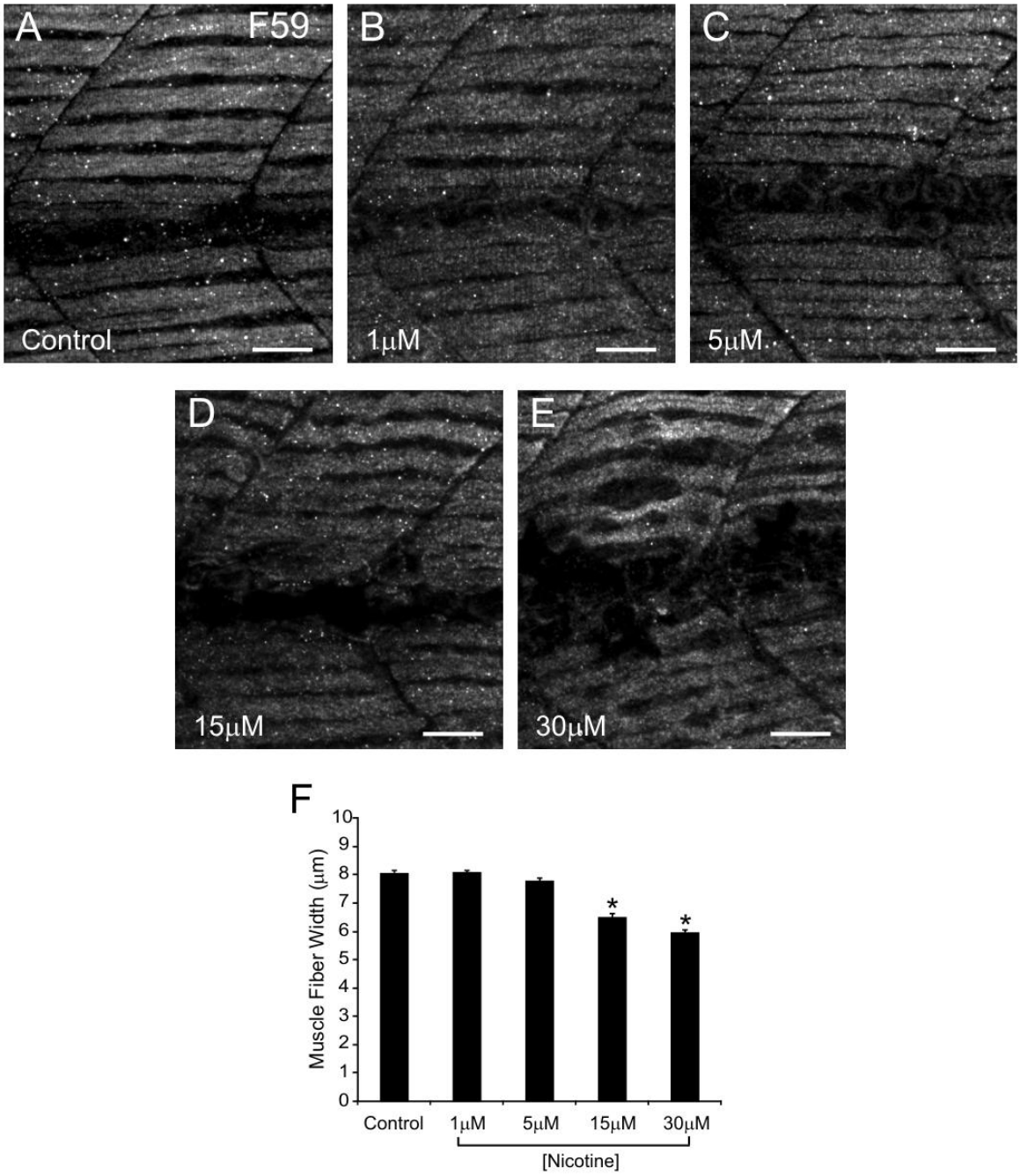

Figure 2.3. Morphology of slow muscle fibers following nicotine exposure (22-72 hpf). F59 immunoreactivity was used to reveal slow muscle fibers in 72 hpf zebrafish embryos exposed to varying concentrations of nicotine, 1μM (B), 5μM (C), 15μM (D) and 30μM (E) from 22-72 hpf. F) Quantification of slow muscle fiber widths in 72 hpf zebrafish. Controls (8.02±0.09 μm, 268 muscle fibers from 7 fish) and nicotine-exposed zebrafish (1μM: 8.08±0.09 μm, 237 muscle fibers from 7 fish; 5μM: 7.78±0.12 μm, 165 muscle fibers from 5 fish; 15μM: 6.49±1.72 μm, 207 muscle fibers from 7 fish; 30μM: 5.97±0.09 μm, 198 muscle fibers from 7 fish). Asterisks denote significance with a p value<0.05. Scale bars, 20 μm.

Zebrafish embryos exposed to 5μM, 15μM, and 30μM nicotine exhibited axonal pathfinding errors in their dorsal (Fig. 2.2C-E, filled arrows), mediolateral (Fig. 2.2C-E, arrowheads), and ventral (Fig. 2.2C-E, open arrows) projecting SMN axons.

Zebrafish myotomal segments were examined to quantify the abnormal phenotypes exhibited by the secondary motoneuron axons following nicotine exposures (Fig. 2.2F). Hemisegments possessing all three axonal trajectories dorsal, ventral, and mediolateral projecting axons were scored as abnormal if at least one of the three main axonal trajectories was abnormal. This quantification revealed that nicotine-exposed (1-30μM) zebrafish had more hemisegments with abnormal motoneuron trajectories when compared to their stage-matched controls (Fig. 2.2F).

At high nicotine concentrations (15 and 30μM), the axonal pathfinding errors coincided with abnormal slow muscle morphology (Fig. 2.3D and E) in the form of smaller fiber widths (Fig. 2.3F) when compared to control zebrafish (Fig. 2.3A). At low nicotine concentrations (1 and 5μM, Fig. 2.3B and C), the presence of axonal pathfinding errors did not coincide with abnormal muscle morphology (Fig. 2.3F). These findings suggest that the axonal pathfinding errors caused by 1 and 5μM nicotine concentrations are most likely neuronal-specific effects that occur independent of muscle degeneration.

Uncoupling Axonal Pathfinding Errors from Muscle Degeneration: 12-30 hpf Exposure

Zebrafish embryos were exposed to nicotine (1-30μM) at the beginning of neurulation at 12 hpf. Zebrafish embryos were then transferred to fresh embryo media at 30 hpf and raised to 72 hpf. At low nicotine concentrations (1 and 5μM), zebrafish SMN axons projected normally into the periphery (Fig. 2.4B and C) and were indistinguishable from their control counterparts (Fig. 2.4A). However, nicotine exposure at high concentrations (15 and 30μM) resulted in SMN axonal pathfinding errors (Fig. 2.4D and E, arrows). Quantification of the abnormal phenotypes

Figure 2.4. **Nicotine exposure between 12-30 hpf and SMN axon anatomy.** Zn5 immunoreactivity was used to reveal secondary motoneuron axons and their somata in ventral spinal cord in 72 hpf control zebrafish (A). Zebrafish embryos exposed to varying concentrations of nicotine, 1μM (B), 5μM (C), 15μM (D) and 30μM (E) from 12-30 hpf. Note the abnormal motoneuron axon trajectories of the nicotine-exposed when compared to their control counterparts. F) At 72 hpf, the percent (%) of hemisegments that had normal projecting SMN axons (dorsal, ventral, and mediolateral) was determined. Nicotine-exposed zebrafish (1μM: 80.6±2.2%, 176 segments from 7 fish; 5μM: 76.8±3.0%, 139 segments from 6 fish; 15μM: 68.7±4.1%, 125 segments from 5 fish; 30μM: 62.6±2.7 %, 146 segments from 6 fish) and stage-matched controls (84.6±1.7 %, 152 segments from 6 fish). Arrows indicate errors in dorsal projecting axons. Asterisks denote significance with a p value <0.05. Scale bars, 20 μm.

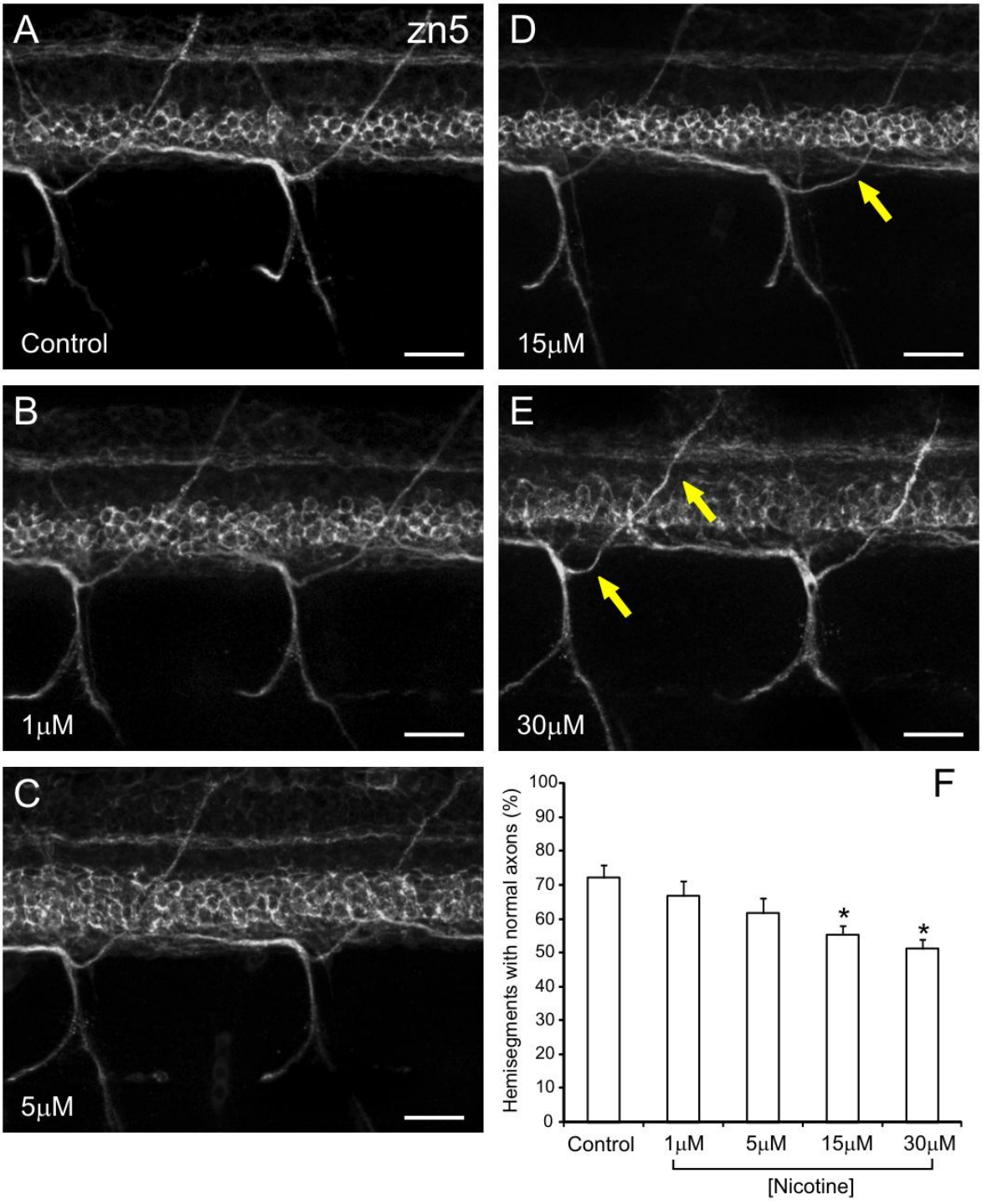
A
zn5
Control
D
15μM
B
1μM
E
30μM
C
5μM
F
Hemisegments with normal axons (%)
100
90
80
70
60
50
40
30
20
10
0
*
*
Control
1μM
5μM
15μM
30μM
[Nicotine]

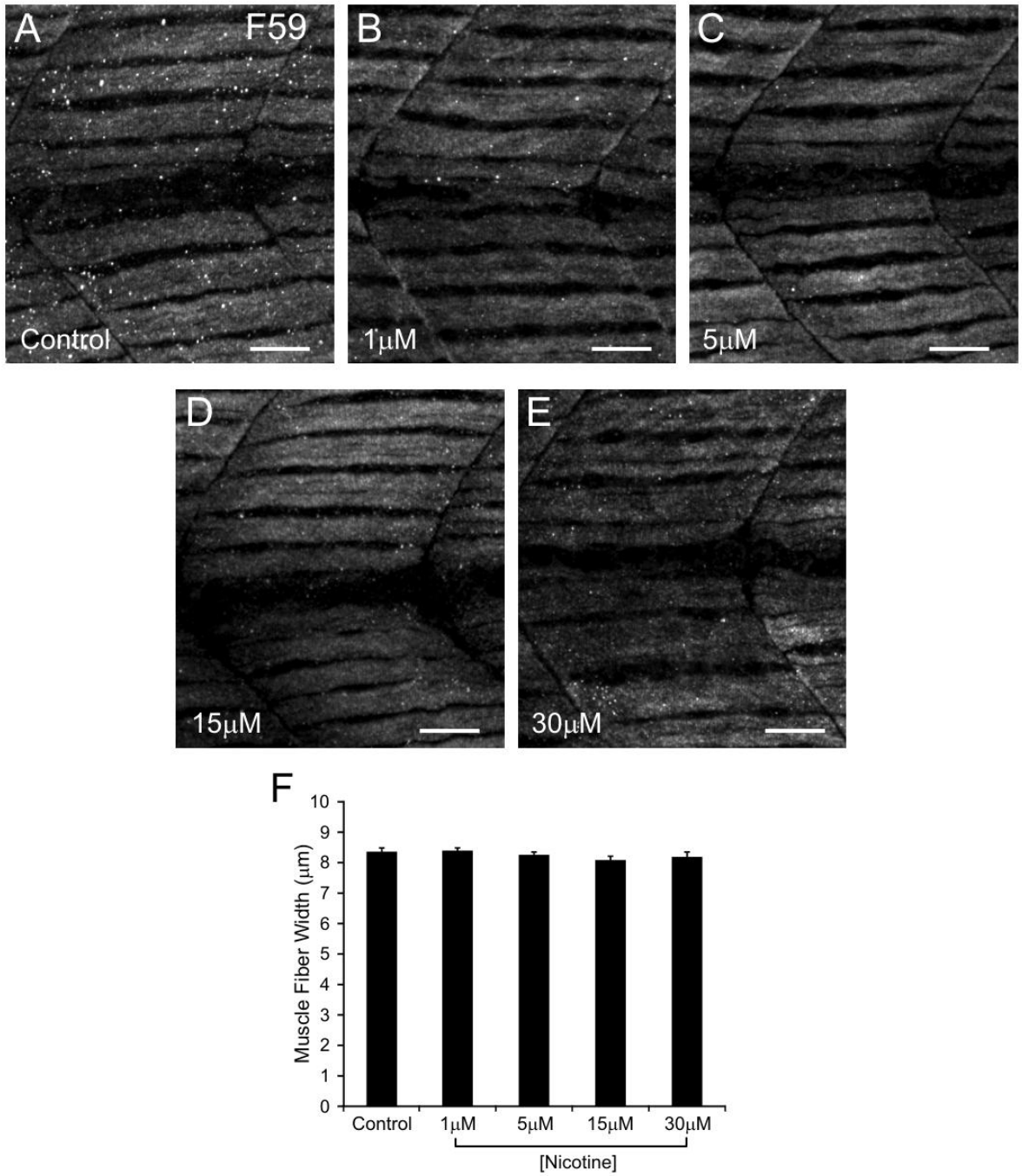

Figure 2.5. Morphology of slow muscle fibers following nicotine exposure (12-30 hpf). F59 immunoreactivity was used to reveal slow muscle fibers in 72 hpf zebrafish embryos exposed to varying concentrations of nicotine, 1μM (B), 5μM (C), 15μM (D) and 30μM (E) from 12-30 hpf. F) Quantification of slow muscle fiber widths in 72 hpf zebrafish. Control (8.38±0.12 μm, 363 muscle fibers from 12 fish) and nicotine-exposed zebrafish (1μM: 8.4±0.11 μm, 256 muscle fibers from 10 fish; 5μM: 8.28±0.10 μm, 463 muscle fibers from 16 fish; 15μM: 8.11±0.11 μm, 398 muscle fibers from 13 fish; 30μM: 8.19±0.17 μm, 204 muscle fibers from 9 fish). There were no significant differences when compared to the controls ($p > 0.05$). Scale bars, 20 μm.

revealed that the number of hemisegments with normal motoneuron trajectories was significantly lower only at high nicotine concentrations (15μM and 30μM, $p<0.05$) when compared to their stage-matched controls (Fig. 2.4F). In these fish, the morphology of slow muscle fibers appeared normal with no significant differences from control zebrafish (Fig. 2.5A-F, $p>0.05$). At this early exposure window, pathfinding of SMN axons was mostly affected only when exposed at high concentrations of nicotine and these pathfinding errors occurred independent of muscle.

Dorsal Projecting Axons Were Mainly Affected Following Nicotine Exposure

Following the nicotine exposure paradigms, it was clear that SMN axons were differentially affected not only with respect to their axonal trajectories (dorsal, ventral, mediolateral) (Fig. 2.6A) but also by the nature of the pathfinding errors (Fig. 2.8). Consequently, we focused our examination on the individual dorsal, ventral, and mediolateral projecting axons in each hemisegment. Following a 22-72-hpf nicotine exposure, the dorsal projecting axons were affected the most at all concentrations when compared to their ventral and mediolateral counterparts (Fig. 2.6B). The mediolateral and ventral projecting axons were primarily affected at high nicotine concentrations (15 and 30μM, Fig. 2.6B). These findings imply that dorsal projecting axons are mainly targeted by nicotine exposures (compare Fig. 2.6B for dorsal projecting axons with Fig. 2.2F). Similar differential target effects were observed following a 12-30-hpf nicotine exposure, where the ventral and mediolateral SMN axons projected normally, but the dorsal SMN axons did not (Fig. 2.6C). These results suggest that dorsal projecting axons are more susceptible to nicotine than ventral and mediolateral axons. These effects also indicate that different mechanisms possibly underlie the actions of nicotine (compare Figs. 2.6B and 2.6C for dorsal projecting axons with Figs. 2.2F and 2.4F, respectively).

Consequently, we then focused our analysis on the dorsal projecting axons regardless of the nature of their pathfinding errors (Fig. 2.7A). The number of dorsal projecting axons that

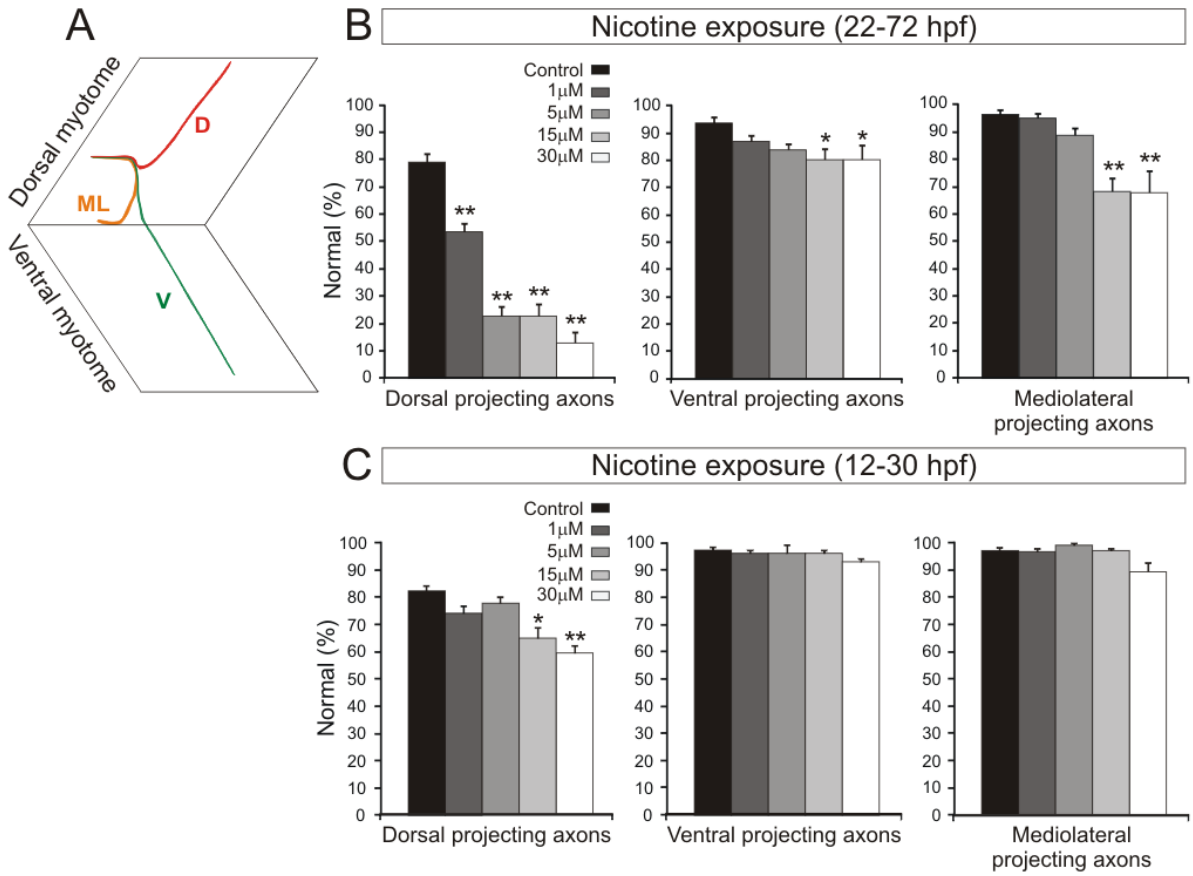

Figure 2.6. Nicotine exposures mostly affect dorsal projecting SMN axons. A) Cartoon illustrating the 3 main trajectories of secondary motoneuron axons: dorsal, ventral, and mediolateral. Hemisegments in 72 hpf zebrafish following nicotine exposures between 22-72 hpf (B) and 12-30 hpf (C) were examined based on their dorsal, ventral and mediolateral trajectories. The percent of hemisegments that possess normal dorsal, ventral and mediolateral projecting axons was quantified (% normal). Asterisks denote statistical significance when compared to the control with a p-value < 0.05 (*) and a p-value < 0.001 (**). See table 5.1 for values. Cartoon is not drawn to scale.

possessed abnormal trajectory phenotypes increased with increasing concentration of nicotine when exposed between 22-72 hpf (Fig. 2.7B). However, when exposed from 12-30 hpf the occurrence of abnormal trajectory phenotypes associated with dorsal projecting axons was increased only at high nicotine concentrations (Fig. 2.7B)

Nicotine-Induced Pathfinding Errors of Dorsal Projecting Axons

In order to understand the differential effects of nicotine exposure on the nature of the pathfinding errors observed, it was necessary to categorize the errors of dorsal projecting axons

Table 2.1. Hemisegments with normal dorsal, ventral, and mediolateral axons in 72-hpf control and nicotine-exposed zebrafish

		Normal (%)			Analyzed
		Dorsal	Ventral	Mediolateral	Hemisegment
12-30 hpf					
Control		82.18±2.25	97.53±0.89	97.18±1.15	145 (n=6)
Nicotine	1μM	74.04±2.88	96.16±1.37	96.60±1.41	163 (n=7)
	5μM	77.67±2.16	96.35±2.82	98.96±0.81	155 (n=6)
	15μM	64.89±3.67*	96.17±1.24	96.91±0.95	121 (n=5)
	30μM	59.34±2.80**	93.05±1.35	89.23±3.02	147 (n=6)
22-72 hpf					
Control		78.83±3.29	93.50±2.29	96.17±1.96	260 (n=10
Nicotine	1μM	53.39±3.27**	86.78±2.29	95.19±1.59	316 (n=11
	5μM	22.74±3.44**	83.86±2.34	88.62±2.64	223 (n=8)
	15μM	22.89±4.24**	80.04±4.23*	68.38±4.82**	268 (n=10
	30μM	12.85±3.83**	80.11±5.46*	67.98±7.61**	232 (n=9)

Values are means±SEM, The number (n) of zebrafish analyzed is indicated in the parenthesis. Asterisks denote statistical significance when compared to the control with a p-value < 0.05 (*) and a p-value < 0.001 (**).

based on their resulting abnormal phenotypes. Four phenotypically distinct groups emerged that specifically described abnormal dorsal projecting SMN axons (Fig. 2.8). The first abnormal phenotype was strictly characterized by distinct "trajectory errors." Dorsal projecting axons that fell into this group successfully reached their dorsal-most targets in the periphery. However, as they navigated through dorsal muscle, they failed to turn dorsally at an intermediate turning point (Fig. 2.8B, arrowheads) and rather extended pass that point ("drift") in the posterior side of the somite rather than in the center. In some cases, they made very distinct sharp turns (Fig. 2.8B, arrows) as they navigated within the myotome. The second category of abnormal SMN axonal phenotypes included dorsal projecting axons that exhibited "fork"-like phenotypes as they projected into the dorsal myotome along the dorsoventral axis of spinal cord (Fig. 2.8C, filled

arrows). In this case, a subset of axons separated from the main dorsal SMN nerve bundle and extended in different directions. This resulted in axon splitting which resembled a fork.

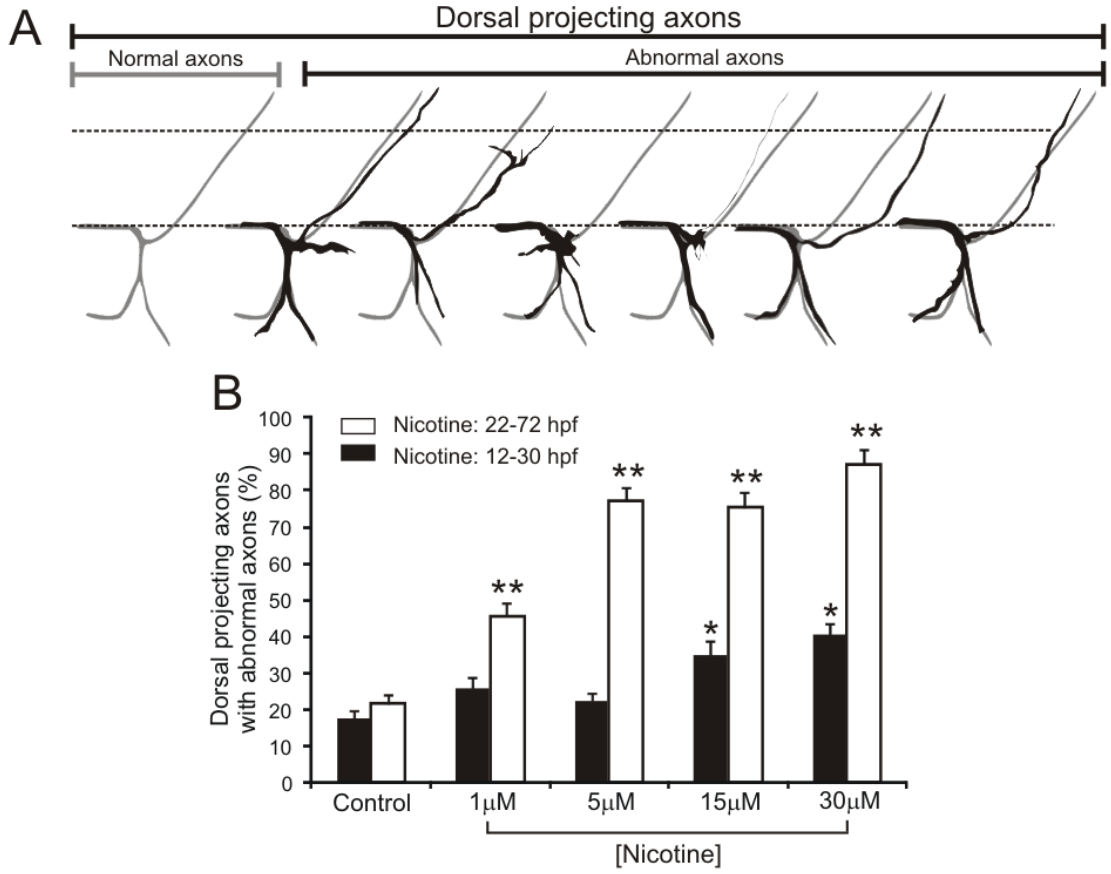

Figure 2.7. Effect of embryonic nicotine exposure on dorsal projecting axons. A) Cartoon depicts the normal dorsal projecting axons (grey) superimposed with observed nicotine-induced abnormal phenotypes. Examples of abnormal phenotypes include forked axons, stalled axons and trajectory errors. B) Dorsal projecting axons in 72 hpf zebrafish with abnormal phenotypes following a nicotine exposure between 12-30 hpf or 22-72hpf. Dotted line denotes the boundaries of spinal cord. Asterisks denote statistical significance when compared to the control with a p-value < 0.05 (*) and a p-value < 0.001 (**). Dotted line in A indicates the boundaries of spinal cord. Cartoon not drawn to scale.

The third phenotypically distinct group was characterized by stalled dorsal projecting axons that fail to reach their dorsal most targets as one fasciculated nerve bundle (Fig. 2.8D). In some instances, even though it was evident that the dorsal projecting axons stalled at the ventral root (Fig. 2.8D, circle), a subset of dorsal projecting axons could be detected appearing as a thin thread and successfully reached the dorsal-most periphery (Fig. 2.8D, arrowheads).

Figure 2.8. Abnormal phenotypes of dorsal projecting SMN axons following embryonic nicotine exposure. A) Left, low magnification photomicrograph (zn5 immunoreactivity) reveals normal motoneuron axon trajectories (scale bar, 50 μm). Middle, diagram illustrates the normal trajectories of dorsal, ventral, and mediolateral motoneuron axons and the red box outlines the dorsal projecting axon. Right, high magnification photomicrograph reveals the normal trajectory path of the dorsal projecting axon. Nicotine-induced phenotypes of dorsal projecting axons were categorized as "trajectory error" (B), fork (C) and stall (D). B) Trajectory error phenotypes include dorsal motoneuron axons that reach their dorsal most target but they drift (arrowheads) pass their turning point and make sharp turns as they traject (open arrows). C) Dorsal projecting motoneurons fork (filled arrows) as they extend in the periphery. D) Motor axons completely stall (dotted circle) as they exit the ventral root and fail to reach their dorsal most targets in the periphery. Arrowheads in D denote a pool of motor axons that successfully reached their dorsal target. Scale bars, 20 μm.

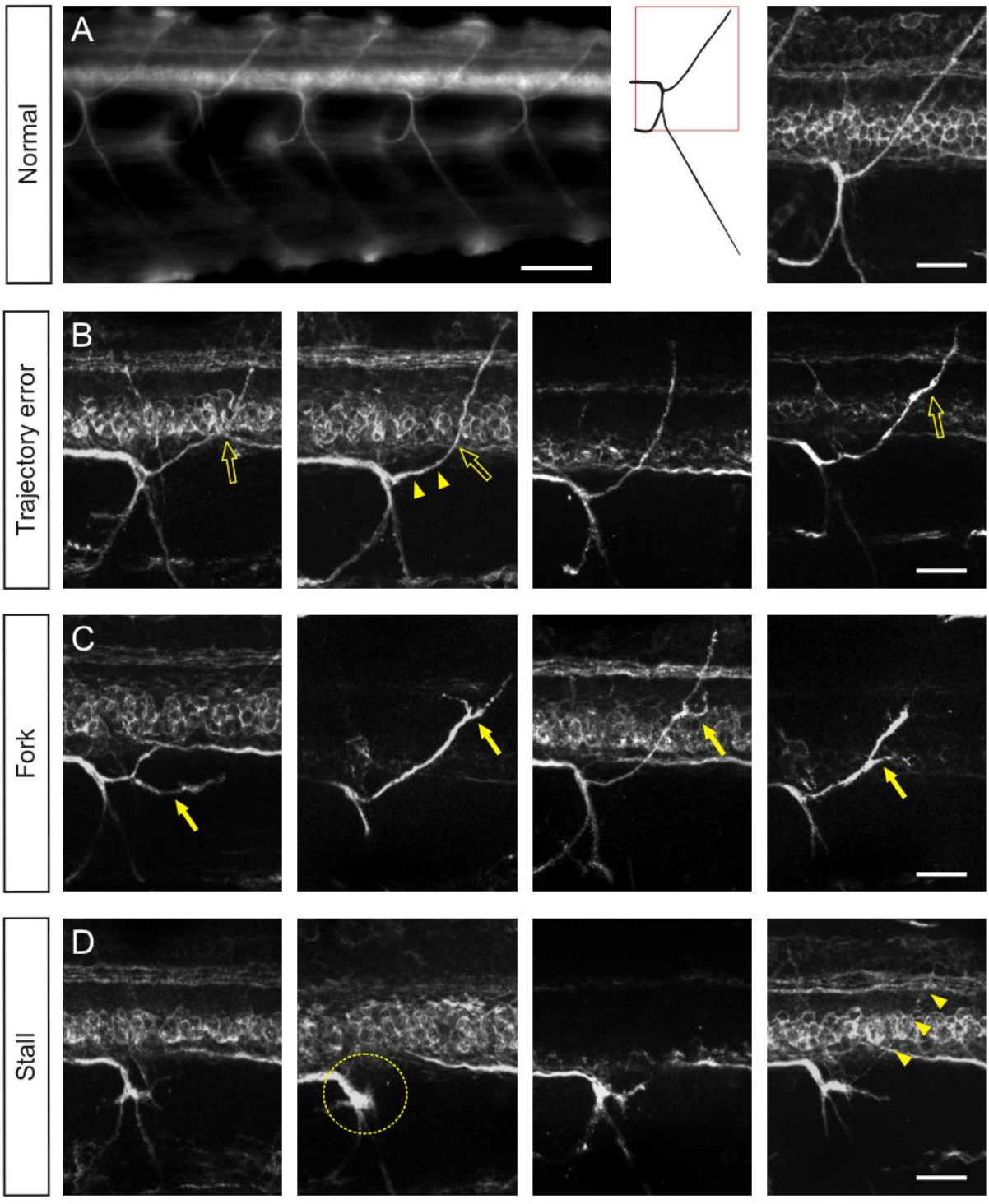
Normal
A
Trajectory error
B
Fork
C
Stall
D

A fourth phenotypically distinct pathfinding error that did not follow any of the above criteria exhibited a duplicated ventral axon in between two hemisegments (Fig. 2.9A and B). Even though these duplicated axons projected ventrally, they stayed confined in the dorsal myotome and did not extend their axons pass the midline in the ventral myotome. This phenotype occurred more frequently in nicotine-exposed zebrafish and appeared to be unique to the long nicotine exposure window (22-72 hpf) (Fig. 2.9C).

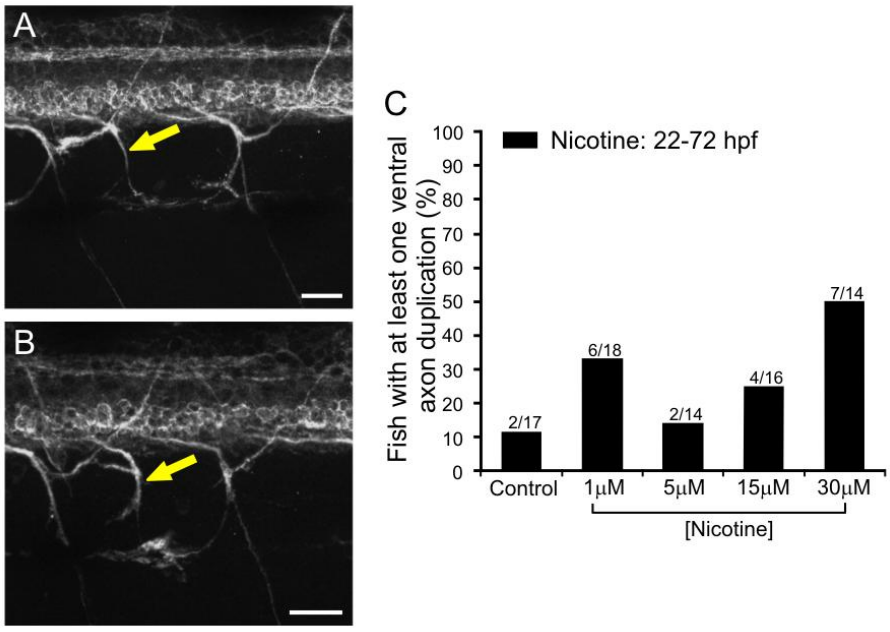

Figure 2.9. Nicotine-induced duplication of SMN axons. Examples of ventral axon duplication (yellow arrows) following nicotine exposure between 22-72 hpf (A and B). C) Percent of 72-hpf zebrafish that possess at least one duplicated ventral axon. Scale bars, 20 μm.

Zebrafish following nicotine exposure from 22-72 hpf exhibited trajectory errors in their dorsal projecting axons at all concentrations of nicotine (Fig. 2.10A). This was also evident in zebrafish exposed to high nicotine concentrations (15 and 30μM, Fig. 2.10A) but not at low concentrations (1 and 5μM, Fig. 2.10A) from 12-30 hpf. There was also a larger number of dorsal projecting axons that forked (Fig. 2.10B) and stalled (Fig. 2.10C) when exposed in 5, 15 and 30μM nicotine between 22-72 hpf. This suggests that 1μM nicotine exposure between 22-72

hpf strictly results in trajectory errors. Also, zebrafish exposed to 5 and 15μM nicotine at 22-72 hpf exhibited more dorsal projecting axons that forked (Fig. 2.10B) whereas, stalled dorsal projecting axons were typically observed in embryos exposed at 30μM nicotine (Fig. 2.10C).

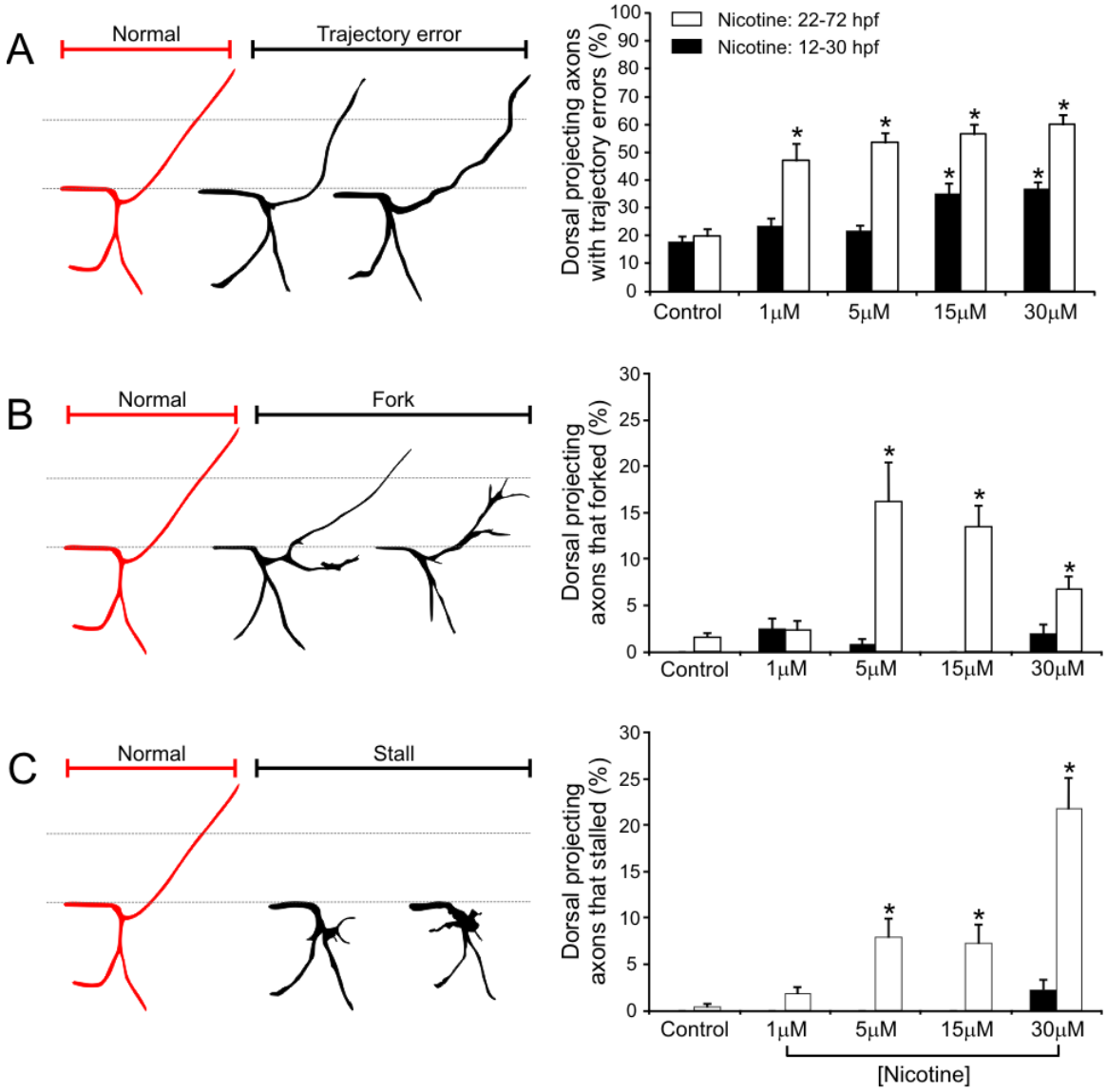

Figure 2.10. Three unique nicotine-induced phenotypes of dorsal projecting SMN axons are dependent on the length of the exposure and nicotine concentration. A-C) Left, diagrammatic illustration of dorsal projecting axons with normal and abnormal phenotypes. Right, Quantification of the dorsal projecting axons that possess the corresponding abnormal phenotypes shown to the left (trajectory errors, A; forked axons, B; stalled axons, C). Normal motoneuron axon phenotypes are shown in red and abnormal phenotypes are shown in black. Dotted line denotes the boundaries of spinal cord. Asterisks denotes significance with a p value <0.05.

Discussion

Uncoupling Axonal Pathfinding Errors and Muscle Degeneration

Embryonic nicotine exposure affects motoneuron axon pathfinding and muscle morphology (Figs. 2.2-2.4). In this chapter, we show that nicotine-induced axonal pathfinding errors can occur in the presence or the absence of muscle defects depending on nicotine concentration levels and exposure duration. When wildtype embryos were exposed from 22-72 hpf to 15 and 30μM nicotine, axonal pathfinding abnormalities and muscle degeneration occurred concurrently (Fig 2.3). However, when zebrafish are exposed to lower concentrations of nicotine (1 and 5μM, 22-72 hpf), abnormalities in axonal targeting occurred independent of muscle effects (Fig. 2.2 and Fig. 2.3).

It was also apparent that axonal pathfinding errors are far more robust at nicotine concentrations where muscle degeneration is present. This suggests that defects in muscle morphology can be a factor for the abnormal motoneuron phenotypes observed following nicotine exposure. It is widely accepted that nerve-muscle interaction is important for proper axon growth and target selection (Funaksoshi et al., 1995). In zebrafish, one of the requirements for proper migration and guidance of spinal motor axons are certain muscle-derived cues (Feldner et al., 2005; Schweitzer et al., 2005; Schneider and Granato, 2006). Nicotine-induced abnormalities in muscle morphology may impair the ability of the muscle to provide the appropriate cues back to the spinal motor axons. In this case, then axons would either be misrouted to inappropriate targets or completely stall at an intermediate target point (Knobel et al., 1999).

Zebrafish embryos exposed to nicotine from 12-30 hpf did not exhibit muscle degeneration at nicotine concentrations that would normally result in slow muscle defects during a longer exposure paradigm (22-72 hpf). The spinal motor axon effects following nicotine

exposures uncouple from muscle defects at 1 and 5μM nicotine following a 22-72-hpf exposure and at 15 and 30μM following a 12-30-hpf exposure. Altogether, these results suggest that the action of nicotine is mediated in part through neuronal-specific substrates.

Differential Nicotine-Induced Effects on Dorsal, Ventral, and Mediolateral Projecting SMN Axons

Nicotine-induced motoneuron axon pathfinding errors appear to predominately affect dorsal projecting axons when compared to their ventral and mediolateral counterparts in the same spinal hemisegment. Embryonic motoneurons exit ventral spinal cord at relatively precise exit points and either extend their axons ventrally or dorsally. Ablation experiments in zebrafish showed that in the absence of ventral primary motoneurons (CaP), SMN extend their axons properly and reach their targets (Pike et al., 1992). However, in the absence of the dorsal primary motoneurons (MiP), dorsal projecting axons failed to project properly and extended towards incorrect paths. Also, dorsal and ventral motoneurons have different transcription factor profiles, which enables them to use in essence distinct signaling pathways for axon extension and targeting (Guthrie, 2007; Sharma et al., 2000). This differential ability of dorsal, ventral, and mediolateral SMN axons to establish their normal pathways suggests that different guidance cues govern path choice. Therefore, nicotine exposure could alter signaling pathways and guidance cues specifically needed by the dorsal projecting axons to make correct path choices.

Mechanisms Underlying Nicotine-Induced Motoneuron Axon Phenotypes

The nicotine-induced effects observed on motoneuron axons were characterized by phenotypically distinct pathfinding errors and were divided into four categories. Trajectory errors were among the most commonly observed axon pathfinding errors following nicotine exposures (12-30 hpf and 22-72 hpf). These trajectory errors occurred at all nicotine concentrations (22-72 hpf) regardless of muscle degeneration but when exposed between 12-30 hpf (15 and 30 μM

nicotine) the effects of nicotine were strictly neuronal. These findings imply that muscle degeneration does not contribute to the occurrence of the trajectory errors of dorsal projecting axons suggesting direct nicotine-induced neuronal effects.

There are at least two possible mechanisms that could produce the trajectory errors observed in zebrafish. First, altering the frequency of rhythmic bursting activity during motoneuron axon outgrowth can result in pathfinding errors (Hanson and Landmesser, 2004, 2006). Zebrafish embryos exhibit spontaneous activity between 17-28 hpf (Saint-Amant and Drapeau, 1998, Thomas et al., 2009). This intrinsic spontaneous activity is associated with Ca^{2+} transients in the motoneuron soma and growth cones (Hanson and Landmesser, 2003) and results in the activation of nicotinic receptors by the release of acetylcholine (Wang et al., 2009). We also know that transient nicotine exposure dramatically increases the embryonic motor activity in zebrafish (Thomas et al., 2009). Therefore, nicotine application during motoneuron axon outgrowth can alter the frequency of their bursting activity through activation of nAChR, thus potentially disrupting motor axon pathfinding decisions in zebrafish.

Second, nicotine-induced alterations of primary motoneuron axons can occur even before SMNs start extending their axons into the periphery. This would subsequently result in the abnormal pathfinding of SMNs axons. In zebrafish, it is known that secondary motoneurons extend their axons following a path previously established by primary motoneurons (Pike et al., 1992). In some of the experiments reported here, zebrafish embryos were exposed to nicotine before the dorsal projecting primary motoneuron (MiP) axons start to extend in the dorsal myotome. If nicotine exposure altered the normal trajectory of MiP axons, this could influence SMN axon pathfinding. For example, SMN dorsal projecting axons could follow the incorrect path set by MiP axons and at 72 hpf, this would be detected as a trajectory error.

Forked dorsal projecting axons were mostly observed in hemisegments of zebrafish exposed to 5μM nicotine between 22-72 hpf and were rarely or never seen when embryos were exposed between 12-30 hpf. Thus at this concentration, the actions of nicotine may be SMN-specific in that the exposure directly affects secondary motor axons after they have extended their axons out in the periphery.

Stalled motoneuron axons were mainly observed in zebrafish that were associated with an exposure paradigm which often resulted in muscle fiber degeneration (30μM, 22-72 hpf). However, axon retraction and growth cone stalling are also associated with high frequency Ca^{2+} transients. When axons stall at intermediate decision points, they exhibit a high frequency of Ca^{2+} transients and when they begin to turn and elongate towards their target, Ca^{2+} transients are abolished (Gomez and Spitzer, 1999). Upon nicotine exposure, activation of neuronal and muscle AChRs occurs. This over-activation of nAChRs during critical periods of axon growth can result in high frequency Ca^{2+} transients, thus leading to axon stalling. In chick ciliary ganglion neurons, activation of α-bungarotoxin-sensitive nAChRs by nicotine application causes neurite retraction and inhibits neurite extension in a calcium-dependent manner (Pugh and Berg, 1994). In zebrafish, motoneuron axons stall because they lack the *stumpy* gene that may not allow them to receive attractive signals and prevent them from extending beyond their intermediate targets (Beattie et al., 2000). This suggests that altering the frequency of intracellular Ca^{2+} transients along with changes in the environment (such as muscle degeneration), play critical roles in proper axonal extension.

The presence of duplicated ventral motor axons appearing as additional exit points in the dorsal myotome is not unique to our exposure paradigms. In zebrafish, blocking the expression of neuropilin-1 and plexin A3, the receptors for the axon-repellent semaphorins, induces additional exit points of spinal motor nerves from spinal cord (Feldner et al., 2005; Palaisa and

Granato, 2007). This axon duplication mainly occurs at the posterior end of the somite, where semaphorins are highly concentrated thus restricting the extension of spinal motor axons in the anterior part of the somite. Therefore if motoneuron axons fail to express axon-repellent receptors, they would be unable to detect signals that would normally restrict them from entering the posterior end of the somite.

Taken together, nicotine exposure can elevate Ca^{2+} transients through the activation of AChRs on neuronal and muscle substrates. Cholinergic signaling appears to differentially mediate axonal pathfinding of spatially distinct trajectories in each hemisegment. Increased frequency of Ca^{2+} transients during critical stages of spinal motor axon outgrowth can lead to significant errors in pathfinding. The frequency and strength of Ca^{2+} transients has been shown to effectively modulate gene activity and differentially activate signaling pathways (Dolmetsch et al., 2007; Greer and Greenberg, 2008). Therefore, inappropriate nicotine-induced activation of nAChRs at critical developmental stages can disrupt the normal course of gene expression thus disrupting the expression profiles of axon pathfinding-specific molecules. These findings also raise the possibility that errors in pathfinding of motoneuron axons may be permanent and potentially persist in the adult zebrafish.

CHAPTER 3

SECONDARY MOTONEURONS IN JUVENILE AND ADULT ZEBRAFISH: AXONAL PATHFINDING ERRORS CAUSED BY EMBRYONIC NICOTINE EXPOSURE*

***This chapter was reprinted and modified with permission from Wiley Interscience published in the Journal of Comparative Neurology, 512, Menelaou, E, Svoboda, KR, Secondary motoneurons in juvenile and adult zebrafish: axonal pathfinding errors caused by embryonic nicotine exposure, pp. 305-322, 2009.**

Introduction

In Chapter 2, experiments were performed that focused upon the short-term consequences of embryonic nicotine exposure on secondary motoneuron axon pathfinding and slow muscle morphology. Nicotine exposure altered the pathfinding of distinct motoneuron axon trajectories. Therefore, we sought to determine whether the phenotypes observed following embryonic nicotine exposure were transient and recovered over time or if they were permanent and persisted into adulthood.

In order to address this, we had to develop a method where we could reliably examine and track nicotine-induced alterations in motoneuron axons at different stages of development. *In vivo* live imaging offers many advantages over immunohistochemical analysis of fixed tissues as it eliminates fixation artifacts that could obscure histological features and also the ability to track morphological features in the same animals. Live imaging has become a powerful tool for studying axonal regeneration in injured spinal cords in animal models including mice (Kerschensteiner et al., 2005), lamprey (Zhang et al., 2005) and zebrafish (Bhatt et al., 2004). Also, *in vivo* imaging in transgenic zebrafish expressing green fluorescent protein (GFP) has aided in the visualization and characterization of the vascular (Lawson and Weinstein, 2002) and lymphatic systems (Yaniv et al., 2006).

We initially took advantage of two characteristics of the zebrafish model. First, zebrafish are genetically accessible with several transgenic lines readily available which are routinely used to facilitate anatomical studies. Second, zebrafish embryos/larvae are translucent making high resolution *in vivo* imaging feasible. It was first necessary to choose the appropriate transgenic zebrafish line that would allow visualization of secondary motoneuron axons. In this case, two transgenic GFP reporter fish were chosen. In the *Tg(isl1:GFP)* zebrafish (Higashijima et al., 2000) referred to as *isl1* from here onward, GFP is expressed in a subpopulation of secondary

motoneurons innervating the dorsal myotome (Zeller et al., 2002). In the *Tg(gata2:GFP)* zebrafish (Meng et. al, 1997), referred to as *gata2* from here onward, GFP is expressed in a subset of secondary motoneurons which innervate the ventral myotome (Zeller et al., 2002). Before we could proceed with nicotine exposures, we had to characterize these two transgenic lines early in larval development using a well-characterized antibody, zn5 (Chapter 2).

In this chapter, we characterize the motoneuron axon trajectories in 72-hpf *isl1* and *gata2* larvae, and based on this characterization, chose the *isl1* zebrafish to address the long-term consequences on secondary motoneuron pathfinding. Using a live imaging technique, we show that axonal pathfinding errors resulting from embryonic nicotine exposure persisted into adulthood. These findings indicate that exposure to nicotine during embryonic development can have long-term consequences for motoneuron anatomy in zebrafish.

Materials and Methods

Zebrafish Maintenance

Animal protocols were approved by the Institutional Animal Care and Use Committee at Louisiana State University. Fertilized eggs were obtained from natural spawnings of *Tg(isl1:GFP), Tg(gata2:GFP),* and several wild-type lines according to the Zebrafish Book (Westerfield, 1995). Adult fish were maintained at 28^{o}C with a lighting schedule of 14 h light and 10 h dark. Embryos were collected within 3 hours of spawning, rinsed, and placed into 100 mm petri dishes containing embryo medium. Stage matched control and nicotine-exposed fish were raised in system water following 5 days post fertilization (dpf), cleaned daily (20% water change) and raised on a diet of baby fish food from 5-10 dpf and brine shrimp following 10 dpf. Both experimental and control fish were maintained under the same conditions for the duration of the experiments.

Nicotine Exposures

Zebrafish embryos at 19-22 hours post fertilization (hpf) were exposed while in their chorions to nicotine (5-30µM, Sigma, St. Louis, Missouri, USA, catalog # N3876-5ml) made in embryo medium (pH 7.2). Nicotine stock solutions were made fresh daily as needed in distilled water and then the stock solution was diluted in embryo medium to obtain final concentrations. Embryos were continuously exposed in 35 mm petri dishes until 72 hpf. At 48 hpf, all nicotine-exposed and stage matched control embryos were manually dechorionated. At 72 hpf, nicotine-exposed larvae were transferred into nicotine-free embryo medium and a sample of those larvae (nicotine-exposed and stage match controls) were fixed in 4% paraformaldehyde. The remaining nicotine-exposed and stage matched unexposed (control) larvae were transferred into one-liter beakers containing system water at 5 dpf and raised for examination at later developmental stages.

Immunohistochemistry

Whole mount immunohistochemistry was carried out using a modified version of our previously published protocol (Svoboda et al., 2001 & 2002; Pineda et al., 2006). Briefly, larval zebrafish were first fixed in 4% paraformaldehyde overnight at 2-4^{o}C and then stored in PBST (PBS, pH 7.3, containing 0.1% Tween 20). After permeabilization, they were incubated in primary antibody overnight at 2-4^{o}C. The monoclonal antibodies zn5 (dilution 1:500) and F59 (dilution 1:250) were obtained from the Developmental Studies Hybridoma Bank (The University of Iowa, Iowa) and were used to reveal secondary motoneuron somata and their axons (Fashena and Westerfield, 1999) and slow muscle fibers (Devoto et al., 1996), respectively. The following day, the larvae were washed for 90 minutes and then incubated for another 90 minutes in an anti-mouse fluorescent secondary antibody conjugated to Alexa 546 or Alexa 488 (1:1000 dilution in PBST; Molecular Probes). They were then rinsed in PBST for another 60 minutes and

prepared for image analysis. The zn5 mouse monoclonal antibody recognizes a thick band (doublet) at about 75 kilo Daltons on western blots. The zn5 antigen peptide sequences (peptide 1: KHVTGPNQVSTPDTFQIRYPQ, peptide 2: KVSLQVVSQSPITEG) match a stretch of 37 amino acids within the extracellular domain of the zebrafish DM-GRASP sequence (Fashena and Westerfield, 1999). The zn5 antibody in this study revealed the same stereotypical morphology of secondary motoneurons and their axons as well as the apposed membrane regions of slow muscle fibers (Fashena and Westerfield, 1999; Devoto et al., 1996; Ott et al., 2001). The antibody zn5 is currently available as zn8 from the Developmental Studies Hybridoma Bank. The antibodies zn5 and zn8 are duplicate isolates of the same hybridoma (Kawahara et al., 2002). The mouse monoclonal antibody F59 is raised against chicken myosin (Crow and Stockdale, 1986) and this antibody is specific for the fast isotypes of myosin heavy chain in chicken. The specific isotypes of myosin heavy chain recognized by F59 in zebrafish are not known. Staining with this antibody (F59) revealed the distinct labeling pattern of slow muscle fibers in zebrafish (Devoto et al., 1996).

Neuromuscular Junction Staining

Tetramethylrhodamine conjugated to α-bungarotoxin (Rh-α-btx) (Molecular Probes, Eugene, OR) was used to identify potential sites of neuromuscular junctions. Transgenic larval zebrafish were processed for immunohistochemistry and then incubated in Rh-α-btx (10 μg/mL) for 90 minutes before image analysis. For double labeling experiments in wild-type larvae, incubation in Rh-α-btx (10 μg/mL) for 90 minutes was performed first before adding the zn5 antibody to the primary solution (overnight at 2-4^{o}C). The following day, the larvae were washed for 90 minutes and then incubated for another 90 minutes in an anti-mouse fluorescent secondary antibody conjugated to Alexa 488 (1:1000 dilution) to reveal zn5 labeling.

Image Acquisition and Analysis of Morphological Data in Fixed Tissue

Fixed transgenic zebrafish (3-30 dpf) were mounted laterally on a slide in PBST, lightly cover slipped and sealed. Images were obtained using a Zeiss Axiovert 200M inverted microscope equipped with epifluorescence and a Zeiss ApoTome. Images were acquired using a 40x oil immersion objective (N.A. 1.30) and z-stacks (20-60 μm thick) were collected at 0.5-0.8 μm intervals. When imaging α-bungarotoxin (α-btx) signals, the step size interval of the z-stacks was 0.3 μm. The GFP and rhodamine signals were visualized using separate filter cubes. The image stacks were obtained over the yolk sac extension (Fig. 3.1), including at least one complete side (hemi-segment) of spinal cord, and reconstructed in three-dimensional volumes using Imaris 5.7.2 (Bitplane Inc., Saint Paul, MN). Volume rendering analysis included 360^{o} rotations in all directions to reveal motoneuron morphology. All of the rotational views presented in this work were always rotated horizontally around the dorsal-ventral axis with rostral regions moving away and caudal regions moving out from the plane of the page (illustrated in Fig. 3.1). A total of 268 z-stacks were acquired and analyzed in this study and the model of axonal trajectories in larvae and juvenile *isl1* zebrafish was generated based on observations pertaining to these z-stacks. The stacks were obtained from 45 control zebrafish at different developmental stages (3-30 dpf). All images are presented with the rostral region at the left and dorsal to the top as shown in figure 3.1. Photoshop 7.0 (Adobe, San Jose, CA) and CorelDraw Graphics Suite 12 (Ottawa, Ontario, CA) were used to crop and organize the figures, respectively.

Live Imaging

Isl1 zebrafish were first anesthetized in 0.008% tricaine methanesulfonate (MS222) at 17 dpf and in 0.02% MS222 in fish older than 24 dpf. Once completely anesthetized, the fish were placed in a single drop of MS222 on 1 mm-thick slides and imaged live on a Zeiss fluorescent stereomicroscope (Lumar V.12) equipped with an eGFP filter set using a Neolumar S 1.5x

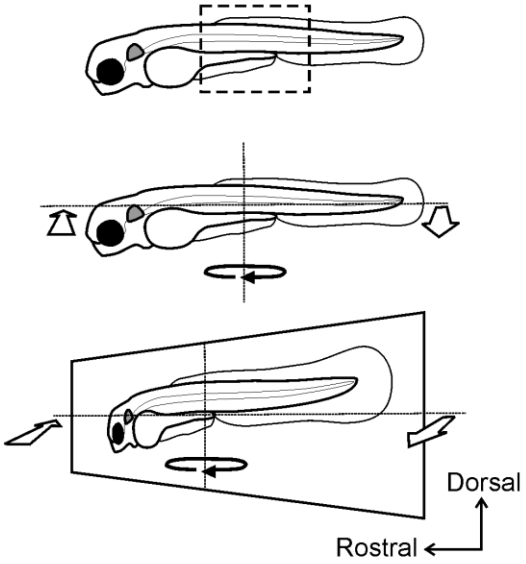

Figure 3.1. Illustration depicting imaging methodology in fixed tissue. Zebrafish at various ages were analyzed via fluorescent microscopy with the aid of an ApoTome. All zebrafish were mounted on the side. Image stacks were acquired within the region denoted by the dashed box (top) and subsequent examinations using Imaris software included volume rendering allowing rotations in any direction. All rotations shown in this work are presented as horizontal rotations of the dorsoventral axis (middle, black arrow indicates rotational direction) with rostral regions moving away (bottom, left open arrow) and caudal regions moving out of the plane of the page (bottom, right open arrow).

objective (150x maximum magnification). Single focal plane images were captured using an AxioCam MRc 5 digital camera. The time interval for live examination was closely monitored. We were able to image anesthetized zebrafish (17 dpf) for 8-10 minutes before they had to be "rescued" and returned back to their individual containers containing system water. In fish older than 2 months of age, the imaging interval could be extended to 15-20 minutes. Two or three consecutive live imaging examinations were performed for the same fish given that the fish was allowed to recover from anesthesia for at least one hour. This permitted examination of both sides of the fish. During live imaging, fish were kept moist by adding a few drops of MS222. Examination was performed initially at 17 dpf and long-term investigation tracking motoneuron changes in the same fish was carried out every week beginning at 37 dpf and continued until 86

dpf (~3 months old). At the end of the long-term investigation, all zebrafish were transferred back to their own individual tanks in our zebrafish facility. All acquired images during live examination were digitally processed with the aid of Adobe Photoshop 7.0 (Adobe, San Jose, CA). The invert function was used to convert the GFP signals to a black-and-white image.

Statistics

All values are reported as means ± standard error of the mean (SEM). The Mann-Whitney *U* test was performed to test for significance and was assigned if the p value was <0.05.

Results

Zebrafish Secondary Motoneuron Axons

There are different developmentally regulated populations of motoneurons in the zebrafish spinal cord. Secondary motoneurons have a distinct morphology, physiology, and timing of their development (Myers et al., 1986; Westerfield et al., 1986). They are born during later stages of development following the primary motoneurons and start extending their axons around 22-23 hpf (Beattie et al., 1997; Pike et al., 1992). Secondary motoneuron somata are numerous and are located within ventral spinal cord (Myers, 1985). Their axons exit each segmental root as a nerve bundle following the path established by primary motoneuron axons. They extend into the myotome to contact either medially located (fast, white) or laterally located (slow, red) myotomal muscle fibers (Pike et al., 1992; Westerfield et al., 1986; Devoto et al., 1996; Fetcho, 1986).

In our previous work, secondary motoneuron development and axonal pathfinding was examined using the *isl1* GFP reporter fish and the zn5 antibody which recognizes the adhesion molecule DM-GRASP (Burns et al., 1991). However, the use of zn5 is limited in younger zebrafish (younger than 8 dpf; Svoboda et al., 2002) and it can only be used in fixed tissue. Our goal of determining whether nicotine-induced abnormalities in secondary motoneuron axons

persisted in fish older than 8 dpf required that we identify other markers of secondary motoneuron axons which could be imaged in living fish.

Transgenic lines of zebrafish provide a great opportunity to visualize GFP expression within axonal trajectories in older living fish. In the *isl1* zebrafish line, GFP expression is driven under direction of the *islet1* promoter. In *isl1* zebrafish older than 54 hpf, GFP can be detected in secondary motoneurons (Higashijima et al., 2000). These motoneurons can be identified according to their ventral positions in spinal cord and their axons which travel in nerve bundles projecting into the dorsal musculature (Svoboda et al., 2002; Zeller et al., 2002; Ott et al., 2001). In the *gata2* transgenic line, GFP is expressed in a subpopulation of ventrally projecting secondary motoneuron axons (Meng et al., 1997; Pineda et al., 2006).

Zn5 immunoreactivity exhibits stereotypical labeling of secondary motoneuron somata and their axons which extend within the ventral and dorsal myotome (Fig. 3.2B). When analyzed in 3 dpf *isl1* zebrafish, dorsally projecting GFP-positive motoneuron axons were zn5-positive (Fig. 3.2A-C, F). Similar examination in *gata2* zebrafish revealed that zn5 labeled the main GFP-positive ventrally projecting nerve (Fig. 3.2D, E). When examining zn5 immunoreactivity within spinal cord we noticed that a subset of zn5-positive cells corresponded to GFP positive somata in *isl1* zebrafish (Fig. 3.2G) as well as in *gata2* zebrafish (Fig. 3.2H). In the *isl1* line, GFP/zn5-positive cells lie within mid-dorsal spinal cord (Fig. 3.2G). In the *gata2 line*, GFP/zn5-positive cells were confined to more ventral spinal cord (Fig. 3.2H). In *gata2* zebrafish, the dorsally located GFP-positive cells which are zn5-negative are most likely interneurons (Fig. 3.2H; arrowheads, Hale et al., 2001). Mating crosses of *isl1* and *gata2* transgenic GFP reporter fish resulted in transgenic zebrafish expressing GFP in both subpopulations of motoneurons. GFP expression associated with both populations of motoneurons was correlated with most of the zn5-positive cells (Fig. 3.2I). However, it appeared that not all zn5-positive cells were expressing

Figure 3.2. Zn5 labeling of secondary motoneuron somata and their axons in *isl1* and *gata2* zebrafish. A) Photomicrograph of a projected z-stack from a 72 hpf *isl1* zebrafish reveals GFP-positive motoneuron somata located in ventral spinal cord. Secondary motoneurons extend their axons dorsally to innervate dorsal musculature (filled arrow). B) Zn5-positive axons extend both ventrally and dorsally into the myotome. C) The merged image reveals that dorsally projecting GFP-positive axons are recognized by zn5. The GFP signal was saturated to reveal motoneuron axons. D) Projected z-stack from a 72 hpf *gata2* zebrafish reveals GFP-positive motoneuron somata and ventrally projecting axons (filled arrowhead) and zn5-positive axons extending both ventrally and dorsally into the myotome. The GFP signal was saturated to reveal motoneuron axons. Expanded views from C and D merged images (E and F, respectively) show zn5 labeling of ventrally projecting GFP-positive motoneuron axons in a *gata2* larva (left) and on dorsally projecting GFP-positive motoneuron axons in an *isl1* larva (right). GFP-positive cells located more dorsally are presumably interneurons (open arrowhead). Single focal plane images selected from a series of stacks from *isl1* (G), *gata2* (H) and *isl1/gata2* (I) zebrafish indicating that zn5 labels a population of motoneurons other than just the GFP-positive motoneurons in *isl1* or *gata2* zebrafish. Motoneuron somata that express GFP driven by the *islet1* promoter (G) are detected by zn5 and are positioned in mid-dorsal spinal cord. Only a subpopulation of zn5-positive motoneuron somata, which are located in ventral spinal cord, is GFP-positive in *gata2* zebrafish (H). Some interneurons located dorsally are not zn5-positive (open arrowheads). Zn5 immunoreactivity in *isl1*/*gata2* transgenic zebrafish (I) detects most GFP-positive motoneurons. The presence of zn5-positive/GFP-negative cells indicates the presence of other secondary motoneuron subpopulations. A total of 21 fish were analyzed for this figure. Scale bars, 20 μm. A-C share the scale bar in C and G-I share the scale bar in I.

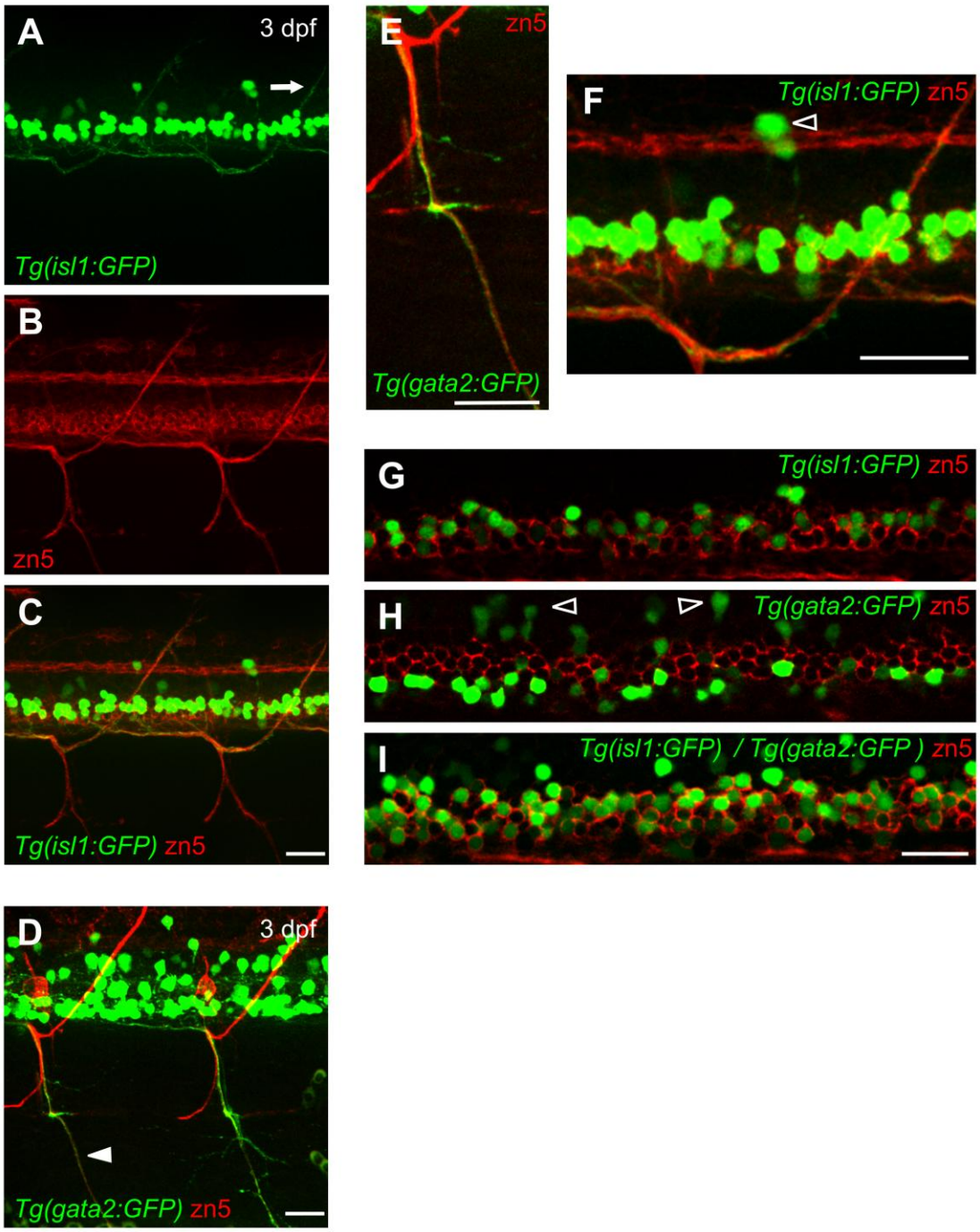
A
3 dpf
Tg(isl1:GFP)
B
zn5
C
Tg(isl1:GFP) zn5
D
3 dpf
Tg(gata2:GFP) zn5
E
zn5
Tg(gata2:GFP)
F
Tg(isl1:GFP) zn5
G
Tg(isl1:GFP) zn5
H
Tg(gata2:GFP) zn5
I
Tg(isl1:GFP) / Tg(gata2:GFP) zn5

Figure 3.3. Secondary motoneuron axons in *isl1* and *gata2* zebrafish. A) Lateral view of a maximum projection from a z-stack (0^o rotation) from a 72 hpf *gata2* zebrafish labeled with zn5 reveals ventrally projecting motoneuron nerves exhibiting secondary and tertiary branches. B) Three-dimensional rendering at a 45^o rotation reveals axons exiting ventral spinal cord that exhibit branching extending laterally within the myotome. C) At a 90^o rotation, the spinal cord (half spinal hemisegment) is to the right (open arrow) with the most superficial (lateral, zn5-positive) side of the fish to the left. Note the extensive branching from the ventral main nerve within the myotome (GFP signal below the white arrowheads). D) Lateral view (0^o rotation) from a z-stack from a 72 hpf *isl1* zebrafish reveals zn5 immunoreactivity in dorsally- and ventrally projecting axons in addition to the slow muscle boundaries. E) Three-dimensional rendering at a 45^o rotation reveals zn5-positive axons that project to reach the lateral edge and then take a dorsal path along the segmental boundaries at the most lateral part of the fish (open arrowheads). F) The 90^o rotation reveals the cross-sectional view showing the left side of the spinal cord to the right (open arrow) with the superficial/lateral side of the fish to the left (open arrowheads). Both zn5- and GFP-positive axons are evidently extending from a medial plane (ventral of spinal cord) out into the most lateral surface of the fish (open arrowheads in E and F). Note the GFP-positive axonal trajectories located within the dorsal myotome (region above the white arrowheads). A total of 21 fish were analyzed for this figure. White arrowheads indicate the midline in C and F. Scale bars, 20 μm. A-C share the scale bar in C and D-F share the scale bar in F.

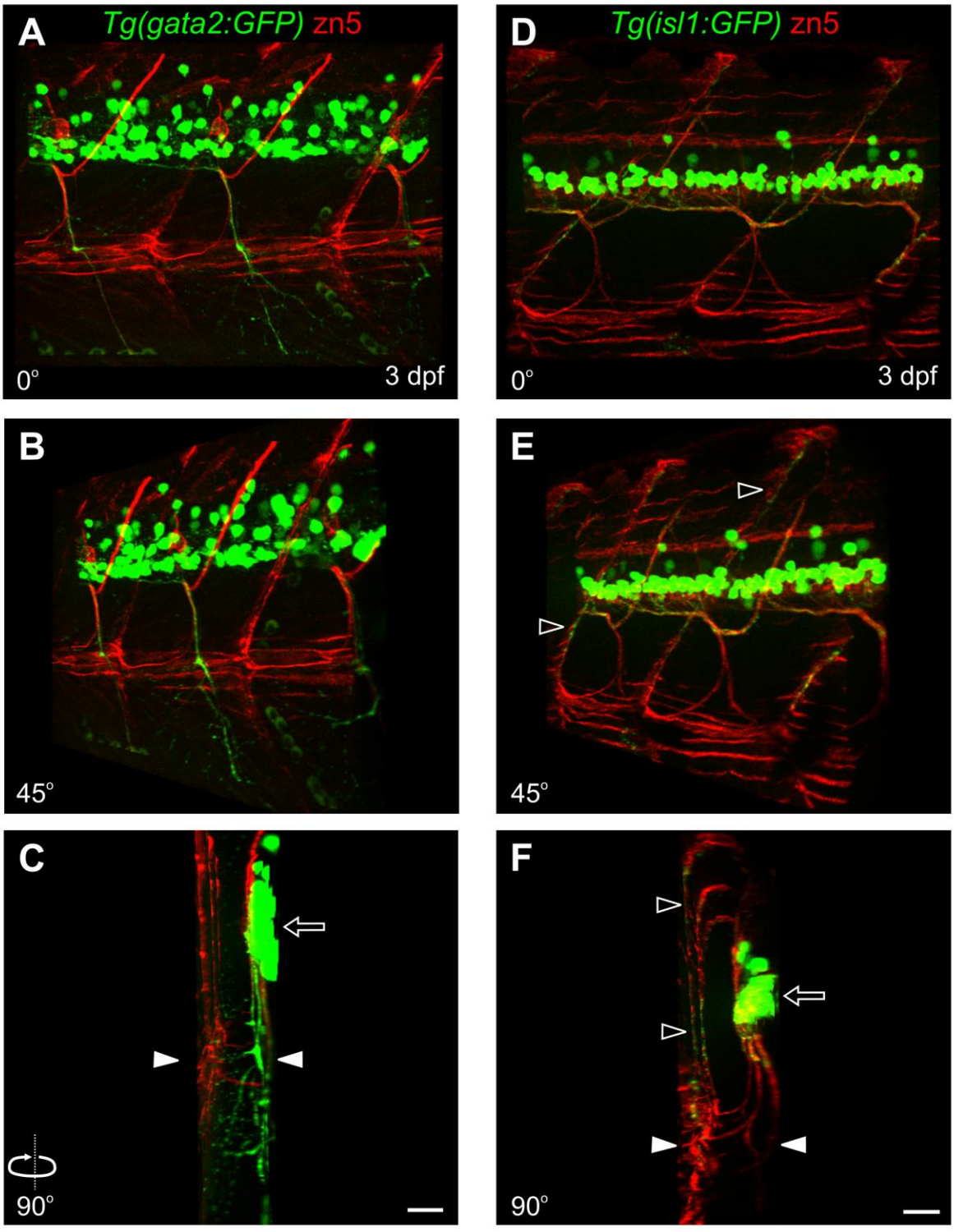
A
Tg(gata2:GFP) zn5
0°
3 dpf
D
Tg(isl1:GFP) zn5
0°
3 dpf
B
45°
E
45°
C
90°
F
90°

GFP driven by either the *islet1* or *gata2* promoters. This suggests that there is yet another sub-class of secondary motoneurons, which is zn5-positive.

The zn5 antibody also detects the most lateral (superficial) region of the zebrafish where it labels the boundaries of slow muscle fibers (Fashena and Westerfield, 1999). These slow muscle fibers are superficially located just beneath the skin (Devoto et al., 1996). Volume rendering analysis in *gata2* zebrafish (Fig. 3.3A-C) indicated that the GFP-positive ventrally projecting main nerves had numerous branches extending from them. These axonal branches did not extend to the most superficial layer of the zebrafish, which was revealed by zn5 immunoreactivity, when rotated 90^{o}. (Fig. 3.3C and data not shown). The axons were located within the region where fast muscle fibers make up the myotome and were juxtaposed to Rh-α-btx-positive nicotinic acetylcholine receptors (Fig. 3.4).

Similar analysis was performed in *isl1* zebrafish and revealed GFP-positive motoneuron axons extending dorsally to innervate medially and laterally located musculature (Fig. 3.3D-F). The zn5 labeling at the segmental boundaries in the lateral periphery were in the same focal plane as superficially located slow muscle fibers (Fig. 3.5A-C). The lateral axonal trajectory in *isl1* larvae appeared to contact zn5-positive structures at these segmental boundaries (Fig. 3.5D, E). Neuromuscular junction staining revealed the presence of nicotinic acetylcholine receptors on zn5-positive segmental boundaries and muscle fibers located laterally within the myotome (Fig. 3.5F-H). Rh-α-btx labeling of the V-shaped segmental boundaries (myosepta) does not necessarily represent synapses (Chen et al., 1990; Ono et al., 2004). The spatial distribution of the *isl1* axonal trajectories in the lateral myotome suggests that different subpopulations of axons within the main nerve bundle target either fast or slow muscle fibers (Fig. 3.4). Zn5 labeling thus served as a reference marker of the lateral periphery of the zebrafish myotome and guided us in distinguishing between medially and laterally located motoneuron axons.

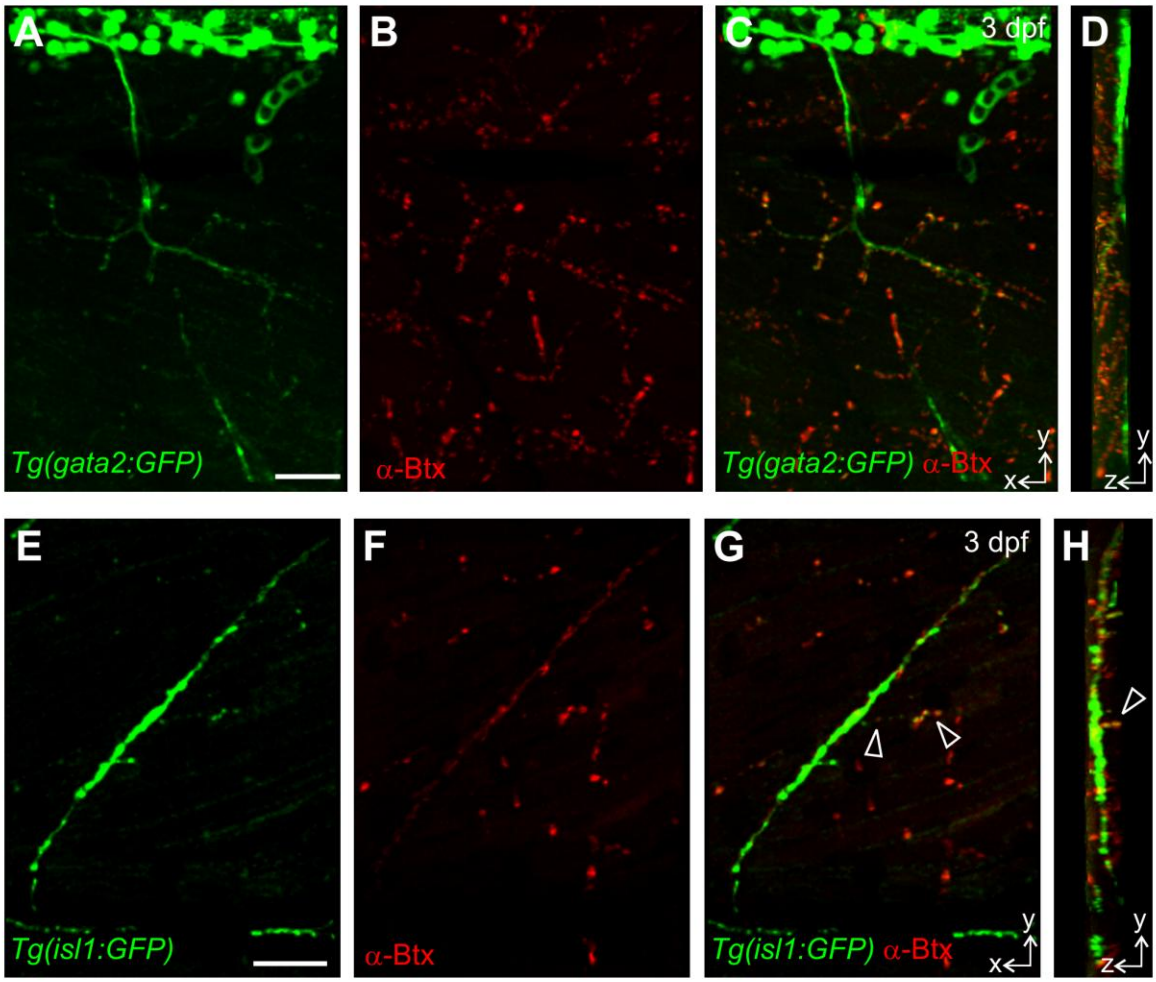

Figure 3.4. Neuromuscular junction staining in *isl1* and *gata2* zebrafish. Staining with Rh-α-btx reveals nicotinic acetylcholine receptors in 72 hpf *gata2* and *isl1* transgenic lines of zebrafish. A) Lateral view of a 72 hpf *gata2* zebrafish reveals the main ventral nerve with some secondary and tertiary branches. B) Rh-α-btx labeling is evident throughout the myotome. C) The merged image of A and B demonstrates that the ventrally projecting nerve and its branches make contacts with adjacent musculature. D) A side view (90^{o} rotation) of the image in C demonstrates the spatial extension of the axonal trajectories within the medial myotome in *gata2* zebrafish. The most superficial/lateral side was not included in this projection to emphasize Rh-α-btx staining within the medial myotome. E) Lateral view of a 72 hpf *isl1* zebrafish reveals the dorsally projecting nerve at the lateral region of myotome with some branches extending out into the periphery. F) Neuromuscular junction staining reveals muscle nicotinic acetylcholine receptors at the lateral region of the fish along the segmental boundaries similar to the GFP-positive axons. G) The merged image demonstrates some branches projecting off the main lateral trajectory (open arrowheads). H) Side view (90^{o} rotation) of the image in G (superficial side is to the left and medial is to the right) shows the distribution of muscle nicotinic acetylcholine receptors at the lateral myotome and the arrowhead points to the same branch shown in G which appears to innervate laterally located fast muscle fibers. A total of 7 fish were analyzed for this figure. Scale bars, 20 mm. A-C share the same scale bar in A and E-G share the same scale bar in E.

Figure 3.5. Axonal trajectories in *isl1* zebrafish are associated with laterally located muscle fibers. A) Photomicrograph of 72 hpf wild-type larval zebrafish labeled with the antibody F59 to detect slow muscle fibers located at the most superficial part of the fish under the skin. B) Zn5 immunoreactivity localizes on superficial muscle cells only on their surfaces apposed to other slow muscle cells. C) The merged image reveals double antibody staining with F59/zn5. D) In 72 hpf *isl1* zebrafish, GFP-positive secondary motoneuron axons extend into the dorsolateral myotome as shown by localization of the zn5 signals with GFP-positive axons. E) A magnified view of the boxed area shown in D demonstrates close association of the lateral most GFP-positive axons with zn5 signals (white arrows). F) Rh-α-btx labeling reveals muscle nicotinic acetylcholine receptors at the lateral region of the fish along zn5-positive segmental boundaries. G) Magnified lateral view of the boxed area shown in F shows the distribution of muscle nicotinic acetylcholine receptors at the lateral myotome. H) Side view (90^{o} rotation) of the area shown in G reveals the spatial distribution of the muscle nicotinic acetylcholine receptors both at the slow (filled arrowheads) and fast muscle (open arrowheads) levels. Superficial/lateral side is to the left and medial is to the right. A total of 16 fish were analyzed for this figure. Scale bars in A-C, 25 mm and D-F, 20 μm. Scale bar in G, 5 μm. A-C share the scale bar in C.

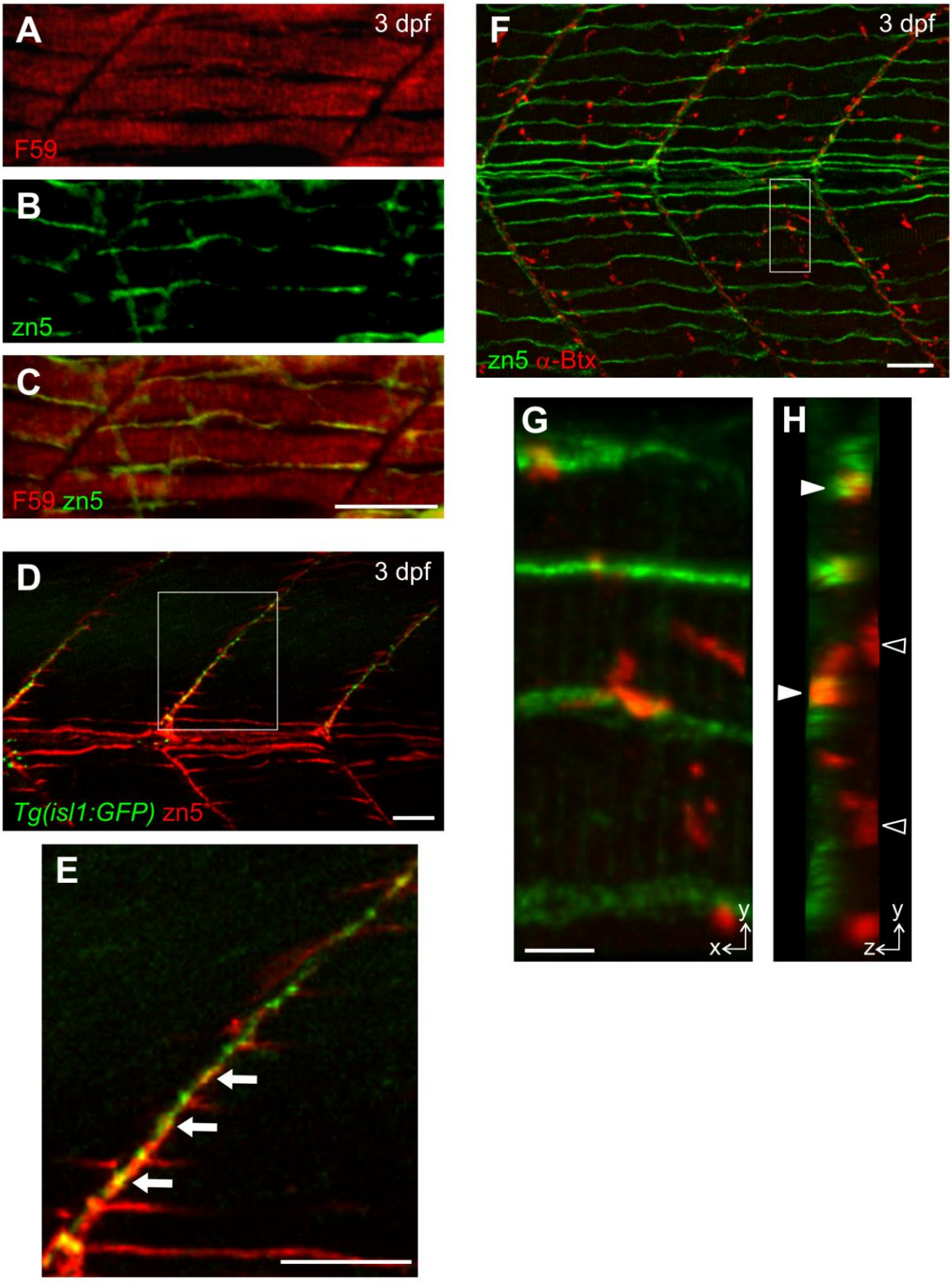
A
3 dpf
F59
B
zn5
C
F59 zn5
D
3 dpf
Tg(isl1:GFP) zn5
E
F
3 dpf
zn5 α-Btx
G
y
x
H
y
z

The zn5 antibody helped us characterize and identify a suitable transgenic reporter fish for live imaging experiments. The *isl1* line was better suited for our experimental endeavors for the following reasons. First, our previous work showed that zn5-positive dorsal axons of nicotine-exposed embryos exhibited pathfinding errors. Since the zn5 antibody labeled dorsally projecting GFP-positive axons in *isl1* fish, we hypothesized that the nicotine-induced abnormalities detected by zn5 immunohistochemistry would also be present in GFP-positive dorsal axons in *isl1* zebrafish at later stages of development. Second, the *isl1* zebrafish line expresses GFP in more secondary motoneuron axons (dorsomedial, dorsolateral) but with less axonal arborization (in fixed tissue analysis) early in development. This minimal axonal branching would facilitate the detection and monitoring of nicotine-induced changes. Third, the axonal trajectories in the *gata2* fish exhibited extensive arborization early in development, making it potentially difficult to detect and monitor any nicotine-induced changes, especially if those changes were subtle in nature.

*Isl1 Z*ebrafish: A Working Anatomical Model of Axonal Trajectories

Isl1 zebrafish were morphologically characterized in fixed tissue at various developmental stages (3, 5, 8, 10, 12, 15, 17, 24, 30 dpf). Optical sectioning was performed to obtain images starting from the most lateral surface of the fish and ending within mid spinal cord. This ensured that entire axonal trajectories would be analyzed as they exit spinal cord and extend into the periphery. Volume rendering of z-stacks helped us identify secondary motoneuron axons as they extended into the myotome at different developmental ages (Fig. 3.6 and data not shown).

Early in development (3 dpf), motoneuron axons in *isl1* zebrafish have two main distinct trajectories (Fig. 3.6A-C). First, a bundle of axons exits from each mid-segmental root and takes a dorsal path, with a characteristic “check” pattern (Fig. 3.6A, B; open arrowheads) extending

Figure 3.6. Anatomical characterization of secondary motoneuron axons in *isl1* zebrafish. The developmental progression of secondary motoneuron axons was examined and four distinct secondary motoneuron axon subpopulations were classified based on their anatomical position. A-F) Projected images from a 3 dpf (A-C) and a 24 dpf *isl1* zebrafish (D-F) are shown at 27^{o} (A and D), 54^{o} (B and E), and 90^{o} (C and F) rotations. One population of axons exits ventral spinal cord from mid-segmental roots and then takes a dorsal turn ("check") (open arrowheads) to extend and innervate musculature within dorsomedial myotome (filled arrowheads). A second population of axons ("loop"-like trajectory) projects ventrally to the midline, then it takes a lateral turn to reach the most lateral periphery and finally project dorsolaterally. A third class of axons exits from ventral spinal cord and continues to project ventrally passing the midline to innervate the ventral-most musculature of the fish (filled arrows, D,F). At later stages in development, a fourth spatially distinct axonal trajectory is present, extending ventrally at the most lateral part of the fish (open arrows, E,F). G) A projected image (49^{o} rotation) of a 24 dpf zebrafish reveals that the axons extending dorsoventrally at the most lateral region of the fish are originating from the same nerve ("loop"-like). H) Magnified view of the boxed area in G reveals the divergence of the two axonal trajectories (dashed arrows), each taking their own path innervating either dorsolateral or ventrolateral musculature. Scale bars, 20 μm. A-C share the scale bar in C and D-F share the scale bar in F.

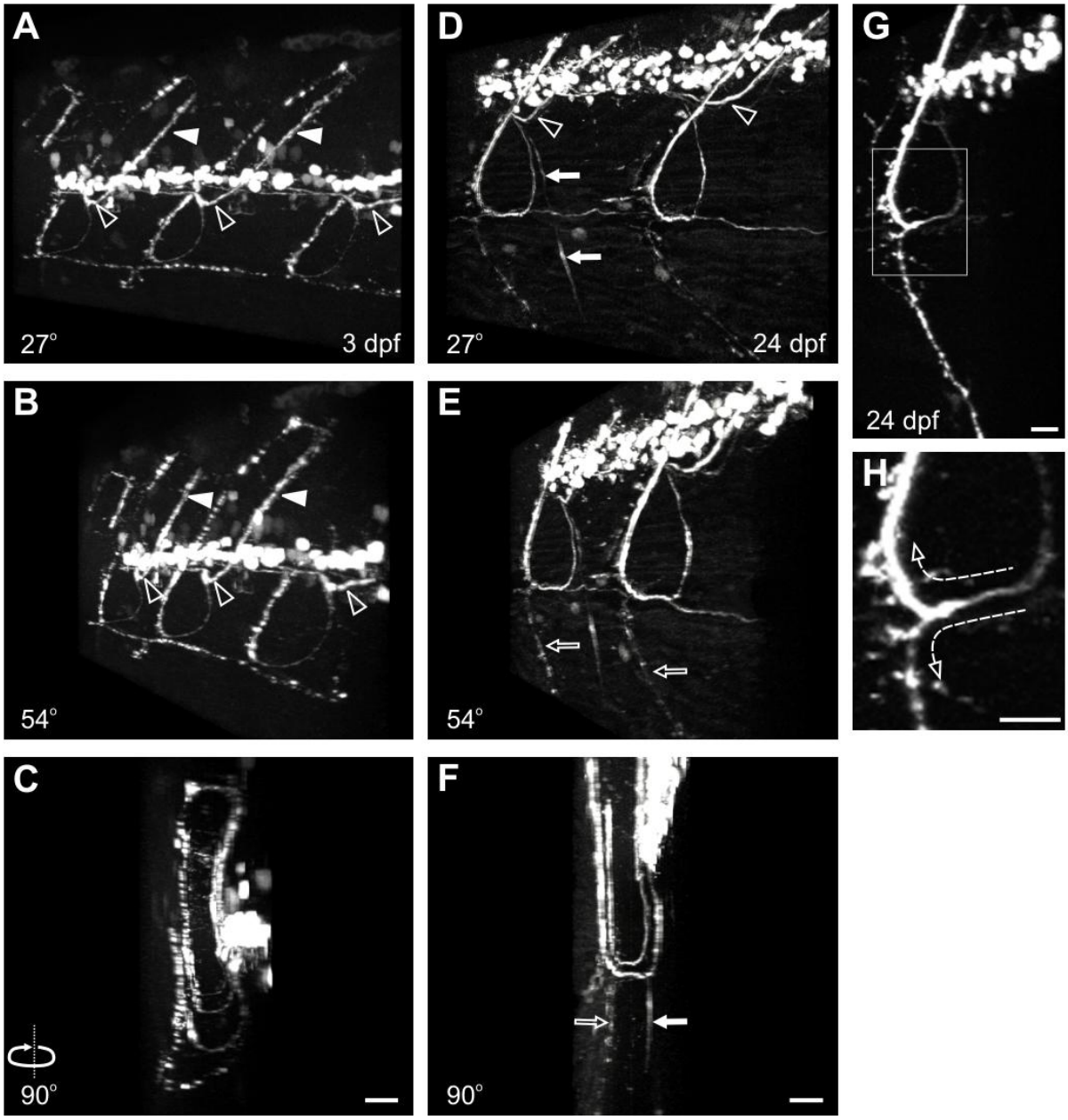
A
27°
3 dpf
D
27°
24 dpf
G
24 dpf
B
54°
E
54°
H
C
90°
F
90°

within the dorsomedial myotome (Fig. 3.6A, B; filled arrowheads). The second class of axonal trajectories exits at the mid-segmental root and initially extends ventrally and medially. Once these axons reach the horizontal myoseptum, they take a lateral path. When they reach the lateral region of the myotome, they then project dorsally. These axonal trajectories have a characteristic "loop"-like pattern (Fig. 3.6A-C). When rotated 90^{o}, their three-dimensional nature was evident (Fig. 3.6C).

By 5 dpf, a third class of GFP-positive axonal trajectories was evident. These trajectories exit at mid-segmental roots to extend within the ventromedial myotome. These trajectories were also evident at 24 dpf (Fig. 3.6D, F; filled arrows). A fourth population of GFP-positive axons was also evident by 5 dpf (data not shown) and was easily visualized in the most lateral region of the fish. There, these axons take a ventral path to target muscle fibers located within the ventrolateral myotome. These axons were clearly visualized in 24-dpf juvenile zebrafish (Fig. 3.6E, F; open arrows). Closer examination revealed that these ventrolateral trajectories originated from the same population of axons that make up the "loop"-like trajectories (Fig. 3.6G). Evidently, these axons extend laterally along the horizontal myoseptum and reach the lateral region where they diverge either dorsally or ventrally (Fig. 3.6H). This lateral region may act as an important guidance choice point where secondary motoneuron axons commit to either the dorsal or ventral path as they project towards lateral muscle fibers.

This anatomical characterization revealed four distinct subpopulations of secondary motoneuron axonal trajectories which were classified based on anatomical position. They are schematically illustrated in figure 3.7. Axons of GFP-positive motoneuron somata located in ventral spinal cord (Fig. 3.7) exit from each ventral root in each segment and extend into the myotome. At 3 dpf, the first detectable axonal trajectories were seen projecting into the dorsal myotome (Fig. 3.7, red and blue axons). At later ages of development, the main nerve projecting

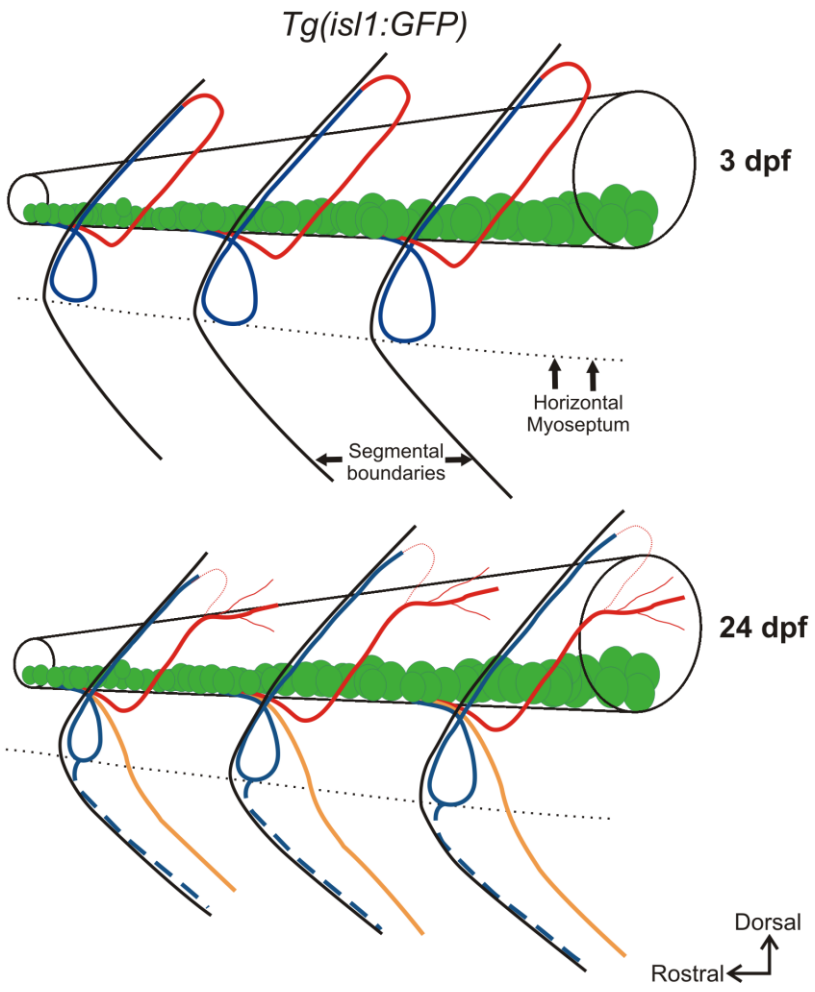

Figure 3.7. Diagrammatic illustration of the motoneuron axons in *isl1* zebrafish. Cartoons depict the patterning of the secondary motoneuron axons in the *isl1* zebrafish according to our characterization shown in figure 5. GFP-positive motoneuron somata located in ventral spinal cord are shown in green. Dotted line indicates the horizontal myoseptum. Continuous black lines (V-shaped) represent segmental boundaries. At 3 dpf, a subset of motoneuron somata extend their axons to exit from mid-segmental roots, where they travel shortly in a ventral path and then take a dorsomedial turn (red). Another population of secondary motoneurons axons (shown in blue) exits the same mid-segmental root to follow a ventral path until they reach the horizontal myoseptum. There they turn laterally and finally take a dorsolateral path. At 24 dpf, the motoneuron axons shown in red and blue at 3 dpf maintain their trajectories with the exception that the nerve bundles extending dorsomedially (red) at 24 dpf are putting out secondary and tertiary branches in the dorsomedial myotome. At later stages of development, another nerve is located ventrally and retains a ventromedial trajectory (orange). The motoneuron axons, shown in dashed blue, are diverging from the motoneuron axons shown in blue (dorsolateral) and they take a ventrolateral path. A total of 45 fish between 3-30 dpf were analyzed in generating this model. Cartoons are not drawn to scale.

dorsomedially exhibited secondary and tertiary branches (Fig. 3.7, red axons). Also, additional ventrally projecting axonal trajectories were evident medially and laterally (Fig. 3.7, dashed blue and orange axons, respectively).

Nicotine-Induced Axonal Pathfinding Errors in *isl1* Larval and Juvenile Zebrafish

With the anatomical characterization of the *Tg(isl1:GFP)* zebrafish line complete, we examined the long-term consequences of embryonic nicotine exposure on motoneuron development. At 72 hpf, secondary motoneuron axonal trajectories in control (unexposed) larval zebrafish followed their stereotypical paths, extending both medially ("check"-like) and laterally ("loop"-like) into the dorsal myotome, (Fig. 3.8A). In larval zebrafish (72 hpf) exposed to 5µM nicotine, the overall pattern of axonal trajectories was not largely affected as the "loop"-like trajectory extended and projected properly into the periphery (Fig. 3.8B). In some cases, the presence of duplicated "check"-like axonal trajectories exiting the same ventral root was evident (Fig. 3.8B; open arrowhead). Abnormal trajectories were observed in approximately 55% of the total segments analyzed (17 out of 29 segments) in 5 larval fish (Table 1). A 15µM nicotine exposure had a more robust effect on axonal trajectories (~31% of segments analyzed were normal; table 3.1) in that some dorsally projecting axons failed to extend completely into the periphery (Fig. 3.8C; open arrow). Also, accumulation of GFP at the ventral root was evident indicating axonal stalling at the exit of the root where the axons make their appropriate turns into the periphery. Similar phenotypes were evident in zebrafish embryos exposed to 30µM nicotine (Fig. 3.8D, E). In agreement with our previous work (Svoboda et al., 2002), some dorsally projecting axons ("check"-like nerve) completely failed to extend into the periphery by 72 hpf (Fig. 3.8D, filled arrow). Also, in some segments the "loop"-like nerve bundle failed to loop and project along the dorsolateral extent of the fish (Fig. 3.8E; open arrowheads). GFP accumulation at the exit of the root into the periphery was evident, similar to the 15µM nicotine exposure.

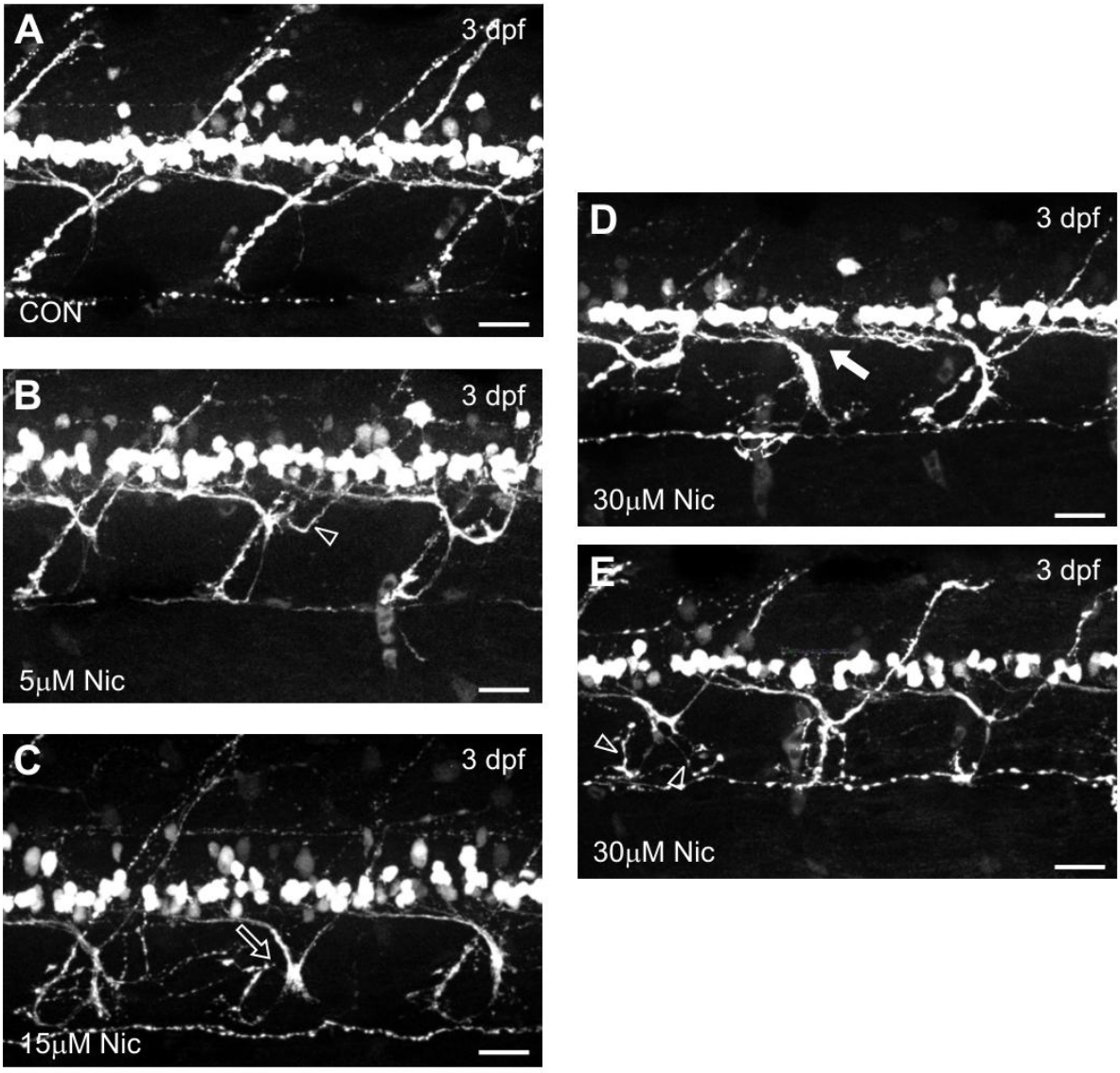

Figure 3.8. Embryonic nicotine exposure causes secondary motoneuron axonal pathfinding errors early in development. A) Projected image from a z-stack shows a stage matched control *isl1* larval zebrafish (n=15 fish) that has the characteristic pattern of the "check"-like trajectories and the ventrally projecting axons that loop laterally to take a dorsolateral path in each segment. B) *Isl1* zebrafish embryos exposed to 5 μM nicotine (n=5 fish) have abnormal trajectories exhibiting duplicated dorsal axons (open arrowhead) but no distinct abnormalities in the main axonal trajectories. C) 15 μM nicotine exposure (n=7 fish) causes pathfinding errors when axons reach the lateral periphery of the fish (open arrow). The axons do not properly loop dorsally and they exhibit extensive branching. D and E) 30 μM nicotine exposure (n=6 fish) produces various axonal pathfinding errors including failure to project dorsal axons in some segments (D, filled arrow). Pathfinding abnormalities associated with axons extending out along the dorsolateral path and abnormal branching at the ventral root (E, open arrowheads) are also evident. Scale bars, 20 μm.

Following a 30μM nicotine exposure, ~26% of the segments analyzed had normal axonal trajectories with the remaining segments exhibiting a wide range of abnormal axonal phenotypes (41 out of 51 segments analyzed were abnormal, Table 3.1).

Axonal pathfinding errors were still evident when analyzed at 24 dpf (3 weeks following nicotine exposure) (Fig. 3.9). Nicotine-exposed embryos exhibited duplications of the "check"-like nerve in between mid-segmental roots (Fig. 3.9B; open arrowheads) and also made inappropriate turns into the periphery (Fig. 3.9C; filled arrow). Abnormalities in the axonal trajectories at the most lateral periphery of the fish were very distinct (Fig. 3.9C; circle) when compared with their stage matched controls (Fig. 3.9A). It appeared that the axons comprising the "loop"-like nerve failed to take their appropriate path and appeared highly disorganized.

The abnormalities at the most lateral periphery were further examined (Fig. 3.10). At these later ages, the "loop"-like motoneuron axons extend to the lateral most side of the fish where they diverge into two distinct trajectories. One population of axons takes a dorsal path and the other population of axons extends ventrally, resembling a V-shaped pattern (Fig. 3.10A, B and D). These axons failed to project to this most lateral region of the fish in the stereotypical manner as observed in stage matched controls. Axonal disorganization in the nicotine-exposed fish was also evident as the "loop"-like axons failed to properly reach the lateral region at the choice point, (compare Fig. 3.10A, B, D arrowheads at the center point and Fig. 3.10 C, E circles) before extending to their appropriate targets (dorsal or ventral) (Fig. 3.10 C, E).

Nicotine-Induced Axonal Pathfinding Errors in *isl1* Adult Zebrafish

Examination in fixed tissue indicated that embryonic nicotine exposure caused pathfinding errors of secondary motoneurons axons. To eliminate the possibility that that some of the phenotypes observed were fixation artifacts we took advantage of fluorescent stereomicroscopy to image living juvenile zebrafish. This would allow us to identify and track

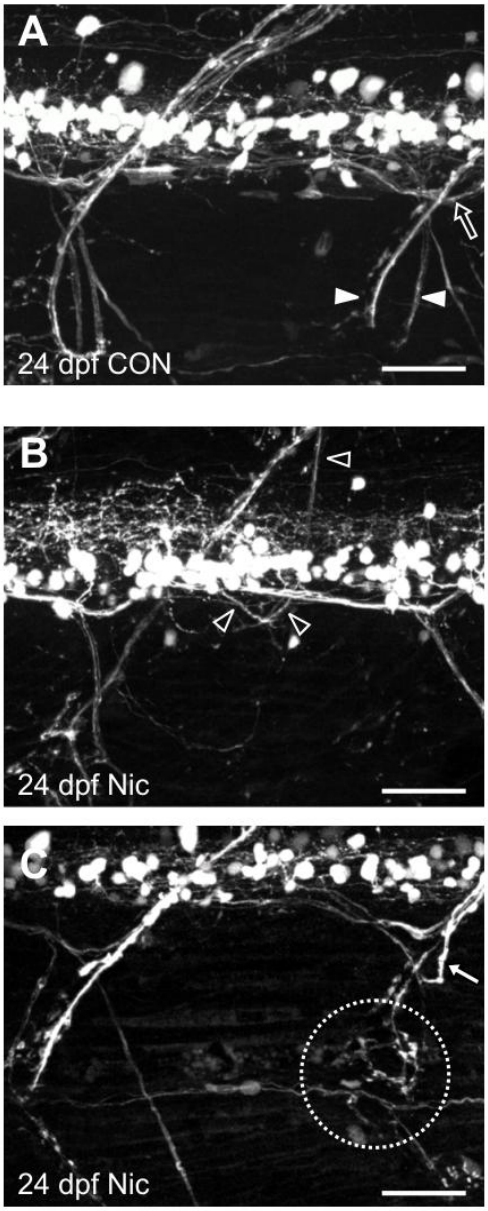

Figure 3.9. Nicotine-induced abnormalities revealed 3 weeks post exposure in fixed tissue. *Isl1* zebrafish embryos exposed to nicotine were raised to 24 dpf for image examination. A) Stage matched controls (n=4 fish), exhibit the characteristic trajectories with the "loop"-like (arrowheads) and the "check"-like patterns (open arrow). B and C) Nicotine exposure (15-30 µM; n=5 fish) results in abnormal motoneuron trajectories with extra axons exiting spinal cord in between segments (open arrowheads in B). In some cases, duplicated "check"-like trajectories were present (white arrow in C). Also, abnormalities were present at the most lateral region of the fish where the "loop"-like nerve diverges into two distinct axonal trajectories to extend either dorsolaterally or ventrolaterally (circle in C). This disorganization at the most lateral periphery was one of the most frequently encountered nicotine-induced phenotypes. Scale bars, 40 µm.

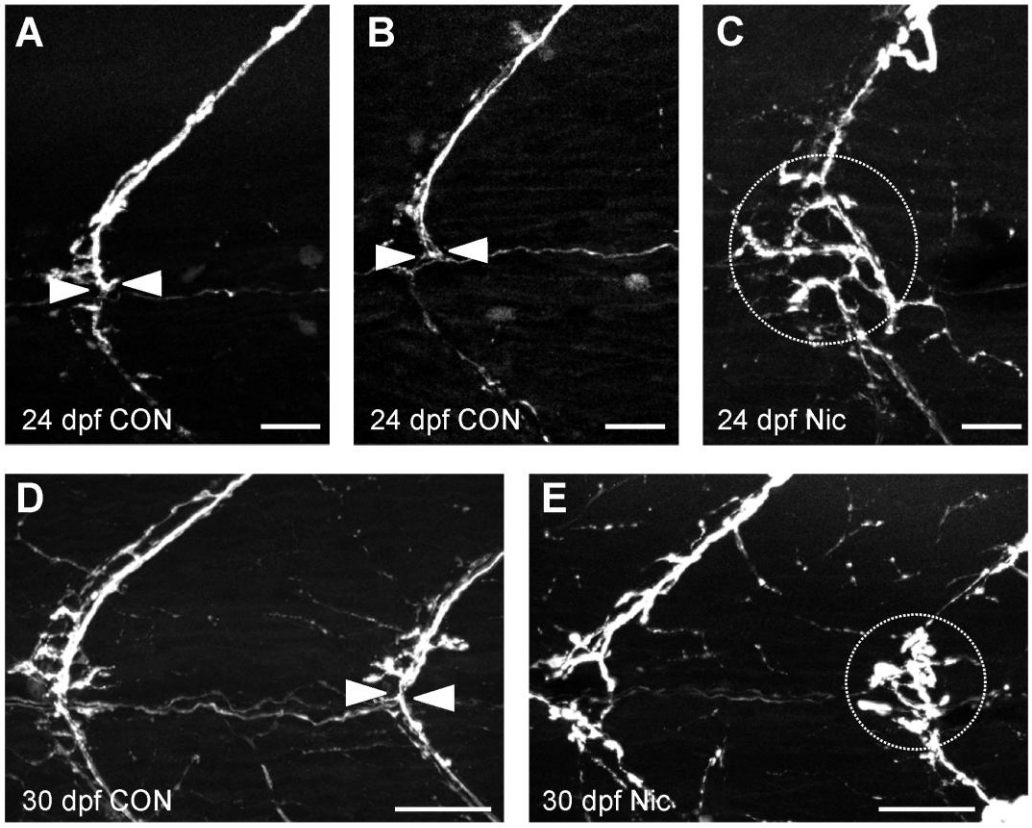

Figure 3.10. Nicotine-induced abnormalities at the lateral region of juvenile zebrafish. *Isl1* zebrafish embryos exposed to nicotine were raised to 24 dpf and 30 dpf. Images shown are from a series of stacked images focusing on the most lateral motoneuronal trajectories. A-C) Images of the most lateral motoneuron axonal trajectories in 24 dpf control (A and B, n=4 fish) and nicotine-exposed (C, n=5 fish) *isl1* zebrafish. Arrowheads in A and B indicate the distinct choice point at the midline where these axonal trajectories diverge to follow their appropriate paths, dorsally and ventrally, along the segmental boundaries. Embryonic exposure to 30 µM nicotine causes axonal abnormalities at this lateral most region of 24 dpf *isl1* zebrafish. The distinct choice point at the midline is not evident or clear in nicotine-exposed zebrafish where no center point can be distinguished. Rather a highly disorganized pattern is observed which is denoted by the white circle. D) Image of a 30 dpf unexposed control *isl1* (n=4 fish) showing the lateral axonal trajectories with a distinct choice point at the midline indicated by arrowheads. E) 30 dpf nicotine-exposed *isl1* zebrafish (n=6 fish) exhibit severe disorganization at this most lateral region of the fish as seen at 24 dpf. This distinct point is not evident in nicotine-exposed zebrafish and is denoted by the white circle to emphasize this abnormal phenotype observed. Scale bars, 40 µm.

such abnormalities in the same fish as they transitioned into adulthood and determine if these phenotypes were permanent in nature. Live imaging in *isl1* fish two weeks following nicotine exposure (17 dpf) revealed the “loop”-like bundles of axons (Fig. 3.11A; open arrowheads) and

the “check”-like trajectories (Fig. 3.11A; open arrows) in each segment of control zebrafish. *Isl1* zebrafish exposed to 15µM nicotine often exhibited duplication of the “check”-like nerve (Fig. 3.11B; arrowheads) and in some instances, the “loop”-like axonal trajectories would exit ventral spinal cord at sites other than the common mid-segmental root, often crossing into adjacent segments (Fig. 3.11C; arrowhead). At the 15µM nicotine concentration, ~47% of the segments analyzed exhibited normal axonal trajectories within the myotome (Table 3.1). Embryonic exposure to 30µM nicotine produced abnormal axonal targeting (Fig. 3.11D; filled arrow) and stalling (Fig. 3.11E; filled arrow). Abnormal axonal phenotypes were observed in 34 out of 53 segments analyzed (~61%; Table 3.1).

Table 3.1. Secondary motoneuron axon examination in *isl1* zebrafish showing number of segments possessing their typical axonal morphology.

	Fish (n)	Normal† segments	Total segments	Segments with normal† axons (%)
3 dpf				
Control	15	79	91	88.93±5.15
5µM Nicotine	5	12	29	45.83±8.94*
15µM Nicotine	7	12	36	31.11±5.44*
30µM Nicotine	7	10	51	26.51±8.20*
17 dpf				
Control	5	42	51	84.37±4.41
15µM Nicotine	5	31	70	47.37±7.54*
30µM Nicotine	6	19	53	39.32±7.62*

†Axonal trajectories were scored as normal if they exhibited the stereotypical “check” and “loop”-like trajectories extending either within the dorsomedial or dorsolateral myotome, respectively. Axonal trajectories that would exit spinal cord in between segments, exhibit duplicated “check”-like trajectories and/or stalling, fail to project to the dorsal myotome either medially and/or laterally were scored as not normal. All results are presented as mean±SEM. Asterisks (*) denote significance with a p-value < 0.05.

We validated the live imaging technique by examining motoneuron anatomy in fixed tissue (24 dpf) from the same fish one week after the initial *in vivo* live imaging (17 dpf). This comparative analysis in the same fish using two microscopy techniques indicated that the

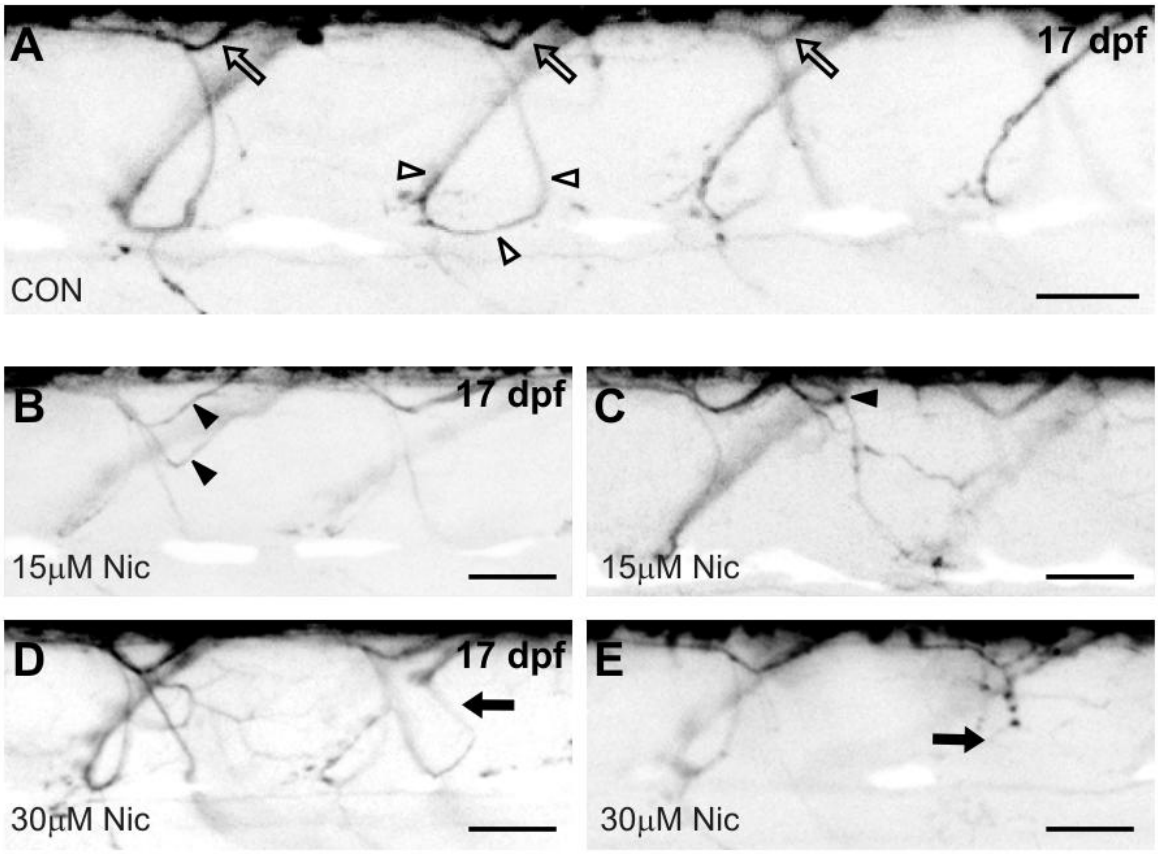

Figure 3.11. *In vivo* live imaging in *isl1* zebrafish at 17 dpf reveals nicotine-induced secondary motoneuron axon pathfinding errors. A) Representative image of an unexposed control (n=5) shows the distinct motoneuron axons that project ventrally and then turn laterally ("loop"-like) (open arrowheads) to project into the dorsal musculature. The open arrows point to the "check"-like trajectories that project dorsally and innervate medially located musculature in every segment. B and C) Photomicrographs of *isl1* zebrafish exposed to 15 μM nicotine (n=5) show a duplicated axonal trajectory (B, filled arrowheads) and extra axons that exit ventral spinal cord in between segments (C, filled arrowhead). D and E) *Isl1* zebrafish exposed to 30 μM nicotine (n=6) exhibit varying abnormal trajectory phenotypes including extra branching medially between segments (D, filled arrow) and stalling of axons extending into the periphery (E, filled arrow). Scale bars, 40 μm.

phenotypes detected in living fish at 17 dpf (Fig. 3.12A) still persisted one week later, when analyzed in fixed tissue (Fig. 3.12B). We optimized the live imaging technique so that we could re-examine the same fish over a period of weeks and determine whether the nicotine-induced abnormalities persisted into adulthood. Since we already established that nicotine-induced axonal pathfinding errors persisted from 17 dpf (2 weeks post exposure) to 24 dpf (3 weeks post

exposure) (Fig. 3.12), we hypothesized that the changes were likely permanent. Thus, we aimed to track these changes further into adulthood.

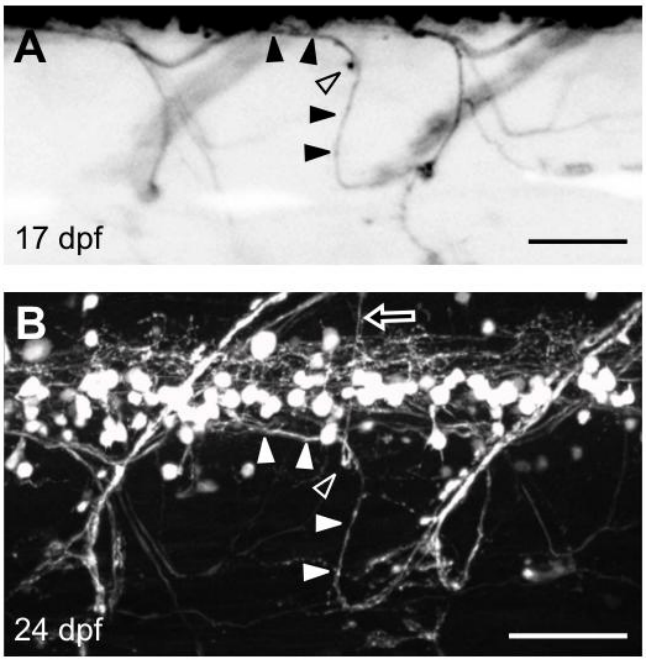

Figure 3.12. The nicotine-induced abnormalities detected with *in vivo* live imaging are confirmed in fixed tissue. A) Photomicrograph of a 17 dpf *isl1* zebrafish obtained during a live imaging session using fluorescent stereomicroscopy. A duplicated axonal trajectory appears to exit ventral spinal cord via an inter-segmental root and extends to the horizontal myoseptum where the "loop"-like axons take either a dorsolateral or ventrolateral path (filled arrowheads). The same fish was raised until 24 dpf and subsequently analyzed using fluorescent widefield microscopy to obtain z-stacks of images. B) Projected image at 24 dpf in the same segments corresponding to the ones observed during live imaging at 17 dpf (A) reveals abnormalities in axonal trajectories (filled arrowheads). A varicosity-like GFP signal was evident during live imaging in 17 dpf fish and most likely this GFP signal represents the turning point of an abnormal trajectory which appears to take a sharp dorsal turn within the myotome (open arrow). Scale bars, 40 µm.

Isl1 zebrafish and their stage matched controls were exposed to nicotine as embryos and raised until 37 dpf (~5 weeks post exposure). Starting at this age, live imaging was performed every week for a total of 7 weeks (37 dpf - 86 dpf) (Fig. 3.13 and data not shown). At these later stages of development, we focused our live imaging analysis to the most lateral region of the fish, primarily because the GFP positive axons located medially deep in the trunk musculature

became obscured as the zebrafish got thicker. Moreover, we already demonstrated nicotine-induced abnormal phenotypes in the axonal trajectories originating from the "loop"-like nerve at the lateral most part of the myotome (refer to figures 3.9 and 3.10). Abnormalities in these most lateral axonal trajectories were also detected at 37 dpf (Fig. 3.14D). Anatomical analysis revealed a great degree of disorganization at the lateral extent of this axonal trajectory when compared to the analogous trajectory in stage matched controls (Fig. 3.13A). Live imaging in unexposed zebrafish identified a varicosity-like GFP signal (GFP "center spot") (Fig. 3.13A-C; arrow) where the "loop"-like axonal trajectories extend laterally (perpendicular and out of the plane of the page) from the medial myotome. The GFP accumulation at the "center spot" was always present as the zebrafish transitioned into early adulthood. Secondary and tertiary branches extended radially from this center point to innervate adjacent muscle fibers (Fig. 3.13G). This axonal pattern was severely disrupted in nicotine-exposed zebrafish with no distinguishable GFP "center spot" (Fig. 3.13H).

Unexposed fish exhibited axonal branching extending from the GFP "center spot" out into the lateral myotome, but this was confined within the segmental boundaries. Axons in nicotine-exposed zebrafish often exhibited crossing in to adjacent segments (Fig. 3.13D-F; arrowheads) which was never observed in any of the unexposed controls.

Discussion

The presence of molecular machinery for synthesizing acetylcholine (ACh) and responding to it during critical periods of embryogenesis suggests that cholinergic stimulation via activation of nAChRs is very important early in development. Co-expression of multiple subunit transcripts with functional nAChRs was detected in premigratory neural crest cells (Howard et al., 1995) and in autonomic neurons early in development (Devay et al., 1994). There is evidence that nicotine exposure during vulnerable developmental stages can also lead to programmed cell

Figure 3.13. Tracking embryonic nicotine-induced motoneuron axonal changes in adult zebrafish using live imaging *in vivo*. *Isl1* zebrafish embryos embryonically exposed to 30 µM nicotine were raised into adulthood and monitored for anatomical changes during motoneuron development. Nicotine-exposed (n=9 fish) and stage matched controls (n=5 fish) zebrafish were imaged weekly starting at 37 dpf for 7 weeks (86 dpf). A-C) Representative photomicrographs of stage matched controls at 37, 51, and 72 dpf, respectively. D-F) Nicotine-exposed fish shown at 37, 51, and 72 dpf, respectively. G-H) Cartoon depicts normal patterns of axonal trajectories in unexposed zebrafish and two examples of nicotine-induced abnormal phenotypes. During these later developmental stages, the unexposed controls have a distinct pattern of dorsally- and ventrally projecting axons located at the most lateral part of the fish. This region (black circle in A) corresponds to the region denoted by white arrowheads shown in Fig. 9A and 9B. A varicosity-like GFP signal (GFP "center spot") (A-C, filled arrows) is evident with additional axons branching from the "center spot" out between segments to where the "loop"-like trajectories extend laterally (perpendicular and out the plane of the page) from the medial myotome. In nicotine-exposed fish, these motoneuron axons have a disorganized patterning associated with the center point at the most lateral periphery. Axons also exhibit crossing over into adjacent segments (D-F, arrowheads) when compared to their stage matched controls. Cartoon in D is not shown to scale. Scale bars, 100 µm.

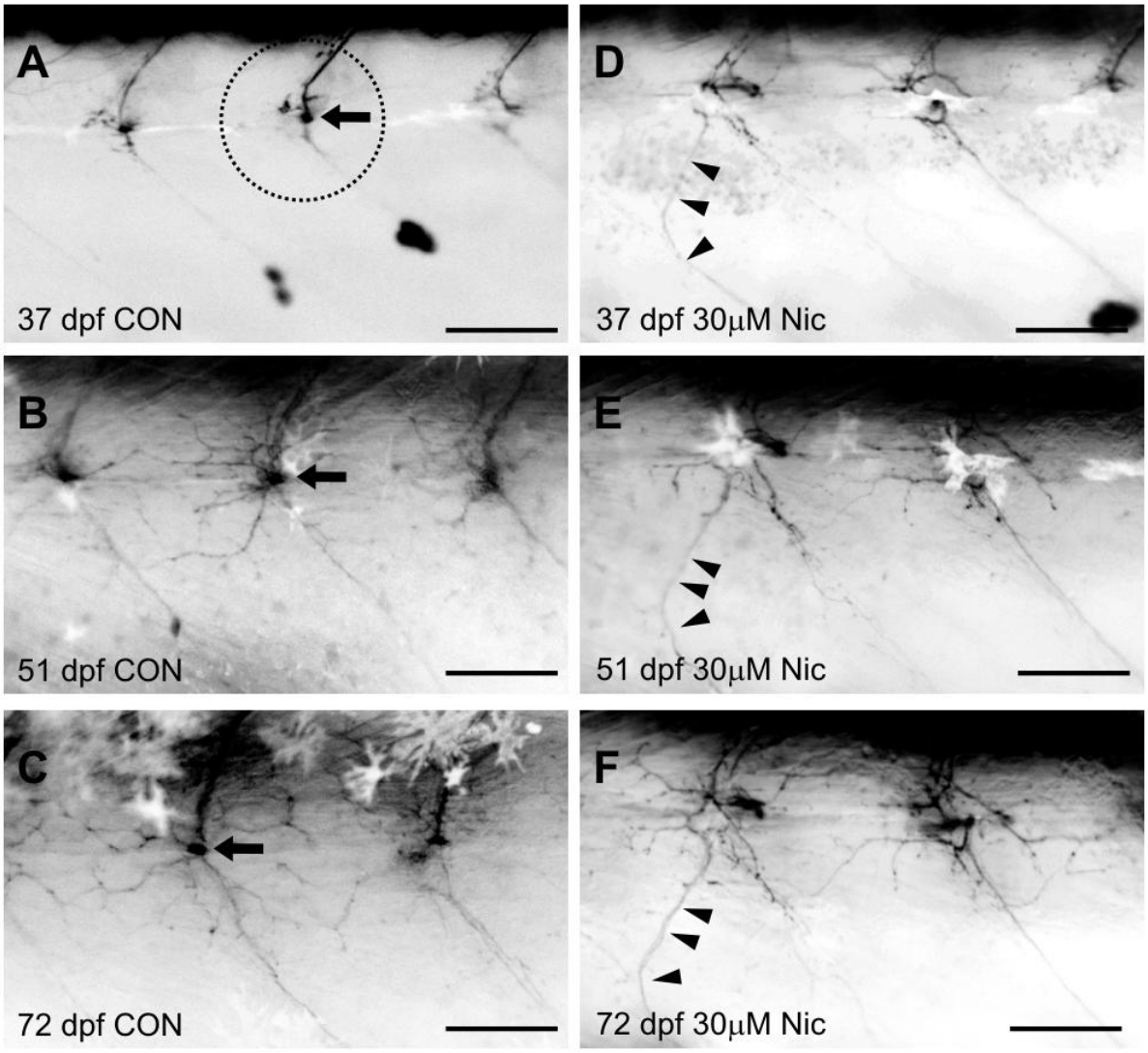
A
37 dpf CON
D
37 dpf 30μM Nic
B
51 dpf CON
E
51 dpf 30μM Nic
C
72 dpf CON
F
72 dpf 30μM Nic

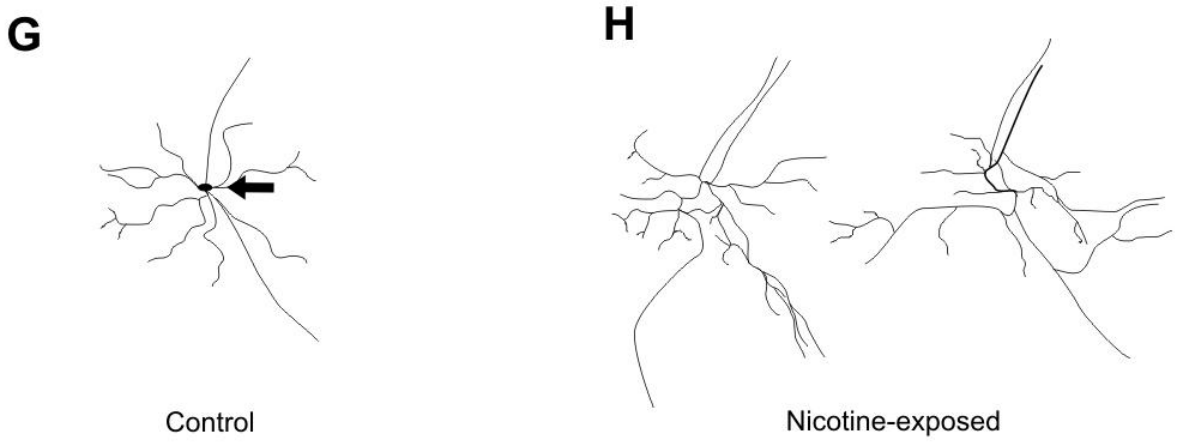
G
H
Control
Nicotine-exposed

death (apoptosis) (Berger et al., 1998; Roy et al., 1998) and inhibit DNA synthesis in the brain (Slotkin, 1998).

Only a few researchers have characterized motoneuron axonal trajectories and innervation patterns in adult zebrafish (Thorsen and Hale, 2007). In that work, the innervation pattern of pectoral fin muscles by motoneurons was analyzed. Ultimately, our research objective was to examine the impact of nicotine exposure not only at the anatomical level but also at the behavioral and physiological levels. Consequently, we have focused on characterizing the anatomy of zebrafish spinal neurons associated with locomotion.

We took advantage of fluorescent microscopy techniques combined with genetically engineered reporter zebrafish (*isl1*) to visualize nicotine-induced alterations in neuronal structures in juvenile and adult zebrafish. We first characterized spinal motoneuron anatomy in larval and juvenile *isl1* zebrafish. This was performed with the aid of widefield fluorescent microscopy in *isl1* zebrafish (3-30 dpf). We then established an anatomical model that described four spatially distinct axonal trajectories distributed within the trunk musculature of *isl1* zebrafish. These axonal trajectories take their appropriate paths in the periphery in a highly organized and stereotypical manner from early (embryonic and larval) to later (juvenile and adult) stages of development.

We found that nicotine exposure resulted in permanent changes in axonal pathfinding examined in the *isl1* GFP reporter line. These pathfinding errors were first detected in larval zebrafish at the end of the nicotine exposure window (72 hpf). These nicotine-induced abnormalities in axonal targeting persisted into juvenile and almost adult stages in zebrafish. The live imaging technique established in this study allowed us to detect nicotine-induced abnormalities and also to monitor and track these changes over time in the same fish as late as 86 days of age. Although applying these techniques in zebrafish is not necessarily unique (Distel et

al., 2006), we believe that this is the first time that a nicotine-induced alteration in neuronal anatomy caused by embryonic exposure has been monitored throughout vertebrate development and imaged in a living model system.

The mechanism underlying nicotine's ability to cause permanent changes in axonal pathfinding was not a primary focus of this study. However, there are two likely scenarios that may account for the long-term nature of the nicotine-induced changes. One possible mechanism may be related to changes in muscle development caused by nicotine exposure. In the zebrafish mutant known as *twister*, a gain-of-function mutation in the chrna1 gene encoding the α-subunit of the muscle-specific AChR, causes the receptor to have longer open times upon binding acetylcholine. This increased muscular activity causes muscle fiber degeneration and motoneuron axonal pathfinding errors (Lefebvre et al., 2004). In this context, exposure to nicotine can also directly over-activate skeletal muscle nicotinic acetylcholine receptors. Nicotine exposures (15-30μM) during the same exposure window used in this study can also lead to muscle degeneration and atrophy (Welsh et al., 2009, see also Chapter 2). The nicotine-induced motoneuron and muscle abnormalities occur in parallel with the possibility that each phenotype exacerbates the other. In *sofa potato* (*sop*) paralytic mutants lacking functional muscle AChRs, motoneuron axonal pathfinding is normal even in the absence of muscle activity (Ono et al., 2001; Welsh et al., 2009). However, when *sop* mutants are exposed to nicotine (15-30 μM) they exhibit motoneuron pathfinding errors without any concurrent muscle degeneration (Welsh et al., 2009). This suggests that muscle over-activity and degeneration is not the exclusive source contributing to the axonal pathfinding errors and that nicotine can directly activate neuronal substrates, possibly motoneurons. Consistent with this, low concentrations of nicotine (1 and 5 μM) can induce motoneuron axonal pathfinding errors with no effect on muscle morphology (see

Chapter 2). This further indicates that nicotine can act directly on the CNS to alter motoneuron axon pathfinding.

The long-term abnormalities in motoneuron axonal pathfinding detected in juvenile and adult zebrafish are likely caused by direct action of nicotine on motoneurons and concurrent over-activation of muscle AChR leading to degeneration. However, if the nicotine-induced degeneration in the muscle is never restored, then this could also contribute to new motoneuron axon pathfinding errors. This would be true of motoneuron axons that begin targeting after the nicotine has been withdrawn. If those axons are destined to target muscle that has now become atrophic due to the nicotine, they would need to be redirected to healthy muscle. We have examined muscle morphology in cross sections at 24 dpf and also later stages of development (~1.5-2 months of age) and we found that muscle fiber recovered from the degenerated phenotypes and appeared rather normal when compared to their control counterparts (data not shown). This further suggests that nicotine is most likely acting on the nervous system and once the motoneurons have mistargeted into the periphery they will establish connections at inappropriate locations.

Since nicotine can directly act on the CNS, nicotine-induced fluctuations in calcium homeostasis may also contribute to axonal pathfinding errors. It is known that nAChR agonists, nicotine and acetylcholine can regulate neurite outgrowth in ciliary ganglion neurons (Pugh and Berg, 1994). In isolated *Xenopus* spinal neurons, acetylcholine-induced turning of nerve growth cones is calcium-dependent (Zheng et al., 1994). Typically, acetylcholine-induced calcium influx is required for extension and turning of growth cones, but a sudden increase in intracellular calcium induces retraction of neurites (Zheng et al., 1994). Also, the frequency of calcium transients in growth cones is inversely proportional to their rate of migration and extension (Gomez and Spitzer, 1999). In zebrafish embryos exposed to nicotine, the presence of nicotine

may over-activate nAChRs during a critical developmental window when motoneuron growth cones are migrating and extending in the periphery. This potentially can disrupt the normal calcium homeostasis leading to abnormal targeting into the periphery due to axon stalling and/or retraction. Consistent with this, we have identified nAChR subunits on motoneuron axons in developing zebrafish (Welsh et al., 2009). This may provide the substrate at the level of the CNS, that nicotine acts upon to influence axonal pathfinding.

In this chapter, we showed that nicotine exposure during embryogenesis could lead to axonal pathfinding errors which are likely permanent in nature. Once the motoneuronal trajectories take inappropriate paths into the periphery with no direction or guidance at the time that is most critical, they are likely to be permanently altered. Even though nicotine can directly act upon motoneurons to induce these errors, it is possible that muscle degeneration resulting from being exposed to high concentrations of nicotine may also contribute to abnormal motoneuron axonal phenotypes during later stages of development.

CHAPTER 4

LOCOMOTOR BEHAVIOR IN ADULT ZEBRAFISH: ALTERATIONS CAUSED BY EMBRYONIC NICOTINE EXPOSURE

Introduction

The effects of prenatal exposure to drugs, such as nicotine have been extensively studied in clinical cohorts and animal studies. There is evidence embryonic nicotine exposure can have long-term behavioral consequences at later stages of development (Ginzel et al., 2007; Cornelius and Day, 2009; Slotkin et al, 1987). We have previously shown in zebrafish that motoneuron axons exhibited pathfinding errors as they targeted into the periphery following embryonic nicotine exposure (Chapter 2). We also showed that these effects on motoneuron anatomy persisted into adulthood (see Chapter 3). In rat pups, chronic exposure to nicotine leads to hyperactivity, which is known to be associated with increased [^{3}H]-nicotine binding sites in the prenatal brain (Tizabi et al., 1997; Slotkin et al, 1987a). In another study, the distribution density of nAChR subunit mRNA expression profiles was changed following embryonic nicotine exposure and these changes persisted into adulthood (Miao et al., 1998). Changes that occur during critical developmental windows could lead to significant disturbances in adult behaviors (Cornelius and Day, 2009). When physiological responses are combined with behavioral and anatomical assays, one can gain great insights into the nicotine-induced abnormalities. Therefore, our goal was to investigate whether long-term physiological consequences accompanied the previously documented long-term changes observed for motoneuron anatomy.

In this chapter we focused on the simple behavior of swimming in zebrafish as an assessable endpoint for studying adult function. The vertebrate spinal locomotor central pattern generator (CPG) is a network of interneurons and motoneurons capable of generating rhythmic motor outputs typified as walking and swimming (for review see Goulding, 2009). Excitation from pre-motor spinal neurons (interneurons) drives motoneurons to produce muscle contractions, which then elicits swimming. Electromyographic (EMG) recordings from freely swimming animals reflect physiological responses that can be either related to muscle,

motoneuron or interneuron activity. Using this approach, we examined long-term physiological consequences in adult zebrafish following embryonic nicotine exposure. Based on the fact that the motoneuron anatomical abnormalities caused by embryonic nicotine exposure persisted into adult stages of development (Menelaou and Svoboda, 2009), we hypothesized that spinal neuron abnormalities could simultaneously affect the physiology and behavior in adult animals.

Materials and Methods

Zebrafish Maintenance

Zebrafish embryos were collected and adult fish were maintained following protocols described under Chapters 2 and 3.

Embryonic Nicotine Exposures

Wildtype zebrafish embryos were exposed to varying nicotine (Sigma, catalog # N3876-5ml) concentrations (5, 15, and 30 μM) while in their chorions between 12-30 hpf and 22-72 hpf as previously described (Chapter 2 and 3). For each exposure paradigm, a different set of unexposed control fish was used from the same clutch of fish. At 72 hpf, zebrafish were sampled from each group and were fixed in 4% paraformaldehyde for whole immunohistochemistry. The remaining zebrafish were raised into adulthood as described in Chapter 3.

Immunohistochemistry, Image Acquisition and Motoneuron Analysis

Whole mount immunohistochemistry using the zn5 antibody (Fashena and Westerfield, 1999) was performed following protocols described under Chapter 2. A Zeiss Axiovert 200M inverted microscope with epifluorescence (Carl Zeiss) was used to capture single focal plane images using a 20x dry objective. Motoneuron axon morphology was assessed and scored as previously described (Chapter 2). Photomicrographs of lateral views of larval zebrafish are shown as rostral to the left and dorsal to the top.

Electrodes and Dissection

Bipolar wire electrodes were made using nichrome wire, 0.001" bare and 0.0015" coated (AM Systems, Sequim, WA). Two twisted wire strands were then twisted together to give a pair of recording electrodes. Then, 1-1.5 millimeters (mm) of insulation were stripped from one end and soldered into fine gold pins. The electrode pair was cut to the desired length (~60 cm) and the free tines on the other end of the electrode were bent back to form two pairs of hooks as illustrated in the inset in Figure 4.1. The hook on each strand of the electrode served as a physical anchor into the muscle at the desired insertion depth (1-2 mm). Great care was taken to avoid nicking the strands (Loeb and Gans, 1986). Electrode pairs were used more than once (but no more than three times) given that their integrity was not compromised during previous recording sessions. Adult zebrafish at ~8 months of age were anesthetized in 0.02% MS222 (Sigma, St. Louis, MO, USA) and placed on a moist tissue under a dissecting microscope. A patch of scales was removed with fine forceps and a sharpened needle was used to puncture the exposed skin. Bipolar hook electrodes were advanced through the hole in the punctured skin into the dorsal muscle on opposite sides of the same segment (Fig. 4.1). Electrode implantation was attempted along the caudal half of the fish between segments 16 and 20 which underlie the dorsal fin as indicated in figure 4.1.

Electromyographic Recordings from Freely Swimming Zebrafish

Following electrode implantation, fish were carefully transferred to a ten-gallon glass aquarium filled with system water and were allowed to recover from anesthesia. The electrodes were plugged into connectors and signals were filtered (300-Hz low cutoff and 5-kHz high cutoff) and amplified (gain 1,000) using an AM Systems 1700 amplifier. Datapac 2K2® software and hardware (Run Technologies) were used for digitization and analysis. A Quest Scientific HumBug was used to remove electrical interferences from signals when needed. A

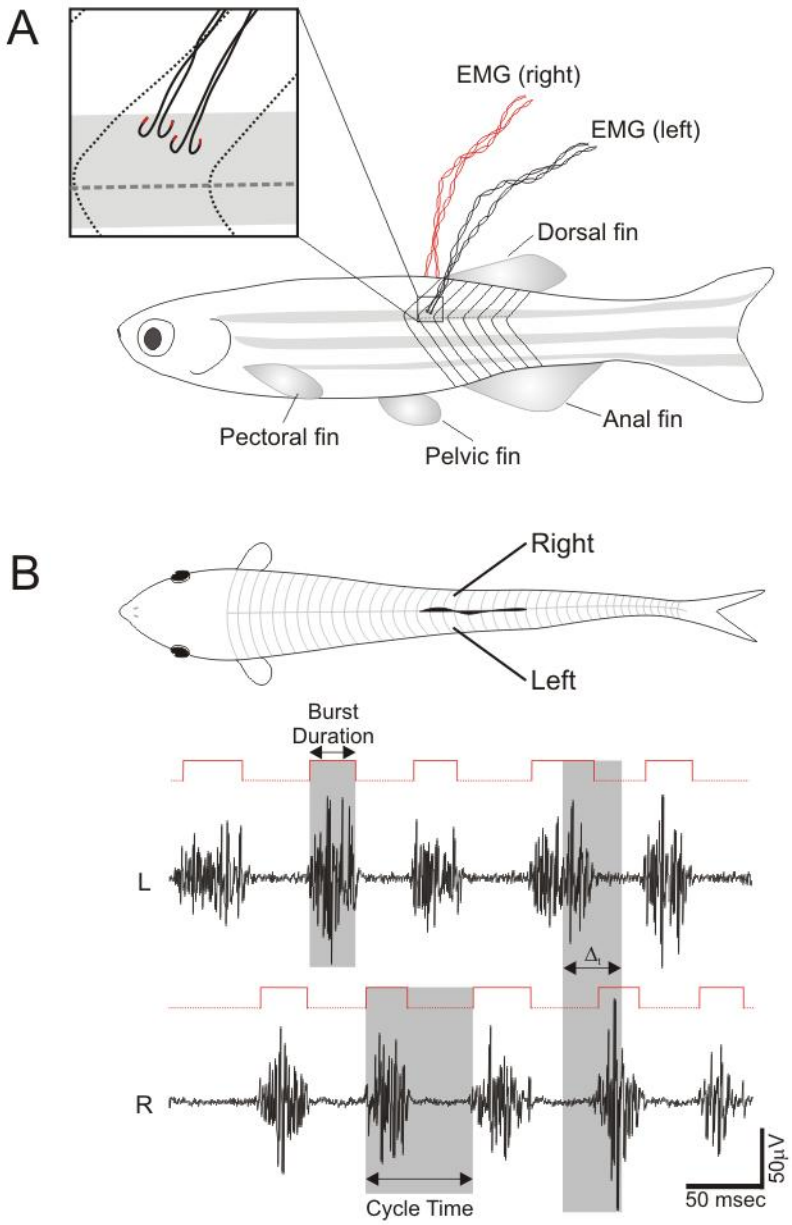

Figure 4.1. Electrode implantation and electromyographic recordings in freely swimming adult zebrafish. A) Adult zebrafish were implanted with a pair of bipolar hook electrodes (inset) in the axial muscle underlying the dorsal fin (body segments 16-20). Each pair of electrodes was implanted on the left (L) and right (R) sides in the same body segment underlying the dorsal fin. Electrodes were stripped off their insulation (bear wire is indicated by red color) to record electromyographic (EMG) activity. B) EMG recording from one swimming bout produced rhythmic motor activity that alternated from left to right sides. Location of the recording sites is shown to the top. EMG recording is shown in black and their corresponding computer-identified burst events are indicated on top of each trace by a histogram bin (red line). Grey shaded boxes indicate the burst duration, cycle time (T) and the time difference between contralateral burst midpoints (Δ_t).

video camera (Canon GL-1) was mounted on the top of the swimming tank to simultaneously capture the swimming behavior of the fish while recording EMG activity. Spontaneous bouts of swimming were recorded and in some instance bouts were elicited by gently tapping the fish tank. Muscle activity was recorded when the implanted muscles were used by the fish to produce movement, make turns and actively swim. Swimming bouts consisted of several bursts of rhythmic alternating EMG activity and each burst was composed of a number of EMG spikes. The length of the recording sessions lasted between 3 and 28 minutes. At the end of a recording session, electrode wires were carefully removed, zebrafish were returned to their individual tanks and housed to our animal facility. The acquired data were processed by a computer with Datapac 2K2® software for storage and analysis.

Electrophysiology Data Analysis

EMG data was analyzed off-line using Datapac 2K2 software. Linear smoothing was applied with a 0.4 ms time constant to the EMG to filter noise before measurements were taken. Using the analysis program, when the voltage of a spike crossed a threshold value, that spike was counted as an event. When consecutive spikes crossed threshold for a certain period, but did not fall below the threshold for more than a given interval (~8ms for fast frequency and ~15ms for slow frequency), a burst event was created and was indicated by a histogram bin. The time between the onset and offset of the bin indicated the duration of a burst. To avoid including spikes in a burst from a subsequent burst, an interrupt filter was used to ensure that all spikes were detected within a given a burst. The threshold criterion was different for each recording channel and was carefully determined based on the quality of the recording. Single spike events were not considered as bursts. For each fish in which EMG activity was recorded, the analysis program was used to characterize the identified bursts with respect to their time between the

bursts (cycle time, T), duration (BD), and their temporal relationship between bursts from opposite sides of the body (contralateral phase, φ_C).

In order to consistently select bouts of activity that closely resembled swimming, a criterion of EMG activity was established where activity needed to be sustained for 5 consecutive bursts on one side of the body which corresponds to at least 4 cycles of alternation at a relatively constant swimming speed. Several bouts of activity were analyzed from each fish with the activity typically covering a wide range of swimming frequencies.

The cycle time (T) was measured as either the interval between the start times of two consecutive bursts (used for the relationship of burst duration and cycle time) or the difference between the midpoints of two successive bursts (used for the relationship of phase and cycle time). The phase relationship between paired recordings obtained from opposite sides of the same segment (contralateral phase, φ_C) was defined as the time difference (Δt) between left and right burst midpoints divided by the cycle time (T) ($\varphi_C = \Delta t/T$) (Fig. 4.1). During swimming, the phase relationship between contralateral paired recordings from the same body segment was ~ 0.5. In some figures, the phase was plotted against the relative burst position (BP) within a swimming bout on a burst-to-burst basis. Specifically, the midpoint of each burst was divided by the duration of the bout of activity. The midpoint of the first burst of the leading side marked the beginning of the bout and the midpoint of the last burst from the same side marked the end of the bout. The BP was expressed as a percentage of the duration of each bout. Instantaneous burst frequency was measured on a burst-by-burst basis as the reciprocal of one cycle time (BF=1/T Hz). Locomotor frequency was defined as the mean burst frequency for each bout.

Each bout of activity consisted of several bursts and each burst is composed of a number of EMG spikes. Therefore, bouts of swimming activity were selected from control and nicotine-exposed (22-72 hpf) animals at varying swimming frequencies and the size distribution of EMG

spikes was examined as previously described (Liu and Westerfield, 1988). EMG spike amplitudes were exported from Datapac into excel for analysis. The number of EMG spikes at each amplitude was plotted and the amplitude distribution was fit to two regression lines consistent with two distinct populations of EMG spikes. Primary (PMN) and secondary motoneurons (SMN) can be distinguished by their spike amplitudes. PMNs produce larger amplitude EMG spikes whereas SMNs produce small amplitude spikes. Individual data points were designated to either of the two lines until the correlation coefficients were maximized. The intersection between the two regression lines was determined and assigned as the threshold amplitude.

Small EMG spikes that fell below the threshold value best described spikes of SMNs whereas larger EMG spikes that were above the threshold were most likely produced by PMNs. This allowed us to account for spike amplitude variation among the recording sessions. Therefore, the amplitude distribution was plotted for each animal and a different threshold value was determined before any comparisons could be made between treatments. To eliminate bias from sampling bouts of activities that had more bursts of activity, we expressed the number of EMG spikes that fell below threshold amplitudes as a percentage of total spikes at different swimming frequencies and were binned every 4 Hz.

Graphs and Statistics

Datapac was used to measure burst duration and cycle times and data were individually checked for accuracy before exporting data from Datapac. Files were then imported into Microsoft excel for graphing. Cartoon figures were created using Corel Draw and the figures were organized using Microsoft PowerPoint. For motoneuron analysis at 72 hpf and spike sorting analysis, all values are reported as means ± standard error of the means (SEM). For differences between three variables, parametric analysis of variance (ANOVA coupled to a Holm-Sidak

post-test) was applied on normally distributed values. Otherwise, Kruskal-Wallis analysis of variance was applied (Dunn's post-test) (SigmaStat3.5, Systat Software Inc., San Jose, USA). For contralateral phase and swimming frequency at different exposure windows and nicotine concentrations values are reported as means ± standard deviation (SD). One way ANOVA (Dunnett's post-test) for multiple comparisons against the controls was performed in SPSS (SPSS Inc., Chicago, IL, USA). Significance was assigned if the p value was <0.05.

The relationship between burst duration and cycle time at different nicotine concentrations and exposure windows, was examined using analysis of covariance (ANCOVA). Both linear plots and power models were considered. Both models had similar fits and it appeared that the assumptions, particularly the assumption for normality, appeared to be better met by the linear model. Linear regression plots are shown is some cases from individual animals. For all linear regression analysis, the regression slope and line intercepts were compared with ANCOVA using SAS 9.1 software (SAS Institute Inc., Cary, NC, USA). For the two different exposure windows, treatment comparisons were performed against the controls from the same experiment. Significance was assigned if the p value was <0.05.

Results

Transient embryonic nicotine exposure causes both short-term (see Chapter 2) and long-term (see Chapter 3) changes in secondary motoneuron axonal pathfinding. Before zebrafish embryos were raised to adulthood for electrophysiological examination, the behavior and anatomy in a subset of the exposed embryos was examined. First, at 48 hpf paralysis was observed in zebrafish embryos exposed to 15 and 30μM at 22 hpf. Second, at 72 hpf whole mount immunohistochemistry was performed to reveal motoneuron axon anatomy using the zn5 antibody. Our results showed that zebrafish exhibited motoneuron axon pathfinding errors when

Figure 4.2. Embryonic nicotine exposures and motoneuron axon morphology at 72 hpf. (A-C) Zebrafish embryos were exposed to 5, 15 and 30μM nicotine from 12-30 hpf and their secondary motoneuron axons were analyzed at 72 hpf with zn5 immunoreactivity. (D-F) Zebrafish embryos were exposed to 5, 15 and 30μM nicotine from 22-72 hpf and their secondary motoneuron axons were analyzed at 72 hpf with zn5 immunoreactivity. Photomicrographs of control zebrafish (A and D) show the normal trajectories of dorsal and ventral SMN axons. B) Representative photomicrograph of a zebrafish larva exposed to 15μM nicotine from 12-30 hpf showing axonal trajectory errors in the dorsal myotome. C) At 72 hpf, the percent of hemisegments that possess normal SMN axons was quantified for controls (69.0±4.5%, 177 segments in 8 fish) and zebrafish exposed to 5μM (62.7±4.5%, 170 segments in 7 fish), 15μM (54.9±3.8%, 183 segments in 7 fish), and 30μM (45.1±5.0%, 150 segments in 6 fish) nicotine. E) A representative photomicrograph from a zebrafish larva exposed to 30μM nicotine from 22-72 hpf showing SMN axons that failed to project to the dorsal myotome as well as a duplicated ventral-projecting axon. F) At 72 hpf, the percent of hemisegments that possess normal SMN axons was quantified for controls (73.9±6.6%, 70 segments in 3 fish) and zebrafish exposed to 5μM (47.4±7.5%, 74 segments in 3 fish), 15μM (29.8±4.8%, 68 segments in 3 fish), and 30μM (18.5±10.7%, 85 segments in 4 fish) nicotine. Asterisks denote significance with a p value <0.05. Scale bars, 50 μm.

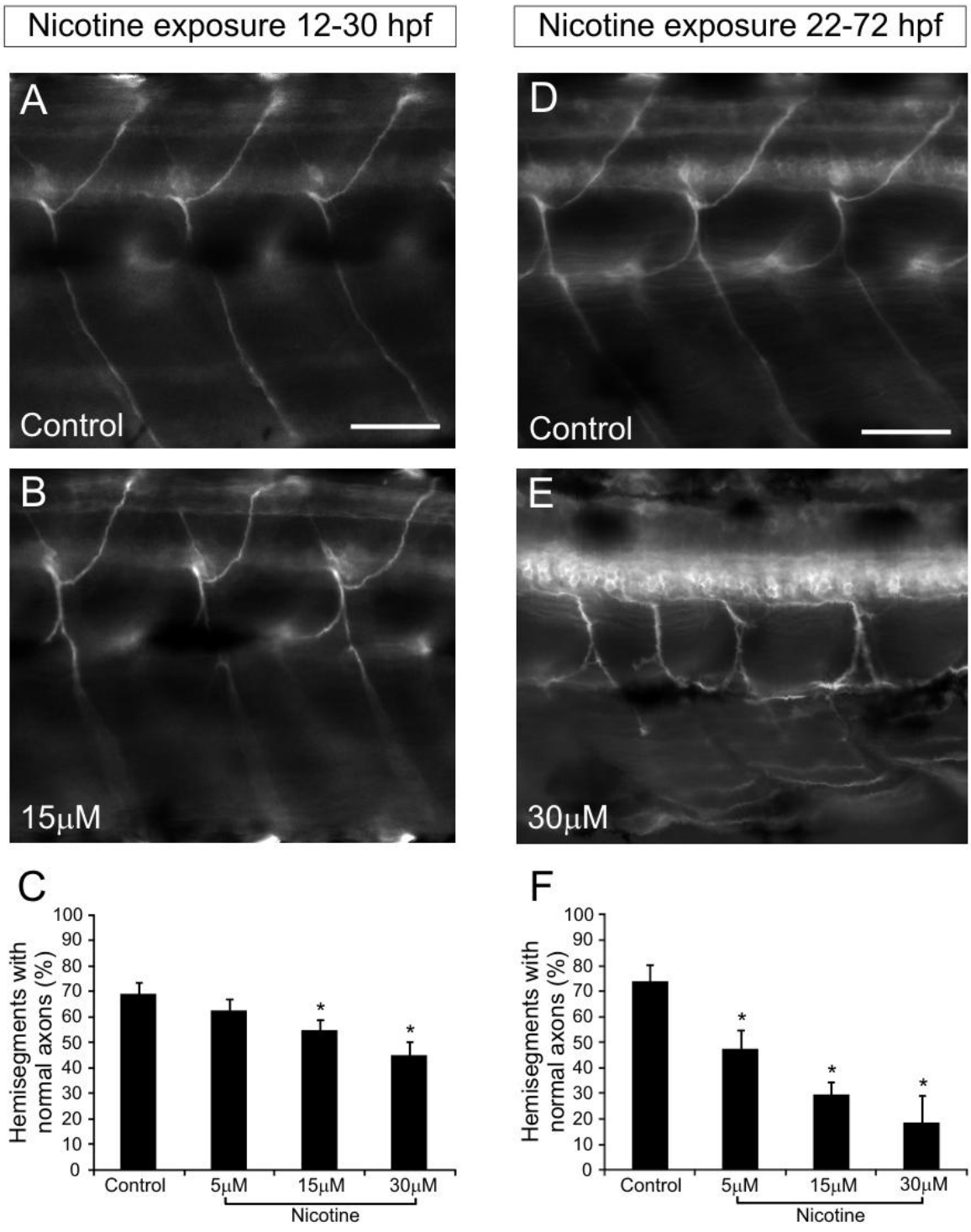
Nicotine exposure 12-30 hpf
Nicotine exposure 22-72 hpf
A
Control
B
15μM
C
Hemisegments with normal axons (%)
100
90
80
70
60
50
40
30
20
10
0
Control
5μM
15μM
30μM
Nicotine
*
*
D
Control
E
30μM
F
Hemisegments with normal axons (%)
100
90
80
70
60
50
40
30
20
10
0
Control
5μM
15μM
30μM
Nicotine
*
*
*

exposed between 12-30 (Fig. 4.2A-C) and 22-72 hpf (Fig. 4.2D-F). These findings were consistent with our previously described results under Chapter 2. Based on this, the remaining nicotine-exposed embryos from a cohort were raised into adulthood to examine their locomotor behavior.

Our findings show that embryonic nicotine exposure did not affect the overall motoneuron activity at different swimming frequencies but caused long-term alterations in several features of the locomotor output of adult zebrafish. Basic features of the locomotor output include: swimming frequency, relationship between burst duration and cycle time and contralateral phase. Zebrafish exposed to nicotine as embryos exhibited alterations in their locomotor output and are best described as follows: 1) slower swimming frequencies when exposed between 22-72 hpf, 2) disrupted relationship between burst duration and cycle time, and 3) altered alternating activity (contralateral phase shift) when exposed to 30μM between 12-30 hpf. In this section, we first describe the basic features of the locomotor pattern to ensure that they resembled the features typical of swimming vertebrates. Then we present in more detail the alterations of the locomotor output in zebrafish exposed to nicotine as embryos.

Locomotor Activity in Freely Swimming Adult Zebrafish

Swimming Frequency

Freely swimming fish generate a propagating wave of activity from head to tail which results in lateral undulatory movements of their body from side-to-side. As the fish body bends, it pushes against the water to generate forward thrust (Altringham and Ellerby, 1999). Here, we focus on the basic features of motor output typical of swimming. Electromyograms (EMGs) were obtained from the muscle of freely swimming, adult zebrafish (~8 months of age, see Methods and Figure 4.1). Zebrafish swam unrestrained in the recording tank for several minutes producing several bouts (episodes) of locomotor activity at varying swimming speeds. Each bout

of activity consisted of several bursts. The total duration of the recording varied among preparations (mean duration of a recording session = 11.7±5.9 minutes from 38 recording sessions) and in many cases, a recording session lasted more than 15 minutes. Each recording session also included silent periods of inactivity when the fish were not swimming. Throughout the recording sessions, the fish swam over a wide range of swimming frequencies (4-38 Hz). In some instances, zebrafish swam at frequencies higher than 40 Hz, but this activity was never sustained; only lasting a few milliseconds. This high frequency activity never lasted longer than the threshold of 5 consecutive bursts of activity which we set as the cutoff for calling a bout of activity swimming, thus we did not classify this activity as swim episodes. On the other hand, zebrafish were able to sustain swimming at lower frequencies and in some cases, these swimming bouts lasted over several seconds (6-8 sec was the longest period analyzed).

Relationship of Burst Duration and Cycle Time

One of the characteristic features of the motor pattern observed in freely swimming fish is the relationship between the duration of a burst and the time between successive bursts (cycle time). When fish swim faster, the cycle time decreases and this is accompanied by a decrease in the burst duration (Fetcho and Svoboda, 1993). We analyzed this relationship in 12 non-exposed fish, and in all cases, the relationship between burst duration and cycle time was strongly correlated. Burst duration increased with increasing cycle time. Examples of this relationship from 5 individual fish are shown in figure 4.3. When we pooled the data from 142 bouts of activity from 12 different fish, the overall relationship between burst duration and cycle time was similar to that observed for individual fish (Fig. 4.3F). This demonstrated that burst duration changed in proportion to cycle time. Across different swimming frequencies, the overall burst duration occupied 36.7±8.1% (1542 bursts in 142 bouts from 12 fish) of the cycle time.

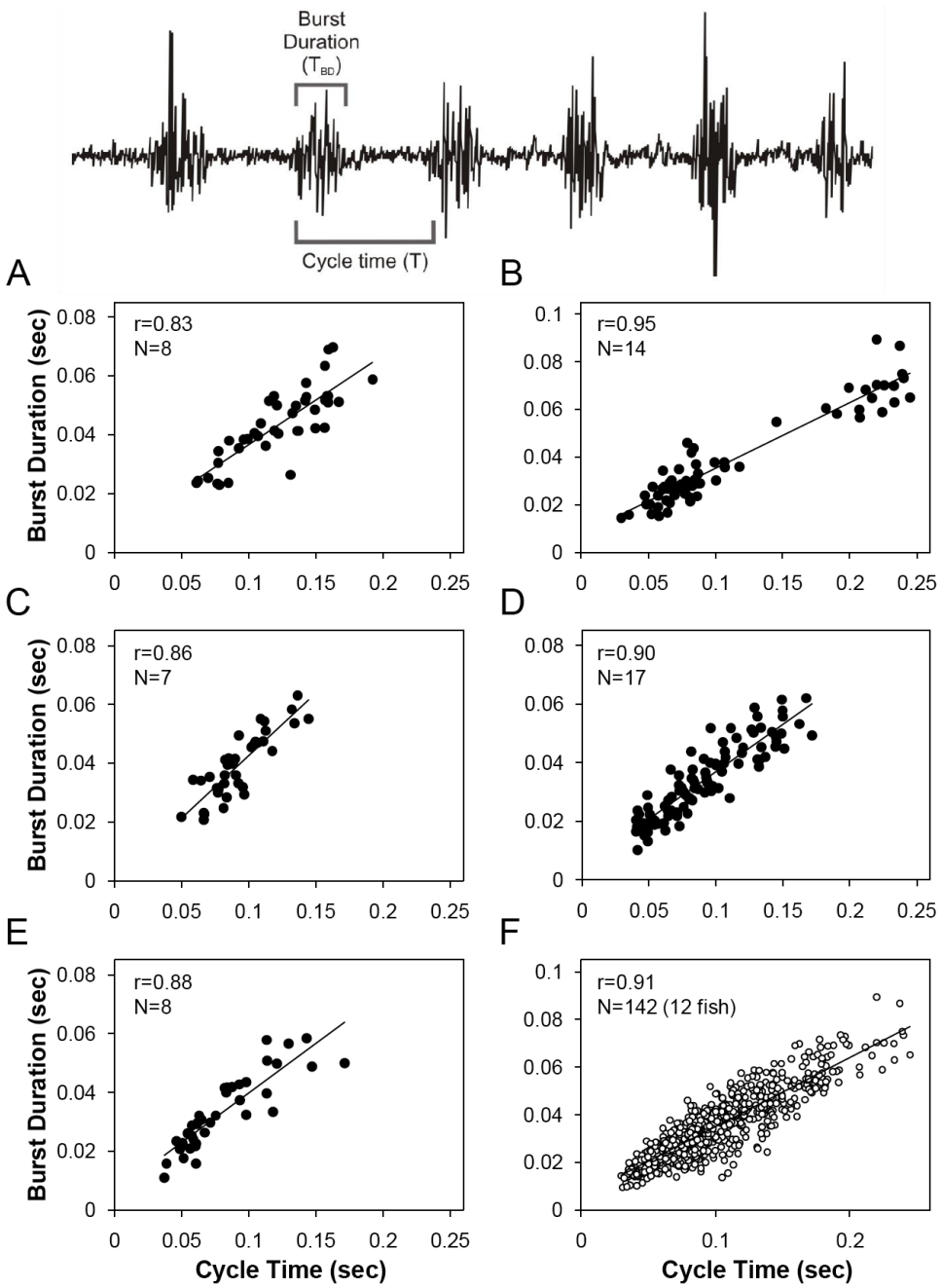

Figure 4.3. Relationship between burst duration and cycle time. Burst duration and cycle time were measured as shown in the top EMG trace from freely swimming adult zebrafish. Plots of burst duration vs, cycle time from 5 individual fish (A-E). Each plot shows several bouts of activity producing a range of 4-11 cycles of activity for each fish. Linear regressions are shown in each plot and burst duration exhibits a strong linear correlation with cycle time as indicated by the correlation coefficient (*r*) in the inset. The number of swimming bouts (N) analyzed for each plot is indicated in the insets. F) Plot of burst duration vs. cycle time contains data from 142 bouts of activity from 12 fish. The pooled data show a strong linear correlation between burst duration and cycle time similar to the individual fish.

Contralateral Phase

Another distinct feature of the swimming behavior is the alternating bursting pattern between both sides of the body. EMG activity was recorded from muscles on opposite sides from the same body segment in order to examine the alternating pattern of activity. The contralateral phase difference was relatively constant from burst to burst when examined at different swimming speeds (fast swimming corresponds with shorter cycle periods). Examples of the relationship between contralateral phase and cycle time are shown in figure 4.4 from 5 individual fish. Data pooled from different fish demonstrated a similar relationship (Fig. 4.4F) and had a mean value of 0.50±0.05 (739 bursts in 142 bouts from 12 fish), indicating that the contralateral phase difference is ~50% of the cycle time.

Zebrafish Locomotor Behavior Following Embryonic Nicotine Exposure

Swimming Frequency

Once the basic features of swimming activity were analyzed and characterized for our preparation, we were able to examine the pattern of motor activity in freely swimming zebrafish that were transiently exposed to nicotine as embryos. The mean swimming frequency of control zebrafish was 12.8±5.1Hz (142 bouts, 12 fish). We categorized the bouts of activity into 3 groups based on the range of swimming frequencies at which those bouts occurred (<9 Hz, 9-16 Hz, and >17 Hz). The number of bouts that occurred within each frequency category was expressed as a percentage of the total bouts analyzed. In control zebrafish, ~58% of the swimming bouts occurred between 9 and 16 Hz, whereas only 26% and 16% occurred at frequencies below 9 Hz and above 17 Hz, respectively (Fig. 4.5A, 61 bouts from 6 fish, mean frequency=12.4±4.5Hz). Figure 4.5B shows bouts of alternating swimming activity from control zebrafish at various swimming frequencies.

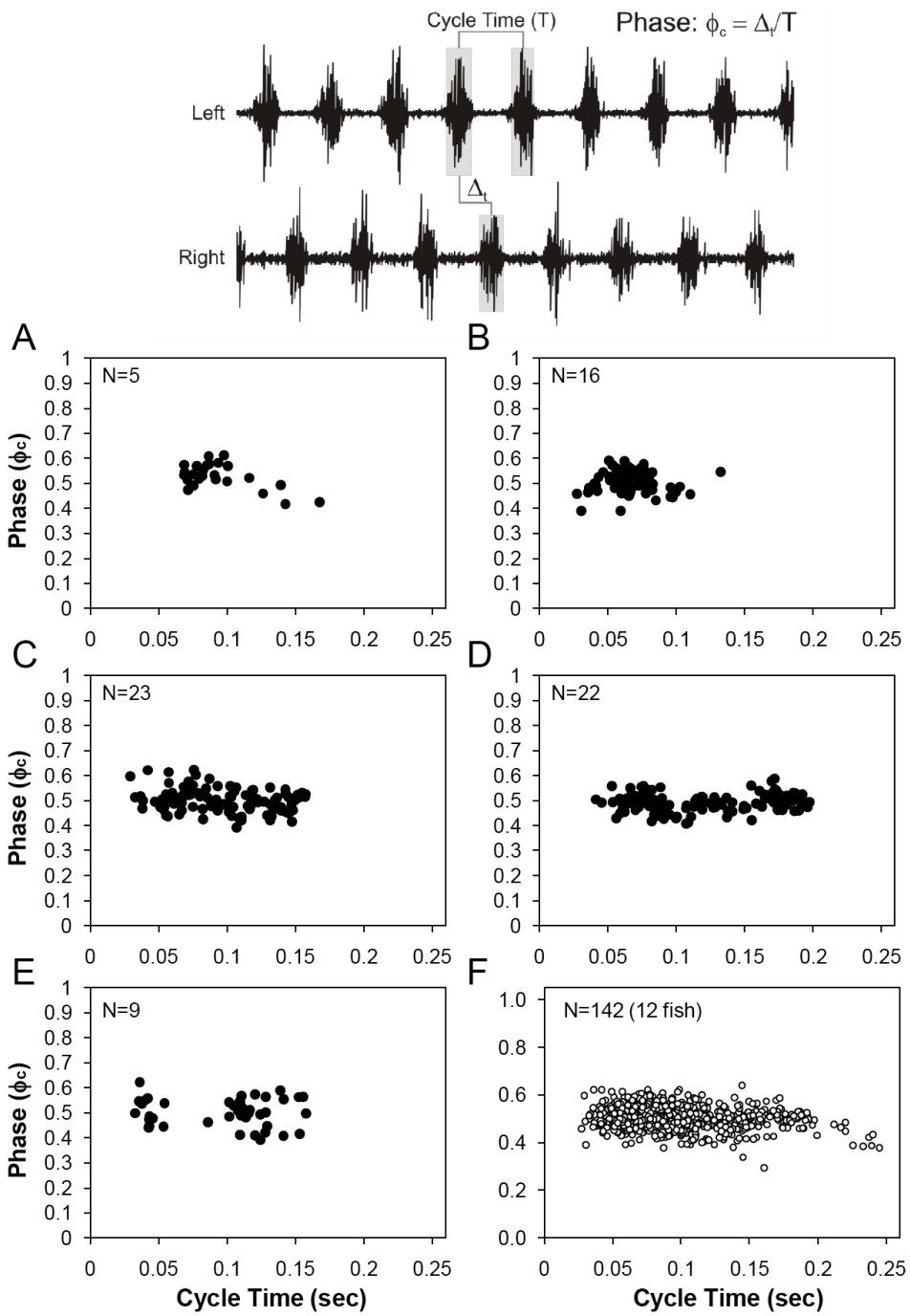

Figure 4.4. Relationship between contralateral phase and cycle time. Top EMG trace shows the alternating pattern of activity from freely swimming adult zebrafish. Contralateral phase (ϕ_C) and cycle time were measured as shown in the EMG recording at the top. Plots of ϕ_C vs, cycle time from 5 individual fish (A-E). Each plot shows individual points from several swimming bouts that ranged between 4-33 cycles (T) of activity at different swimming speeds. The number of bouts (N) analyzed for each plot is indicated in the insets. F) Plot shows the overall relationship between ϕ_C vs. cycle time from 142 bouts of activity from 12 fish. The mean contralateral phase from the pooled data was 0.50±0.05 (mean±SD).

Figure 4.5. Overall swimming frequencies and the effect of embryonic nicotine exposure. Freely swimming zebrafish can swim at different speeds while sustaining a minimum of 4 cycles of activity between 4 and 25 Hz. The percent of swimming bouts that occurred at each range of swimming frequencies (< 9 Hz, 9-16 Hz and > 17 Hz) was quantified. A) Control fish (61 bouts, n=6 fish) had a mean swimming frequency of 12.1±4.4 Hz and appeared to mostly swim between 9-16 Hz. High speed swimming above 17 Hz occurred only in ~15% of the swimming bouts. B) Bouts of activity at 8 Hz, 15 Hz, and 21 Hz swimming frequencies are shown from control fish. C) Zebrafish exposed to 5μM nicotine from 22-72 hpf (64 bouts, n=5 fish) had a mean swimming frequency of 9.1±3.0 Hz and appeared to mostly swim below 9 Hz. Sustained and alternating high speed swimming above 17 Hz only occurred in ~1.5% of the swimming bouts. D) Bouts of activity at 8 Hz, 15 Hz, and 21 Hz swimming frequencies are shown from 5μM nicotine-exposed fish. Note that at swimming frequencies < 17 Hz there was no disruption of sustained alternation in controls and nicotine-exposed fish. When swimming at 21 Hz, nicotine-exposed fish either could not sustain alternation from side-to-side or the left-right pattern of activity was disrupted before 4 cycles were completed (data not shown). Grey boxes are used to highlight alternating activity of the left side. Yellow boxes are used to indicate when overlap of activity occurred between the two sides.

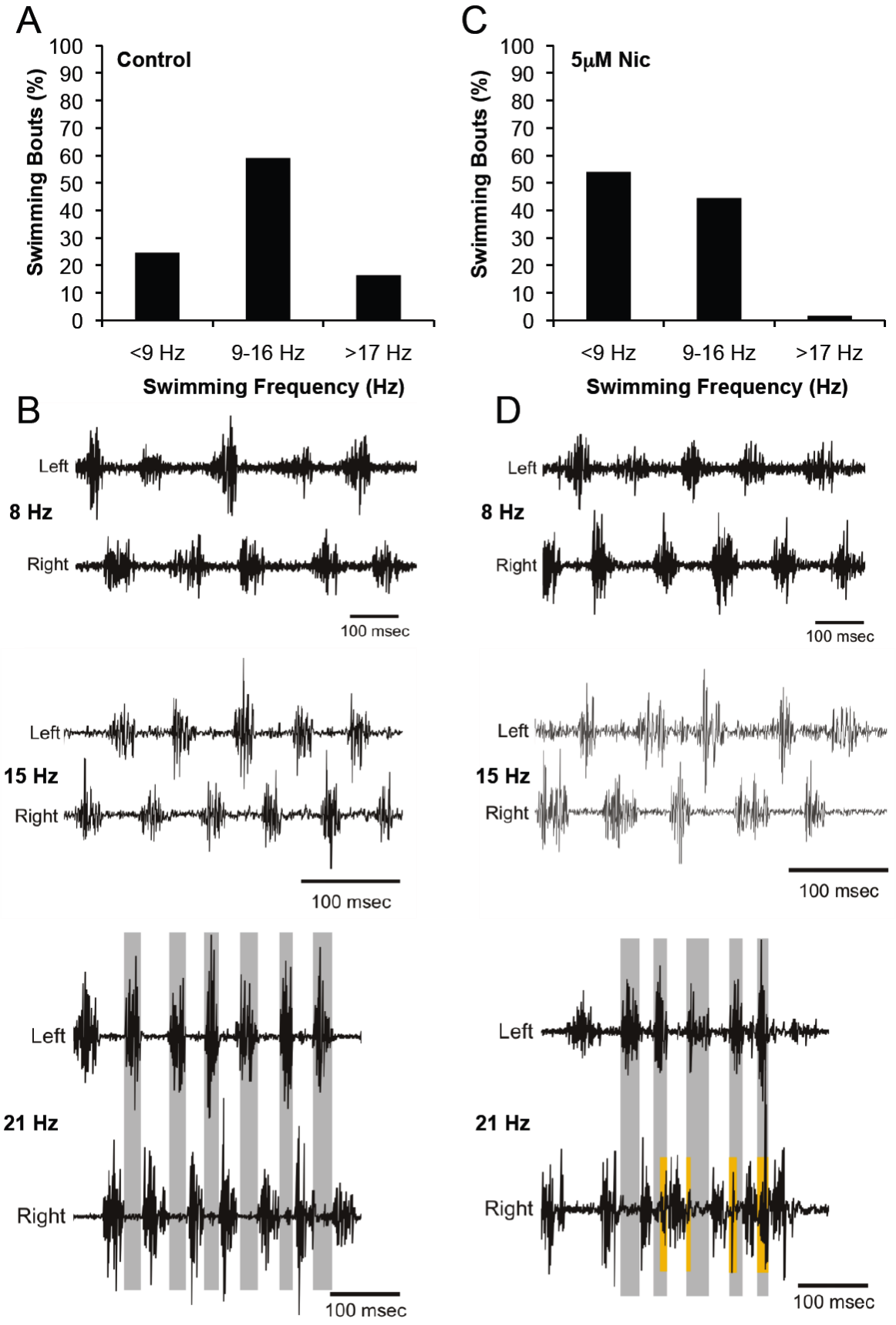
A
Control
Swimming Bouts (%)
100
90
80
70
60
50
40
30
20
10
0
<9 Hz
9-16 Hz
>17 Hz
Swimming Frequency (Hz)
C
5μM Nic
Swimming Bouts (%)
100
90
80
70
60
50
40
30
20
10
0
<9 Hz
9-16 Hz
>17 Hz
Swimming Frequency (Hz)
B
Left
8 Hz
Right
100 msec
D
Left
8 Hz
Right
100 msec
Left
15 Hz
Right
100 msec
Left
15 Hz
Right
100 msec
Left
21 Hz
Right
100 msec
Left
21 Hz
Right
100 msec

In contrast to control fish, zebrafish exposed to nicotine (5μM nicotine, 22-72 hpf) during embryogenesis exhibited a shift towards slower swimming frequencies where twice as many bouts occurred below 9 Hz (Fig. 4.5C, 63 bouts from 5 fish; mean frequency=9.5±3.0 Hz, $p<0.001$) when compared to controls. Fewer than 2% of the swimming bouts were above 17 Hz. For EMG analysis, we selected bouts of activity that were sustained for a minimum of 5 bursts producing 4 cycles of alternating activity. Therefore, in order to eliminate the possibility that our data set was biased towards more low frequency data points, we counted the total number of bouts that sustained alternation for 4 cycles specifically at swimming frequencies above 17 Hz in all control and nicotine-exposed zebrafish. We then normalized the values to the total length of the recording session and found that the frequency of bouts above 17 Hz (# of bouts swimming above 17 Hz/total recording duration) was indeed lower in 5μM nicotine when compared to their controls (data not shown). Nicotine-exposed zebrafish (5μM, 22-72 hpf) could produce some fast bouts of activity above 17 Hz, but this activity was typically sustained for only 2-3 cycles of alternating activity (data not shown). For example, when the right side produced 5 bursts of activity, the activity on left side would be erratic and arrhythmic; the activity did not resemble swimming behavior (Fig. 4.5D, bottom EMG trace). Zebrafish exposed between 22-72 hpf to 15μM also exhibited swimming at significantly slower frequencies (38 bouts from 3 fish, $p<0.05$) but this was not the case for zebrafish exposed to 30μM nicotine (22-72 hpf, 51 bouts from 5 fish, $p=0.094$) (data not shown). In zebrafish exposed to nicotine between 12-30 hpf, there was no significant difference in the mean swimming frequencies when compared to controls from the same experiment (p values>0.05, data not shown).

Relationship of Burst Duration and Cycle Time

We then examined the relationship between burst duration and cycle time in zebrafish exposed to 5, 15 and 30μM nicotine between 22-72 hpf and 12-30 hpf. In all cases, there was a

positive linear correlation between burst duration and cycle time. Cycle time is inversely proportional to swimming frequency. When fish are swimming at slow speeds (longer cycle time), the duration of a burst should increase and when swimming fast (shorter cycle time), burst duration should shorten.

In Figure 4.6, the relationship between burst duration and cycle time and the corresponding linear regressions are shown for controls and zebrafish exposed to nicotine between 22-72 hpf. Each graph shows pooled data from different fish for each treatment group. In control zebrafish, the burst duration was highly correlated with cycle time (Fig. 4.6A). However, the burst duration was only weakly correlated with cycle time in zebrafish embryonically exposed to 5μM nicotine (Fig. 4.6B). Burst duration was shorter in these fish as cycle time increased as indicated by the significantly smaller regression slope ($p<0.0001$) and larger intercept value ($p<0.0001$). In zebrafish exposed to 15μM nicotine as embryos (Fig. 4.6C), the relationship between burst duration and cycle time was not significantly different from controls (slope, $p=0.48$; intercept, $p=0.58$). Even though zebrafish exposed to 30μM nicotine as embryos appeared to have a relatively strong correlation, the regression slope and intercept were significantly different from control values ($p<0.0001$).

In zebrafish exposed to 5μM nicotine as embryos from 12-30 hpf, the relationship between burst duration and cycle time was not significantly different (slope, $p=0.77$; intercept, $p=0.76$) when compared to controls. However, there was a significant difference in the burst duration-cycle time relationship in zebrafish exposed to 15μM (slope, $p<0.05$; intercept, $p=0.39$) and 30μM nicotine (slope and intercept, $p<0.0001$). Note that the difference in the relationship between burst duration and cycle time was not as pronounced in zebrafish exposed to 15μM nicotine as seen in 30μM nicotine-exposed zebrafish. These findings indicate that when nicotine-exposed-fish are swimming at a given frequency, the burst duration is shortened when compared

to control fish swimming at the same frequency. This suggests that the excitatory inputs that drive the duration of a burst are most likely inhibited too early thus resulting in a shorter burst duration.

Contralateral Phase

The relationship between contralateral phase and cycle time was examined in control and nicotine-exposed zebrafish. Phase (ϕ_C) difference between contralateral bursts was

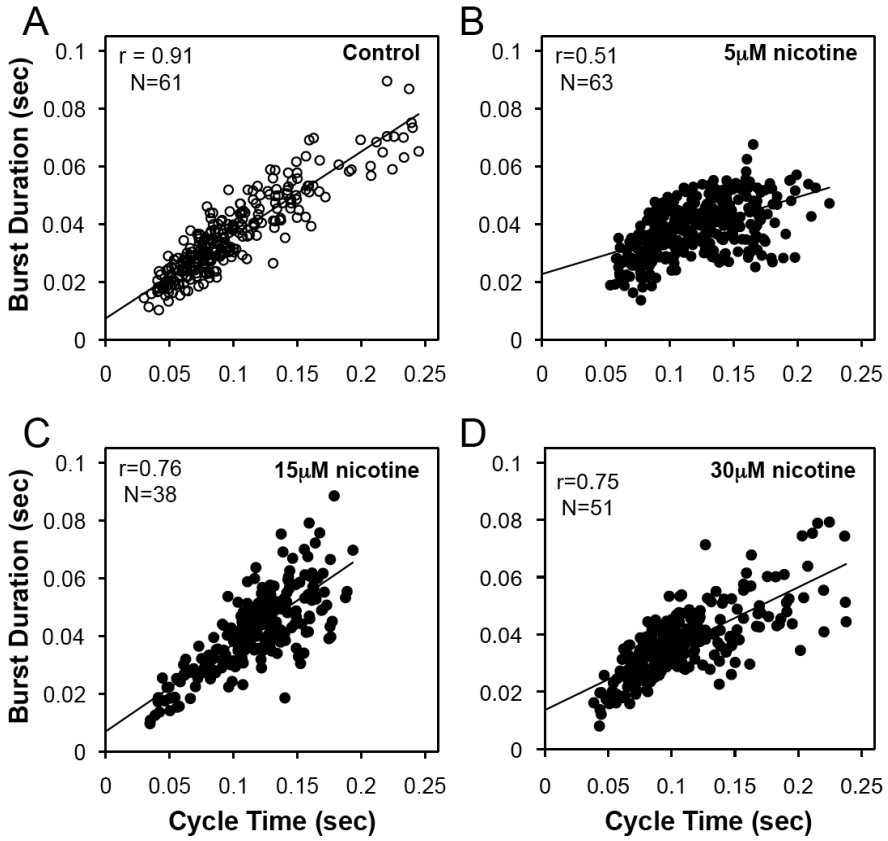

Figure 4.6. Relationship between burst duration and cycle time: embryonic nicotine exposure from 22-72 hpf. Scatter plots of burst duration against cycle time from nicotine-exposed fish between 22-72 hpf and their corresponding controls from the same experiment. Linear regression lines of burst duration against cycle time from controls (A, 6 fish) and zebrafish exposed to 5μM (B, 5 fish), 15μM (C, 3 fish), and 30μM (D, 6 fish) nicotine are shown in each plot. Burst duration in controls exhibits a strong linear correlation with cycle time as indicated by the correlation coefficient (*r*) in the inset. Fish exposed to 5μM nicotine fish showed a weaker linear correlation in the burst duration-cycle time relationship when compared to their control counterparts. The linear relationships for each group were compared to the controls for differences in slopes and intercepts using ANCOVA (see methods and results). N indicates the number of swimming bouts analyzed for each plot.

approximately 50% (0.5±0.04) of the cycle time (Fig. 4.7A, 368 bursts in 81 bouts from 6 fish) and was also normally distributed across recording sessions (Fig. 4.7B). The phase ϕ_C distribution in nicotine-exposed zebrafish (Fig. 4.7C, 301 bursts in 53 bouts from 5 fish) also varied across recording sessions and exhibited a larger spread when compared to the phase ϕ_C values of control fish (Fig. 4.7D). In these nicotine-exposed zebrafish (Fig. 4.7C), the ϕ_C was shifted to a higher range during longer cycles of activity (slower swimming speeds).

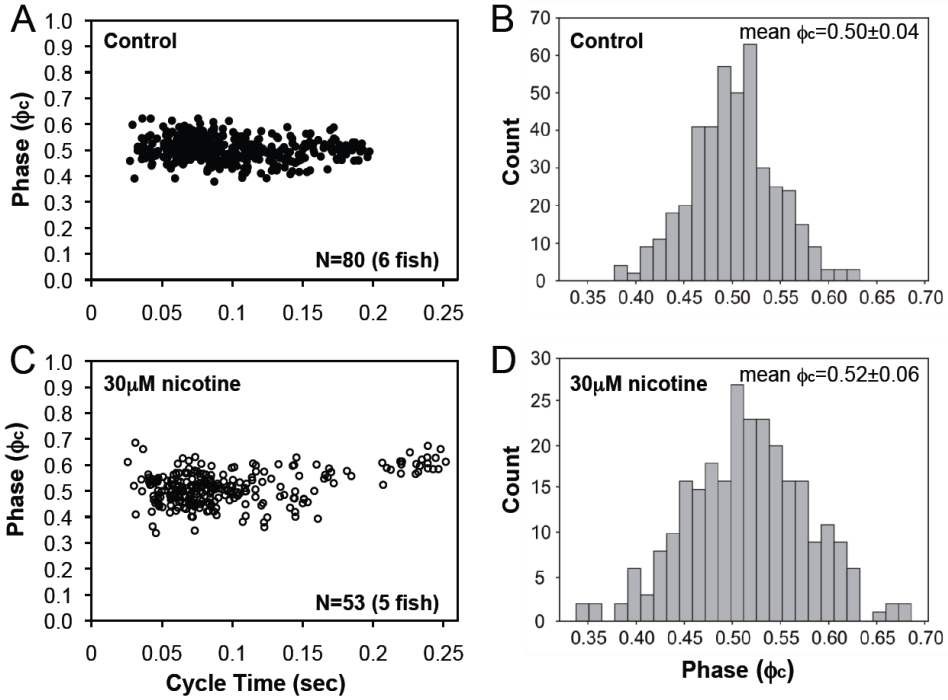

Figure 4.7. Relationship between contralateral phase and cycle time: embryonic nicotine exposure from 12-30 hpf. Analysis of phase (ϕ_C) vs. cycle time in control and nicotine-exposed fish from the same experiment. A) Plot of ϕ_C vs. cycle time from 6 control fish. B) Frequency histogram showing the variability of contralateral phase from all the fish shown in A (mean ϕ_C = 0.50±0.04). C) Plot of ϕ_C vs. cycle time from 5 nicotine-exposed fish (30μM nicotine). D) Frequency histogram showing the variability of contralateral phase from all the fish shown in C (mean ϕ_C = 0.52±0.06). The spread of the histogram in D is larger when compared to the control indicating disrupted contralateral phase in nicotine-exposed fish. Values are means ± SD.

Two representative examples from slow and fast bouts of swimming activity from one control and one nicotine-exposed zebrafish are shown in Figs. 4.8A and 4.8C. The contralateral phase (ϕ_C) was plotted against the relative position of each burst within a single bout from 2

individual fish (Fig. 4.8B, controls; Fig. 4.8D, 30μM nicotine exposure at 12-30 hpf). The contralateral phase of nicotine-exposed fish was elevated at slow (5 Hz) but not at higher (15 Hz) swimming frequencies when compared to controls, indicating that the pattern of alternating activity in nicotine-exposed fish was out of phase (ϕ_C) only at slow swimming speeds.

Motoneuron Activity in Freely Swimming Zebrafish Exposed to Nicotine as Embryos

Lastly, we analyzed intra-burst spikes from several swimming bouts across different swimming speeds. The EMG spikes produced within each burst are the result of primary and secondary motoneuron activity. It was previously shown that PMNs and SMNs could be distinguished based on their EMG spike amplitudes (Liu and Westerfield, 1988). PMNs produce large amplitude EMG spikes which are activated during fast swimming (Fig. 4.9A) whereas, SMNs produce smaller EMG spike amplitudes and are mainly activated during many swimming bouts especially during slow bursting frequencies (Fig. 4.9B). Because the recording quality across preparations varied, direct comparisons of EMG spike amplitudes across recording sessions would be inappropriate. The number of EMG spikes at each amplitude was plotted from each individual fish as previously described (Liu and Westerfield, 1988). The intra-burst spike amplitudes were analyzed in controls (spikes from 184 bursts in 35 bouts from 5 fish) and zebrafish exposed to 5μM (spikes from 184 bursts, 35 swimming bouts, n=5 fish), 15μM (spikes from 184 bursts, 35 swimming bouts, n=5 fish), and 30μM nicotine (spikes from 184 bursts, 35 swimming bouts, n=5 fish). Examples of EMG spike amplitude distribution are shown for a control and a nicotine-exposed zebrafish (Fig. 4.9C, 30μM nicotine from 22-72 hpf in 4.9D). In both cases, the EMG amplitudes could be fit by two lines indicating the existence of two discrete populations of EMG spikes (PMNs and SMNs). Thus, we were able to identify spikes as either PMN or SMN spikes based on amplitude values in individual fish (see Methods for details). In all of the recordings obtained from control or nicotine exposed fish, the EMG spike amplitudes

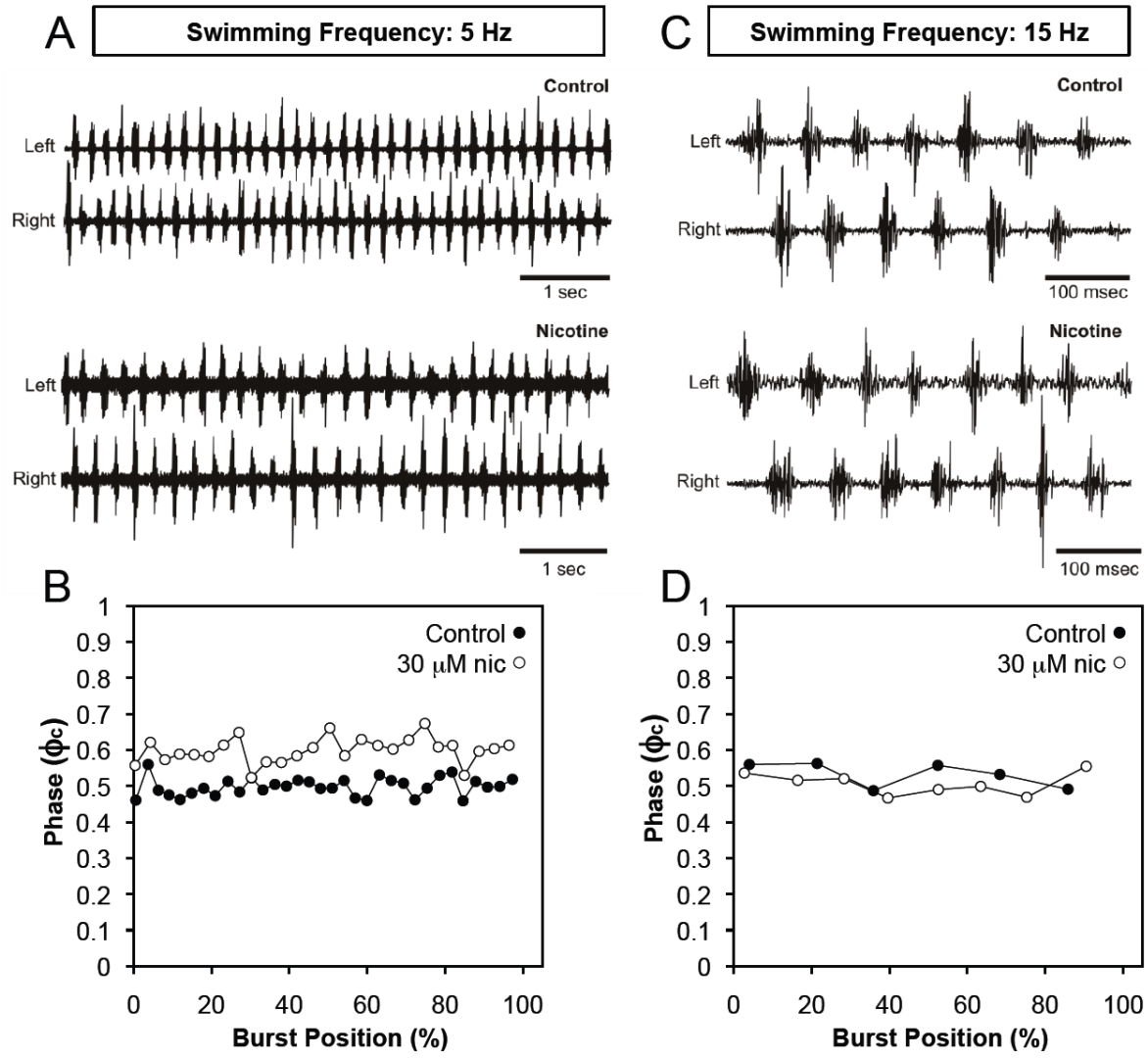

Figure 4.8. Contralateral phase is disrupted at low but not high swimming frequencies. Analysis of contralateral phase and burst position within a single bout of activity from the same experiment shown under Figure 4.7. A) EMG trace from a single bout of activity swimming at 5 Hz from a control fish and a nicotine-exposed. B) Phase (ϕ_C) against burst position (%) within a single swimming bout (see Methods) from the control and nicotine-exposed fish shown in A. Note that contralateral phase in the nicotine-exposed fish was shifted to a higher value when compared to their control counterparts. C) EMG trace from a single bout of activity swimming at 15 Hz from a control fish and a nicotine-exposed. D) Contralateral phase (ϕ_C) against burst position (%) within a single bout of activity from a control and a nicotine-exposed fish.

were always reliably fit by two lines such that no significant differences between controls and nicotine-exposed fish were observed. These results strongly suggest that SMN activation at slow

swimming frequencies, as well as recruitment of PMNs at higher frequencies, were not affected following embryonic nicotine exposure.

Discussion

In this chapter, the locomotor output in freely swimming adult zebrafish that were transiently exposed to nicotine as embryos was analyzed. Before we could make comparisons between control and nicotine-exposed zebrafish, we first examined the basic features of the locomotor pattern to determine if it exhibited characteristics of swimming. This analysis not only allowed us to evaluate the potential long-term effects on locomotive behavior following an embryonic nicotine exposure, but also helped us understand the cellular basis underlying the actions of nicotine.

Freely Swimming Adult Zebrafish: Basic Features of Locomotor Behavior

In order to examine these locomotor behaviors in adult zebrafish, an assay had to be developed where the rhythmic motor activity in adult zebrafish could be examined. We performed electromyographic recordings from axial muscles of freely swimming adult zebrafish. Our analyses demonstrated that the locomotor activity of freely swimming zebrafish possessed basic features indicative of swimming.

During a recording session, zebrafish moved around the tank at various speeds producing several bouts of rhythmic swimming activity with several periods of inactivity in between bouts. The frequency of swimming varied across bouts of swimming activity and ranged between 4-38 Hz. This range of swimming frequencies was similar with the range previously reported in adult freely swimming zebrafish (16-50 Hz, Liu and Westerfield, 1988). Also, in a semi-intact preparation of adult zebrafish, NMDA-induced locomotor frequency averaged ~ 6 Hz and following strychnine application, bursting frequencies increased to ~25 Hz (Gabriel et al., 2008).

Figure 4.9. Primary and secondary motoneuron activity: amplitude distribution of EMG spikes. PMNs and SMNs can be distinguished based on their EMG spike. During swimming, bursts consist of EMG spikes with small and large amplitudes. A) SMNs produce small amplitude spikes shown to the right in the expanded view. B) PMNs produce larger amplitude spikes (right EMG trace is an expanded view of box to the left). As seen here, at fast swimming frequencies (B), PMN are activated and produce the large amplitude EMG spikes (arrow). (C and E) The number of EMG spikes at each amplitude is plotted from an individual control fish (spikes from 53 bursts, 10 swimming bouts) and a nicotine-exposed fish (30 μM from 22-72 hpf; spikes from 66 bursts, 11 swimming bouts). The amplitude distribution fits well in two lines and a threshold amplitude was determined by the intercept of the two lines. The EMG amplitude distribution of the nicotine-exposed fish was similar to the control. (D and F) The number of EMG spikes that fell below threshold was expressed as a percentage of the total EMG spikes. The percent of EMG spikes that fell below the threshold correspond to SMN spikes and was determined at varying swimming frequencies in control (spikes from 184 bursts, 35 swimming bouts, from 5 fish) and nicotine-exposed fish (spikes from 185 bursts, 34 swimming bouts, from 4 fish). The percent of EMG spikes that fell below the threshold amplitude followed the same pattern with the controls in the nicotine-exposed fish. Data were binned at 4-Hz intervals. Values are means±SEM.

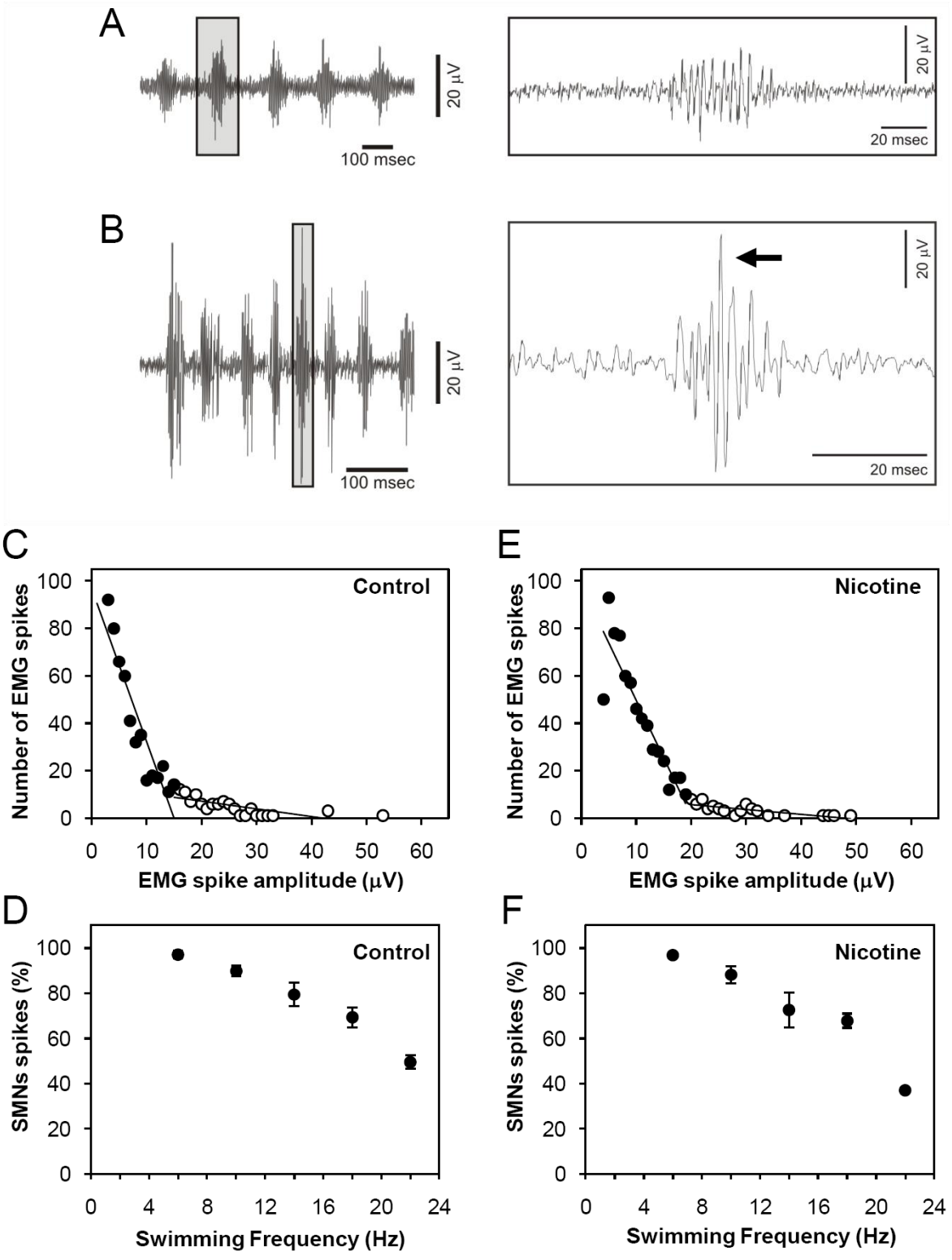
A
20 µV
100 msec
20 µV
20 msec
B
20 µV
100 msec
20 µV
20 msec
C
Control
Number of EMG spikes
EMG spike amplitude (µV)
E
Nicotine
Number of EMG spikes
EMG spike amplitude (µV)
D
Control
SMNs spikes (%)
Swimming Frequency (Hz)
F
Nicotine
SMNs spikes (%)
Swimming Frequency (Hz)

Our results demonstrated that adult locomotor networks have slower swimming frequencies when compared to freely swimming larvae (30-100 Hz in 3 dpf fish, Muller and van Leeuwen, 2004; Muller et al., 2000) and larvae in fictive swimming preparations (20-63 Hz in 4-6 dpf fish, Masino and Fetcho, 2005; 15-75 Hz in 4 dpf fish, McLean et al., 2008). This is consistent with previous reports where the frequency of the motor output decreased as the fish mature (Gabriel et al., 2008).

An alternating pattern of activity from side to side was observed in freely swimming zebrafish, where the burst duration was proportional to the cycle time and the contralateral phase was constant across swimming frequencies. The duration of a burst occupied on average 37% of one cycle which was slightly lower than the expected 50.6% previously reported in goldfish (Fetcho and Svoboda, 1993). Studies from different fish have shown that a 0.5 proportion (50%) is mostly observed in more anterior muscles and this may vary with longitudinal position (28% in zebrafish larvae, Masino and Fetcho, 2005; 36% in lamprey, Wallen and Williams, 1984; 30-45% in mackerel, Shadwick et al., 1998). Under-sampling muscle activity using recording electrodes implanted in a discrete area within a segment could also explain bursts occupying only 37% of the cycle time. This would result in omitting activity within the same segment from muscles that are further away the recording site. Paired contralateral recordings from the same segment showed that the phase between contralateral sides was relatively constant (0.50±0.05) across a wide range of swimming frequencies corresponding to ~50% of one cycle (Masino and Fetcho, 2005; Gabriel et al., 2008).

Secondary Motoneuron Activity in Zebrafish Exposed to Nicotine as Embryos

In these experiments, EMG activity was recorded mostly from white muscle fibers and possibly some intermediate fibers. The local control of muscle movements is regulated by motoneurons in spinal cord and in zebrafish EMG spikes are strongly correlated with the

activation of primary and secondary motoneurons (Liu and Westerfield, 1988). Each white muscle fiber is innervated by a single primary motoneuron and one or more secondary motoneurons (Westerfield et al, 1986). PMN activation causes simultaneous contraction of several muscle fibers to produce large body movements associated with fast swimming and startle responses. On the other hand, SMNs innervate a wider area of adjacent muscle fibers and when activated they control fine movements associated with slow swimming (Liu and Westerfield, 1988).

Intra-burst spike activity from our recordings was consistent with the activation of these two distinct motoneuron populations. During slow bursting frequencies, several small amplitude spikes were detected and as the fish swam faster, more large amplitude spikes were produced. Therefore, we used this feature of intra-burst spikes to describe whether the pattern of activation for primary and secondary motoneurons was affected in zebrafish exposed in nicotine as embryos. Our analysis showed that nicotine-exposed zebrafish produced several small amplitude spikes associated with SMNs at slow swim speeds. At higher swim speeds, less SMN spikes were produced and more, larger EMG spikes were evident, consistent with the recruitment of PMNs. This pattern of motoneuron activation and recruitment was similar in controls. These findings suggest that even though axonal pathfinding of secondary motoneurons was altered in adult stages of development following embryonic nicotine exposure (Menelaou and Svoboda, 2009), their overall recruitment pattern during swimming was not different from unexposed zebrafish.

Zebrafish possess ~20 SMNs per hemisegment and not all motoneuron axons were affected following embryonic nicotine exposure (Chapter 2). This was not surprising, since motoneuron innervation at the neuromuscular junction becomes more elaborate to accommodate more muscle fibers added in their body to accommodate a wider range of movements as

zebrafish develops (Panzer et al., 2005). This may suggest that adjacent motoneuron axons may compensate for motoneuron axons that failed to reach their appropriated targets at the periphery. If this compensatory mechanism was true, then no overall changes would be observed in the summed EMG activity of muscle fibers.

However, one must be careful in interpreting these results, since electromyographic recordings provide the summated activity of several motoneurons from adjacent muscle fibers. Therefore, EMG recordings may not be appropriate to resolve differences in single motor units (a pool of motoneurons innervating a single muscle fiber). Intracellular recordings from individual motoneurons would help to investigate changes in physiological responses caused by embryonic nicotine exposure. These experiments would also provide information as to whether potential changes in motoneuron physiology correlated with a disruption in the swimming behavior of zebrafish.

Altered Patterns of Locomotor Behavior in Zebrafish Embryonically Exposed to Nicotine

Swimming Frequency

Following a basic characterization of EMG activity patterns in freely swimming zebrafish, we assessed the potential effects of embryonic nicotine exposure on the adult locomotor behavior. Several changes in locomotor activity were detected in zebrafish exposed to nicotine as embryos. We first noticed a shift in the preferred swimming frequency. Zebrafish exposed to 5 and 15μM nicotine between 22-72 hpf swam at lower frequencies (9.5±3.0 Hz and 9.7±3.3 Hz, respectively) when compared to controls (12.1±4.4 Hz). Several possible cellular substrates may explain this shift. First, glycinergic interneurons of the CPG are known to project to the opposite side of spinal cord and during swimming, they provide mid-cycle inhibition resulting in a coordinated left-right alternation of axial muscles (Sillar et al., 2002). Evidence from *Xenopus* embryos suggested that the strength of glycinergic inhibition at mid-cycle controls

the swimming frequency. For example, increasing glycinergic inhibition slows down swimming (Dale, 1995). In another study, adult zebrafish locomotor frequency monitored in a semi-intact preparation was increased five-fold following brief application of strychnine; a pharmacological agent that blocks or decreases glycinergic neurotransmission (Gabriel et al., 2008). Taken together, these studies suggest that embryonic nicotine exposure could potentially affect the development and physiology of inhibitory interneurons involved in governing swimming frequencies.

Additional studies in zebrafish larvae have shown that different interneuronal networks govern the distinct motor patterns associated with slow and fast swimming (McLean et al., 2008). During early development, excitatory neurons that produce fast swimming movements in the zebrafish embryos develop first, followed by those governing slower frequency motor activity (McLean and Fetcho, 2009). During slow swimming, excitatory interneurons called MCoDs (multipolar commissural descending) produce swimming behaviors at slow and intermediate frequencies by exciting ventral SMNs. At high swimming speeds, excitatory interneurons called CiDs (circumferential ipsilateral descending) provide direct excitation to PMNs (McLean et al., 2008). CiDs differentiate between 24 and 30 hpf, whereas MCoDs do not begin to differentiate until 72 hpf (McLean and Fetcho, 2009). The distinct developmental patterns of the interneuronal networks between 24 and 72 hpf make them susceptible to perturbations following nicotine exposure between 22-72 hpf. Zebrafish exposed to nicotine at 22 hpf, before CiDs are differentiated, could potentially disrupt the normal course of CiD development which could result in motor defects associated with fast swimming frequencies. If zebrafish were exposed to nicotine at 12-30 hpf, no differences in the overall swimming frequencies would likely occur. Taken together, nicotine exposure after 30 hpf could potentially

affect developmental processes of pre-motor neurons important in governing either slow and fast swimming behaviors.

Relationship of Burst Duration and Cycle Time

Zebrafish exposed to nicotine as embryos also exhibited an altered relationship between burst duration and cycle time. We showed that this relationship is mostly affected at the same concentrations and exposure windows usually associated with SMN axonal pathfinding errors. In zebrafish, the main source of on-cycle excitation to the swimming CPG is provided by rhythmically active CiD interneurons (McLean et al., 2007). Also, glycinergic commissural interneurons from the opposite side of spinal cord are also important for providing mid-cycle inhibition. This ensures that the proportion of burst duration of over cycle time remains relatively constant to produce rhythmic locomotor output. Uncoupling these synaptic connections or altering the physiological properties between these spinal neurons could potentially affect the timing of the burst inhibition thus leading to altered burst durations.

Contralateral Phase

Even though the relationship between burst duration and cycle time was altered in zebrafish exposed to nicotine between 22-72 hpf (5μM and 30μM) and 12-30 hpf (15μM and 30μM), they still exhibited left-right alternation similar to controls. In contrast, in zebrafish exposed to 30μM nicotine (12-30 hpf) as embryos, the alternating pattern of activity was disrupted, but only at slow swimming frequencies. In these fish, a robust left-right alternation was evident, but the time difference between contralateral bursts over cycle time (ϕ_C) was shifted. Altered locomotor-like activities were also reported in embryonic mutant mice that lack choline acetyltransferase (ChAT), the rate-limiting enzyme for acetylcholine biosynthesis (Myers et al., 2005). Even though rhythmically active spinal circuits developed in these mutants, the burst durations were prolonged and the left-right phase relationship was disrupted. Taken

together, cholinergic signaling via nAChRs appears to play an important role in spinal neuron development and functional assembly of spinal motor circuits. Therefore, nicotinic perturbations during critical stages of development may disrupt the normal course of spinal network assembly in embryos resulting in long-term alterations in the adult locomotor behavior.

Modulating Cholinergic Signaling and Rhythmic Motor Patterns

In this chapter, we have provided evidence that embryonic nicotine exposure can disrupt the locomotor behavior in adult zebrafish. The vertebrate locomotor CPG is a spinal neuronal network of interneurons and motoneurons which generates the rhythmic motor pattern of swimming. The role of acetylcholine in spinal neuron development, generation of rhythmic patterns of activity, and the assembly of spinal locomotor circuits has been widely accepted (Hanson and Landmesser, 2003; Myers et al., 2005). During development, the actions of acetylcholine are mediated through nAChR activation and if acetylcholine signaling is disrupted by an exogenous agonist, this could interfere with normal developmental processes.

Based on our analyses of swimming behavior in adult zebrafish, we are in the position to potentially identify cellular substrates for nicotine associated with the abnormal locomotor patterns observed. Inhibitory interneurons within the CPG receive cholinergic transmission from other motoneurons cells (Perrins and Roberts, 1995; Hanson and Landmesser, 2003) indicating that these cells possess nAChRs. Thus, nicotine exposure at stages of development when these cells are just beginning to develop can potentially cause changes in form and function. Any changes in the final assembly or architectural design of the CPG could lead to long-term behavioral effects in the form of altered swimming behavior.

In conclusion, disrupting cholinergic signaling during critical stages of spinal circuit development produced a long-term alteration in locomotor behavior. We took advantage of the basic features that typify swimming behavior in zebrafish to further understand the actions of

embryonic nicotine exposure on underlying physiology. Our approach has led us to identify spinal interneurons as candidate neuronal substrates which likely underlie the long-term changes in locomotor behavior which resulted from the nicotine exposure.

CHAPTER 5

ZEBRAFISH α2-CONTAINING NICOTINIC ACETYLCHOLINE RECEPTORS AND THEIR ROLE IN NICOTINE-INDUCED EMBRYONIC MOTOR OUTPUT

Introduction

Nicotine exposure can cause anatomical and physiological changes in the developing zebrafish that can persist in adulthood (Chapters 2, 3, and 4). It is widely accepted that the presence of nAChRs during embryogenesis can likely mediate the actions of nicotine (Slikker et al., 2005). Studies from other systems have provided a vast amount of information on the molecular, biochemical and anatomical profiles of nAChRs. However, it was only until the last decade that nAChRs have begun to be explored in zebrafish. Therefore, the spatiotemporal expression profiles of receptor subtypes at the time of the nicotine exposure is essential for investigating the role of nAChR in mediating nicotinic responses in embryonic and adult zebrafish. Having this information available would greatly facilitate the identification of potential cellular substrates for nicotine and consequently help in elucidating the underlying mechanisms of nicotine-induced phenotypes in the developing zebrafish.

In mammalian systems as well as *Xenopus*, motoneurons have been shown to receive cholinergic excitation from other adjacent motoneurons or interneurons (Perrins and Roberts, 1995; Zagoraiou et al., 2009). These findings suggest the presence of nAChRs in spinal neurons. In zebrafish, recent studies have provided important information on the mRNA expression profiles of α2, α4, α6, α7 and β3 nAChR subunits (Zirger et al., 2003; Ackerman et al., 2009). We were particularly interested in the α2 subunit because it was shown to localize to a distinct population of neurons in intermediate spinal cord, possibly motoneurons and interneurons (Zirger et al, 2003). In mammalian systems, the nAChR α2 mRNA has been localized in 19% of dorsal spinal neurons (Cordero-Erasquin et al., 2004), in small-to-medium size cells in the rat ventral spinal cord (Ishii et al., 2005), and in human fetal lumbar motor neurons (Keiger et al.,

2003). Based on these expression profiles, we hypothesized that either spinal interneurons or motoneurons in zebrafish would possibly express the α2 subunit.

In this chapter, the spatiotemporal distribution of the nAChR α2 subunit was characterized using a zebrafish-specific antibody. We showed that nAChR α2 expression in embryonic zebrafish is restricted to dorsal spinal cord in a population of mechanosensory neurons called Rohon-Beard (RB) neurons, in olfactory sensory neurons and in the trunk muscle. At later stages of development, strong α2 expression on secondary motoneurons and their axons was evident. The expression of the α2 subunit was then blocked using antisense modified oligonucleotides (morpholinos) to identify the potential roles of α2-containing nAChRs during development. Our results showed that blocking the expression of nAChR α2 subunit did not affect the embryonic spontaneous motor activity but it disrupted the nicotine-induced motor behavior. Disruption of the nicotine-mediated motor behaviors did not affect motoneuron axonal pathfinding, postsynaptic AChR clustering, or responses to touch. Our findings from this chapter, strongly suggest that α2-containing nAChRs localized on mechanosensory Rohon-Beard spinal neurons or interneurons were involved in mediating the nicotine-induced swim-like behaviors in embryonic zebrafish.

Materials and Methods

Zebrafish Embryo Maintenance

Wildtype (EkkWill) and transgenic (Tg(*isl3*):GFP) and (Tg(*isl1*):GFP) adult zebrafish were maintained as previously described (Chapter 2). Embryos were collected immediately after spawning from individual pairs and then placed into 100 mm Petri dishes containing embryo medium prior to microinjection procedures.

Morpholino Design

Morpholino antisense oligonucleotides (MOs) were synthesized by Gene Tools (Philomath, Oregon). One MO was designed to target the predicted translation site of the nAChR α2 subunit (α2 MO) and had the following sequence: 5'-GGATTTCCGCCATGTCCAGCGTC-3'. A second MO that targeted the splice junction site at the exon2-intron2 boundary was also synthesized (α2 MO2) and had the following sequence: 5'-ATGCAAAGTATCAACTTACCACATC-3'. The α2 MOs were fluorescently tagged with fluorescein at the 3' end. Similar results were obtained with both α2 MOs and all the experiments shown here were performed using the α2 MO2. But for simplicity purposes it will be referred to as α2 MO from here on. A standard control MO (5'-CCTCTTACCTCAGTTACAATTTATA-3') was used as a control and was not fluorescently tagged. For all morpholino experiments, MOs were diluted to 3 mM in 1× Danieau's solution (58 mM NaCl, 0.7 mM KCl, 0.4 mM $MgSO_4$, 0.6 mM $Ca(NO_3)_2$, 5 mM HEPES, pH 7.6).

Morpholino Microinjections

Microinjection needles were pulled on a horizontal micropipette puller (Flaming/Brown P-97, Sutter Instruments, Novato, CA) using fire-polished borosilicate glass with filament (outer diameter of 1.2 mm, Sutter Instruments). Morpholino solutions were prepared fresh prior to the microinjection procedure. Control MOs were injected between 0.25-1mM in 0.1% phenol red (Sigma) and 125ng/μL rhodamine-conjugated dextran. Fluorescently tagged α2 MOs were injected at 0.1-2mM in 0.1% phenol red. Each solution was loaded into a micropipette needle and was then injected in the yolk stream of 1-2 cell stage. Following microinjection of the morpholinos, the embryos were individually screened for fluorescence at the animal pole at 5-6 hpf using a 10x objective on a fluorescent microscope and at a minimum light intensity. Embryos lacking fluorescence were removed and were not used in subsequent experiments. Some

embryos were also used as uninjected controls in all of our initial experiments to confirm that control MO-injected embryos yielded similar results when compared to their uninjected control counterparts.

Reverse Transcription Polymerase Chain Reaction (RT-PCR)

Embryos were injected at the 1-2 cell stage with antisense oligonucleotide morpholino directed against the nAChR α2 subunit (α2 MO) or control morpholino (control MO) were collected at 24 and 48 hpf. Embryos (> 20) were directly immersed into TRI reagent (Invitrogen), and RNA was isolated as described previously (Tanguay et al., 1999). The quantity of RNA was analyzed by UV absorbance (DU 800 Spectrophotometer; Beckman Coulter). Reverse transcription reactions were carried out using 1 µg of total RNA and the Superscript II Reverse Transcriptase Kit as per the manufacturer's instructions (Invitrogen). Each 25 µl PCR reaction contained 4 µl cDNA; 0.75 µl 10 mM dNTP; 2.5 µl 10X PCR buffer (Fermentas); 2 µl 25 mM MgSO4; 2 µl of 3.75 µM forward and reverse primers for nAChR-α2; 0.25 µl 500 U Taq DNA Polymerase (Fermentas); and 13.5 µl of nuclease-free water. The reactions were run in a PCR Express Thermal Cycler (Thermo Hybaid) at the following conditions: 95°C 3 min then 95°C for 20 s, 62°C for 30 s, and 72°C for 2 min, for a total of 30 cycles followed by 72°C for 5 min. The PCR products were resolved by electrophoresis through a 2% agarose gel and visualized by ethidium bromide staining.

Nicotine Experiments

The (-)-nicotine used in this study was purchased from Sigma (St. Louis, Missouri, USA, catalog # N3876-5ml) and stock solutions were made fresh daily as needed in distilled water. The stock solution was diluted in embryo medium (pH 7.2) to obtain the desired final concentrations (30-60 µM).

Behavior

Embryos were placed in embryo media in 10mm Petri dishes and videotaped with a Kohu video camera mounted to a Zeiss SV6 dissecting microscope. The baseline spontaneous motor output (spinal musculature bends) of all embryos was recorded for 3-5 minutes. Then the embryos were transferred into a nicotine solution (60 μM) and the motor output was recorded again for 3-5 minutes. The motor activity was quantified as the number of bends in a one-minute epoch. For the dechorionation experiments, 22-25 hpf embryos (while in their chorions) were placed in nicotine solution for only 1 minute and their motor output was recorded. Following the 1-minute nicotine exposure, they were quickly transferred to fresh embryo media for a 20-minute wash period. They were then dechorionated manually using fine forceps and their motor output was videotaped for 3 minutes. The embryo response to tactile stimuli (touch response) was also assessed by mechanically probing the embryo trunk at 31 hpf for a total of a 10 trials (time between trials ~5-10 seconds). Responses were scored as follows: 0, no response (no trunk bend); 1.0 normal response (trunk bend). The behavioral scores from the 10 trials were summed for each fish and the average touch response was taken from all the fish to obtain a touch response index. All behavior experiments were carried out at ~25-26^{o}C.

Generation of Zebrafish nAChR α2 Antibody

The human nAChR α2 nucleotide sequence was queried in GenBank to identify the zebrafish nAChR α2 ortholog (accession number NM_001040327). ClustalW2 was used to align the known human and zebrafish nAChR and an α2 subtype specific peptide (FMRRPEPEKKPKKTA) was designed which spanned positions 357–371 of the zebrafish protein. The KLH-conjugated peptide was delivered in two rabbits to generate a zebrafish-specific anti-nAChR α2 polyclonal antibody (referred to as α2 from here on) (Antibodies Inc., Davis, CA)

Immunohistochemistry

Whole mount immunohistochemistry was performed as previously described (Chapter 2). The monoclonal antibodies zn5, currently known as zn8, (1:500), znp1 (1:250), F59 (1:250), zn12 (1:500) were obtained from the Developmental Studies Hybridoma Bank (The University of Iowa, Iowa) and were used to reveal secondary motoneuron somata and their axons (Fashena and Westerfield, 1999), primary motoneuron axons, slow muscle fibers (Devoto et al., 1996), and Rohon-Beard neurons (Metcalfe et al., 1990), respectively. The monoclonal antibodies anti-Hu (referred to as Hu from here on, Invitrogen) and anti-acetylated tubulin (refer to as aat from here on, Sigma) were used to reveal RB neurons and their processes, respectively. The polyclonal anti-nAChR α2 (1:500) was generated by Antibodies Inc. (Davis, CA). Fluorescent secondary antibodies goat anti-mouse Alexa 546 or 488 (Molecular Probes, Eugune, OR) were used at 1:1000 dilution and goat anti-rabbit Alexa 546 or 488 at 1:5000 dilution to reveal primary antibody labeling. Tetramethylrhodamine conjugated to α-bungarotoxin (α-btx) (Molecular Probes, Eugene, OR) was used to identify AChR clustering at neuromuscular junctions. MO-injected zebrafish were processed for immunohistochemistry and then incubated in α-btx (10 μg/mL) for 90 minutes before image analysis.

Dorsal Mounting in Agarose

Zebrafish embryos were individually mounted in 1.25% agarose (Fisher Scientific, Fair Lawn, NJ) with their dorsal side up. Agarose blocks were then placed into 12-well plate dishes containing PBST for image acquisition. Individual agarose blocks with embedded embryos were placed on a glass bottom petri dish and imaged using fluorescent microscopy as described below.

Image Acquisition and Morphological Analysis

Images were obtained using either a 20x dry or 40x oil (N.A: 1.30) objective mounted on a Zeiss Axiovert 200M inverted microscope with epifluorescence and equipped with an ORCA-

ER digital camera (Hammamatsu, Japan) and a Zeiss ApoTome. For motoneuron axon analysis, the 20x dry objective was used to acquire single focal plane images. Image stacks (step size interval 0.5-0.8 μm) from representative control and α2 MO-injected zebrafish were taken using the 40x oil (N.A. 1.30) objective and the ApoTome. Quantification of motoneuron morphology was performed using the 20x images. For α2 labeling in MO-injected embryos, control and α2 MO embryos were processed in the same tube to ensure consistent antibody labeling in all the animals. Tail clippings were performed to distinguish the control from the α2 MO embryos. Single focal images were acquired using the 20x dry objective for the control MO embryos. Images of the α2 MO embryos were acquired at the same exposure settings as the control MOs. Knockdown of expression was determined based on the single focal plane images. For presentation purposes, serial stacks (step size interval 0.5-0.8 μm) were obtained using the 40x oil objective. Serial stacks through dorsal spinal cord from dorsally embedded zebrafish were acquired for Rohon-Beard neuron migration analysis. RB migration distances were obtained using AxioVision 4.7.1 (Carl Zeiss). First, the midline of spinal cord was determined by taking half of the total distance between the most lateral left and right boundaries of spinal cord. Then, the distance from the center of each RB nuclei to the midline was measured. The migration distance of several RB cells was measured from each animal. Image analysis focused on the 4-6 segments that span the yolk sac extension. Image stacks were reconstructed using Imaris 5.7.2 volume-rendering software (Bitplane Inc., Saint Paul, MN). Images were cropped using Photoshop 7.0 (Adobe, San Jose, CA) and CorelDraw Graphics Suite 12 (Ottawa, Ontario, CA) was used to create cartoon diagrams and organize the figures. Photomicrographs of lateral views are presented with rostral to the left and dorsal to top. Photomicrographs of dorsal views are presented with rostral to the top.

Statistics

All values are reported as means ± standard error of the means (SEM). One way analysis of variance (ANOVA) for repeated measures analysis (with Holm Sidak post-test) was performed to test for significance in SigmaStat3.5. A Mann-Whitney U test was used for comparisons of non-parametric values and Student t-tests were used for comparisons of normally distributed values as indicated. Statistical significance was assigned if the p value was <0.05.

Results

nAChR α2 Subunit Expression on Sensory Structures

nAChR α2 RNA was previously detected in zebrafish spinal cord as early as 24 hpf using in situ hybridization (Zirger et al., 2003). Here we show that nAChR α2 protein was expressed in dorsal spinal cord in a pattern similar to that observed for Rohon-Beard neurons (Fig. 5.1A-C). RB neurons are among the earliest born sensory neurons in embryonic zebrafish (Bernhardt et al., 1990). They are characterized by their large soma and dorsal position within spinal cord. They possess rostral and caudal axonal projections and processes that exit dorsal spinal cord to innervate the skin (Clarke et al., 1984). They are the primary sensory neurons present before dorsal root ganglia are born (An et al., 2002) and have been implicated in initiating and mediating locomotive behaviors (Ribera and Nusslein-Volhard, 1998). The identity of these α2 immunoreactive neurons was confirmed in 24 hpf wildtype embryos using the anti-Hu antibody to label RB neurons and in 22 hpf Tg(*isl3*:GFP) embryos which express GPF on RB neurons (Fig.5.1A-F). The same pattern of expression was evident from 48 to 60 hpf, but by 72 hpf RB neurons no longer expressed the α2 subunit (not shown).

We also observed expression of the α2 subunit in the olfactory organ in what appeared to be olfactory sensory neurons (Sato et al., 2005). The olfactory system is comprised of the peripherally derived olfactory sensory neurons and the olfactory bulb of the central nervous

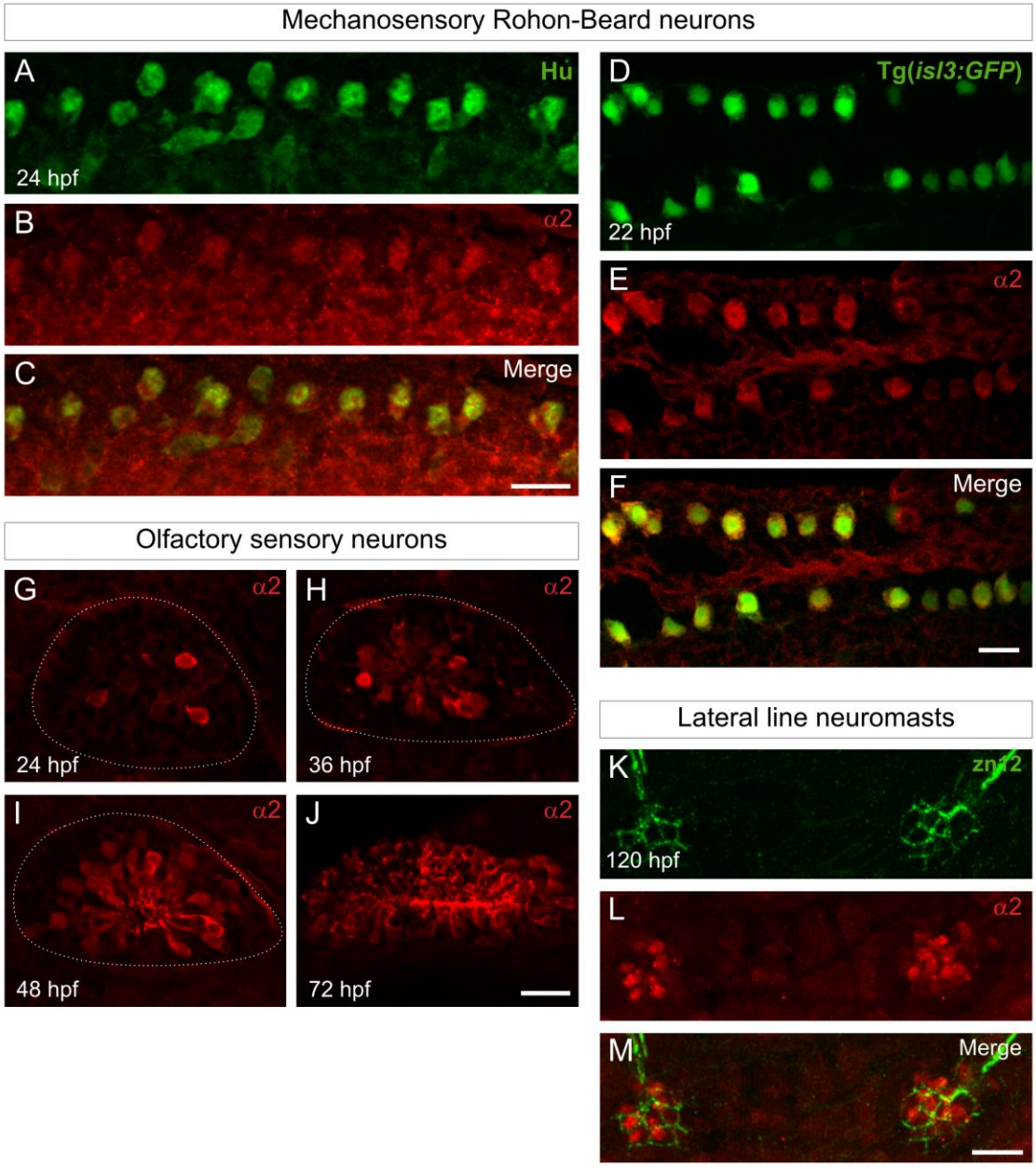

Figure 5.1. nAChR α2 subunit expression is detected in sensory neurons. A) Photomicrograph (lateral view) of a 24 hpf wildtype embryo labeled with anti-Hu. B) α2 labeling in the embryo shown in A. C) Merged image showing α2 labeled RB neurons in the dorsal region of the trunk. D) Dorsal view of RB neurons (green) in a 22 hpf Tg(*isl3*:GFP) embryo. E) α2 immunoreactivity in the embryo shown in D localizes with GFP positive RB mechanosensory neurons. C) Merged image showing α2 immunoreactivity localized to GFP positive RB cells. (G-J) α2 nAChR is also expressed by olfactory sensory neurons. At 24 hpf, the olfactory sensory neurons display weak immunoreactivity (G) and as the embryos age, immunoreactivity becomes stronger and evident in more cells (H-J). The dashed white line indicates the outline of olfactory epithelium. (K-M) Labeling with the zn12 antibody reveals the lateral line nerve (green) and associated neuromasts (red). Cells within the neuromast label with the α2 antibody (red). Merged image shows that neuromasts, but not the lateral line nerve, label with the α2 antibody. Scale bars, 20 μm.

system. The olfactory sensory neurons make connection into the olfactory bulb and the mature olfactory system responds to chemical environmental cues that mediate a variety of behavioral responses (Vitebsky et al., 2005). In the developing zebrafish embryo, differentiation of the olfactory placode occurs very rapidly (Hansen and Zeiske, 1993). Therefore, as the olfactory epithelium appeared to mature (from 24 to 72 hpf), we detected more α2 immunopositive cells (Fig. 5.1G-J). Alpha2 immunoreactivity in the olfactory neurons was evident until 8 dpf which was the latest point analyzed (not shown).

Antibody labeling with anti-α2 also revealed strong immunoreactivity on elements of the lateral line system. The lateral line system in fish consists of the lateral line ganglia and sensory organs known as neuromasts. The lateral line is a sense organ which can detect differences in dynamic water movements and plays a role in prey detection, predator avoidance and schooling behaviors (Whitfield, 2005). Specifically, the α2 subunit was expressed in neuromast cells between 36 and 48 hpf (not shown). At later stages of development, neuromasts migrate ventrally away from the horizontal myoseptum and are innervated by fibers of the lateral line nerve (Becker et al., 2001). At 5 dpf, neuromasts strongly label with the α2 antibody but the lateral line nerve and the innervating fibers, revealed by zn12 labeling, did not express α2 (Fig. 5.2K-M). This pattern of expression was evident until 8 dpf (latest time point analyzed, not shown).

nAChR α2 Subunit Localizes to Secondary Motoneurons and Their Axons

Expression of nAChR α2 subunits was apparent in motoneuron axons as early as 48 hpf (not shown). To test whether secondary motoneurons expressed nAChR α2 subunits, we used the Tg(*isl1*:GFP) line of zebrafish which expresses GPF in a subpopulation of secondary motoneurons and their axons (Fig. 5.2A and D). At 72 and 96 hpf, it was evident that GFP-positive dorsal projecting axons and GFP-positive motoneuron somata in ventral spinal cord

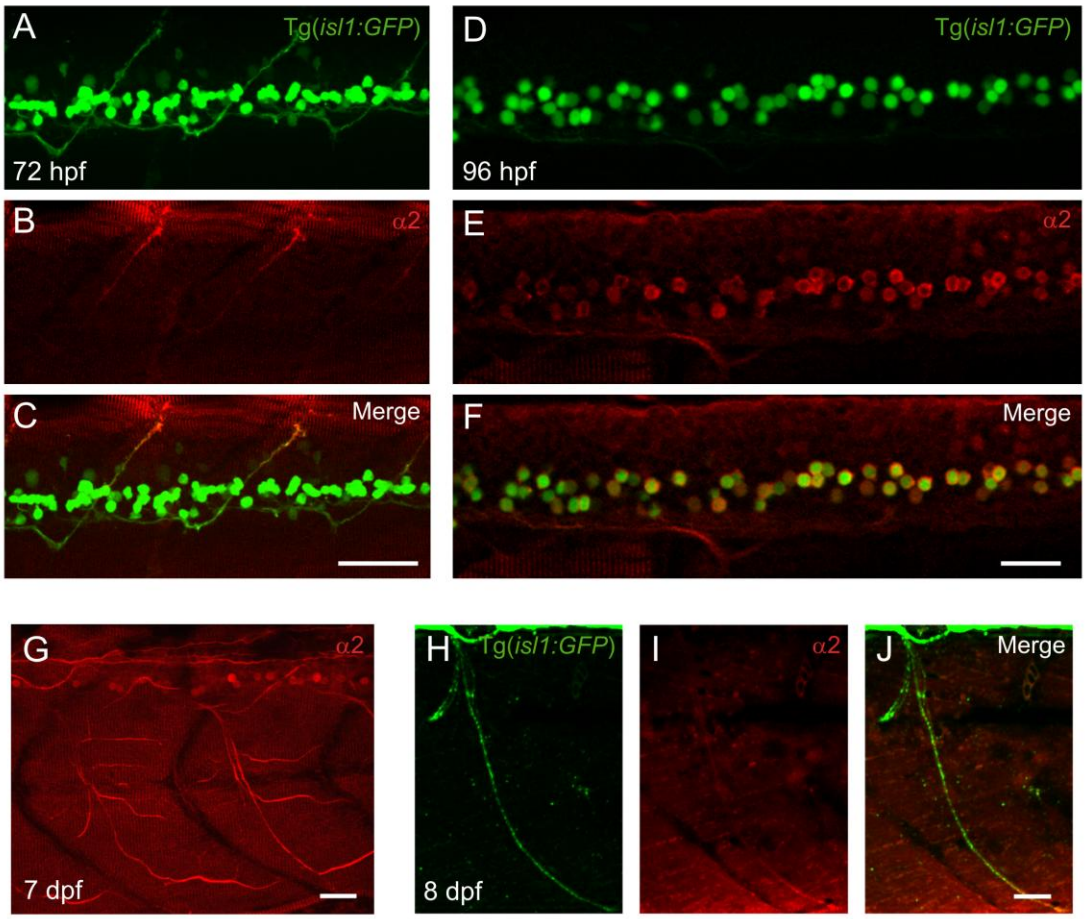

Figure 5.2. nAChR α2 subunit expression in secondary motoneurons. The α2 antibody was used to detect the zebrafish α2 nAChR subunit at various developmental time points. A) Photomicrograph of GFP expression in a 72 hpf Tg(*isl1*:GFP) larva. B) α2 antibody labeling of the larva shown in A. C) Merged image shows that the α2 antibody labeled dorsal projecting, GFP-positive secondary motoneuron axons. D) Photomicrograph of GFP expression in a 96 hpf Tg(*isl1*:GFP) larva. E) α2 antibody labeling in the larva shown in D. F) Merged image shows that α2 antibody labeled GFP positive secondary motoneuron somata. G) α2 antibody labeling at 7 days of age detected elaborate axonal trajectories within the dorsal and ventral myotomes. These are likely motoneuron axon trajectories. H) Photomicrograph of GFP expression in an 8-day old Tg(*isl1*:GFP) zebrafish. I) α2 antibody labeling in the zebrafish shown in H. J) Merged image shows that the α2 antibody labels ventral projecting, GFP-positive secondary motoneuron axons. Scale bars in A-C and G, 40 μm; D-F and H-J, 20 μm.

expressed the α2 subunit (Fig. 5.2A-F). Alpha2 expression was evident at 7 dpf, but at these later developmental stages far more ventral projecting motoneuron axons were expressing the α2 subunit (Fig. 5.2G). At 8 dpf, α2 antibody labeling of the main ventral projecting nerve localized

with GFP positive ventral projecting secondary motoneuron axon in the Tg(*isl1*:GFP) line of zebrafish (Fig.5.2H-J).

Non-neuronal Expression of the nAChR α2 Subunit

nAChRs in the vertebrate skeletal muscle mediate fast excitatory synaptic transmission to the muscle fibers and they are localized on the plasma membrane composed of two α1 subunits and one each of β1, γ, and δ subunits (Kalamida et al., 2007). Zebrafish have slow, fast and intermediate muscle fibers characterized by distinct properties to accommodate a wide variety of swimming behaviors (Fetcho and O'Malley, 1995). Alpha2 antibody labeling revealed strong expression in the nuclei of the mononucleated slow muscle as early as 24 hpf (Fig. 5.3A). A similar pattern of expression was observed at all time points analyzed up to 8 dpf (Fig. 5.3B-D and data not shown). Nuclei of multinucleated fast muscle also expressed the α2 subunit at 24 hpf and 36 hpf (Fig.5.3E and F). Following 36-48 hpf, fast muscle nuclei expression was no longer detected (Fig.5.3G and H).

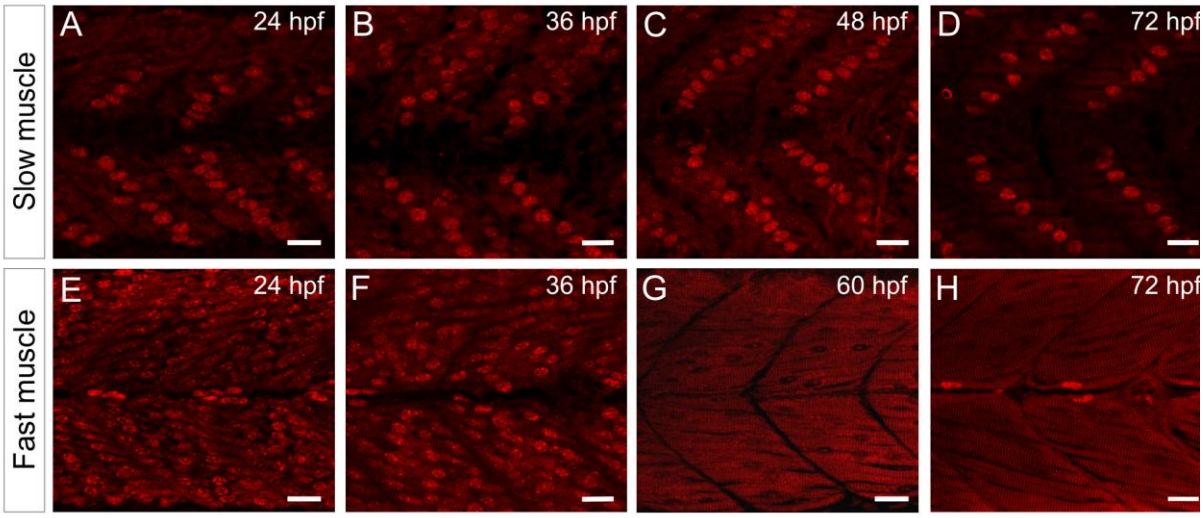

Figure 5.3. Non-neuronal expression profile of nAChR α2 subunit. Anti-α2 antibody labeled fast muscle nuclei (A-D) and slow muscle nuclei (E-H) as early as 24 hpf. The expression of α2 nAChR subunit by the nuclei as indicated by antibody labeling is developmentally regulated. Fast muscle nuclei labeling was absent after 60 hpf, but slow muscle nuclei labeling was present until 8 dpf (latest point analyzed), but presented here at 72 hpf. Scale bars, 20 μm.

Blocking α2 nAChR Expression *in vivo* by Morpholino Antisense Oligos

Antisense morpholino oligonucleotides can be designed to disrupt efficient splicing of its nascent mRNA (Draper et al., 2001). Here, an α2 splice blocking MO was designed to disrupt splicing at the exon2-intron2 boundary of the 6-exon nAChR-α2 transcript, thus resulting in exon 2 skipping during nAChR α2 mRNA processing *in vivo*. (Fig.5.4 A). Reverse transcription polymerase chain reaction analysis (Fig. 5.4B) and immunohistochemistry (Fig. 5.5) were used to assess knockdown success of the α2 subunit following α2 MO microinjection. RT-PCR analysis in 24 and 48 hpf zebrafish confirmed that injection of the α2 MO disrupted effective splicing of its native RNA. This was revealed by the shifted fragment (~450 bp) when compared to its control spliced counterpart (~590 bp) (Fig. 5.4B).

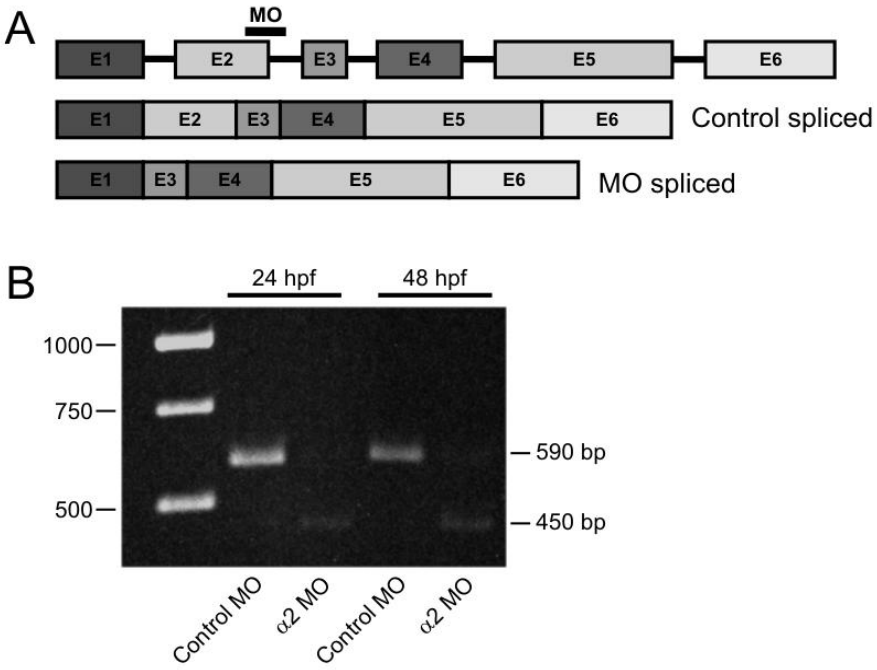

Figure 5.4. Embryos injected with α2 MO blocked mRNA splicing. A) An α2 splice blocking MO was designed to target the exon2-intron2 boundary in the 6-exon nAChR-α2 transcript. The MO is predicted to result in exon 2 skipping during nAChR α2 mRNA processing *in vivo*. Control and α2 MO are expected to amplify at ~590 bp and ~450 bp, respectively. B) RNA from 24 and 48 hpf zebrafish were reverse-transcribed and amplified using α2 subunit specific primers. The PCR products from control MO and α2 MO-injected zebrafish were consistent with the size predicted in A.

Immunohistochemistry was also used to assess the efficacy of the α2 MO in blocking the α2 subunit protein expression. At 33 hpf, wildtype zebrafish embryos injected with a control MO exhibited strong α2 expression in slow and fast muscle (Fig. 5.5A and C, respectively), olfactory neurons (Fig. 5.5E), and Rohon-Beard neurons (Fig. 5.5G). Injection of the α2 MO significantly reduced α2 expression in the muscle (Fig. 5.5B and D), olfactory (Fig. 5.5 F) and Rohon-Beard neurons (Fig. 5.5H and I). We also confirmed that absence of α2 immunoreactivity in RB neurons in α2 MO-injected embryos was not due to lack of RB cells (Figure 5.5J and K). These results indicated that α2 MO injection could successfully block the expression of the nAChR α2 subunit *in vivo*.

Alpha2-Containing nAChRs and Their Role(s) in Nicotine-Induced Motor Output

Zebrafish embryos exhibit spontaneous activity in the form of musculature bends which begins at ~17 hpf when primary motoneurons axons make their initial contacts with muscle fibers (Melancon et al., 1997; Saint-Amant and Drapeau, 1998). This spontaneous motor output peaks at 19-20 hpf and gradually decreases by 27-28 hpf (Saint-Amant and Drapeau, 1998; Thomas et al., 2009). It was previously shown that it can be modulated by cholinergic agonists, such as acetylcholine and nicotine (Thomas et al., 2009). Zebrafish embryos transiently exposed to these agonists elicit a swim-like behavior in the form of rhythmic left-right-left musculature bends. This increased rhythmic motor output is most likely mediated through the activation of nicotinic acetylcholine receptors located on spinal neurons of the central pattern generator (CPG). However, the specific nAChRs underlying these effects are not yet known. Therefore, we took advantage our ability to knockdown the nAChR α2 subunit expression *in vivo* to examine the potential implication of α2-containing nAChRs in mediating these responses.

We first evaluated the baseline spontaneous activity in zebrafish embryos injected with the α2 MO at different developmental stages (Fig. 5.6). Embryonic motor activity was

Figure 5.5. Injection of α2 splice block MO abolished nAChR α2 subunit immunoreactivity. Embryos injected with a control MO displayed nAChR α2 immunoreactivity in slow muscle nuclei (A), fast muscle nuclei (C), olfactory sensory neurons (D) and Rohon-Beard neurons (G, yellow arrowheads). nAChR α2 immunoreactivity was absent in embryos injected with an α2 MO (B,D,F,H and I) indicating that α2 nAChR mRNA was not translated to protein. Dotted line in E and F denotes the boundary of the olfactory sensory organ. J and K) Double antibody labeling using zn12 and α2 antibodies in 31-hpf control MO (J) and α2 MO-injected embryos (K). The zn12 antibody was used to label RB neurons in dorsal spinal cord to confirm the specific knockdown of the α2 subunit expression specifically in RB neurons**.** Scale bars in A-F, 40 μm; G-K, 20 μm.

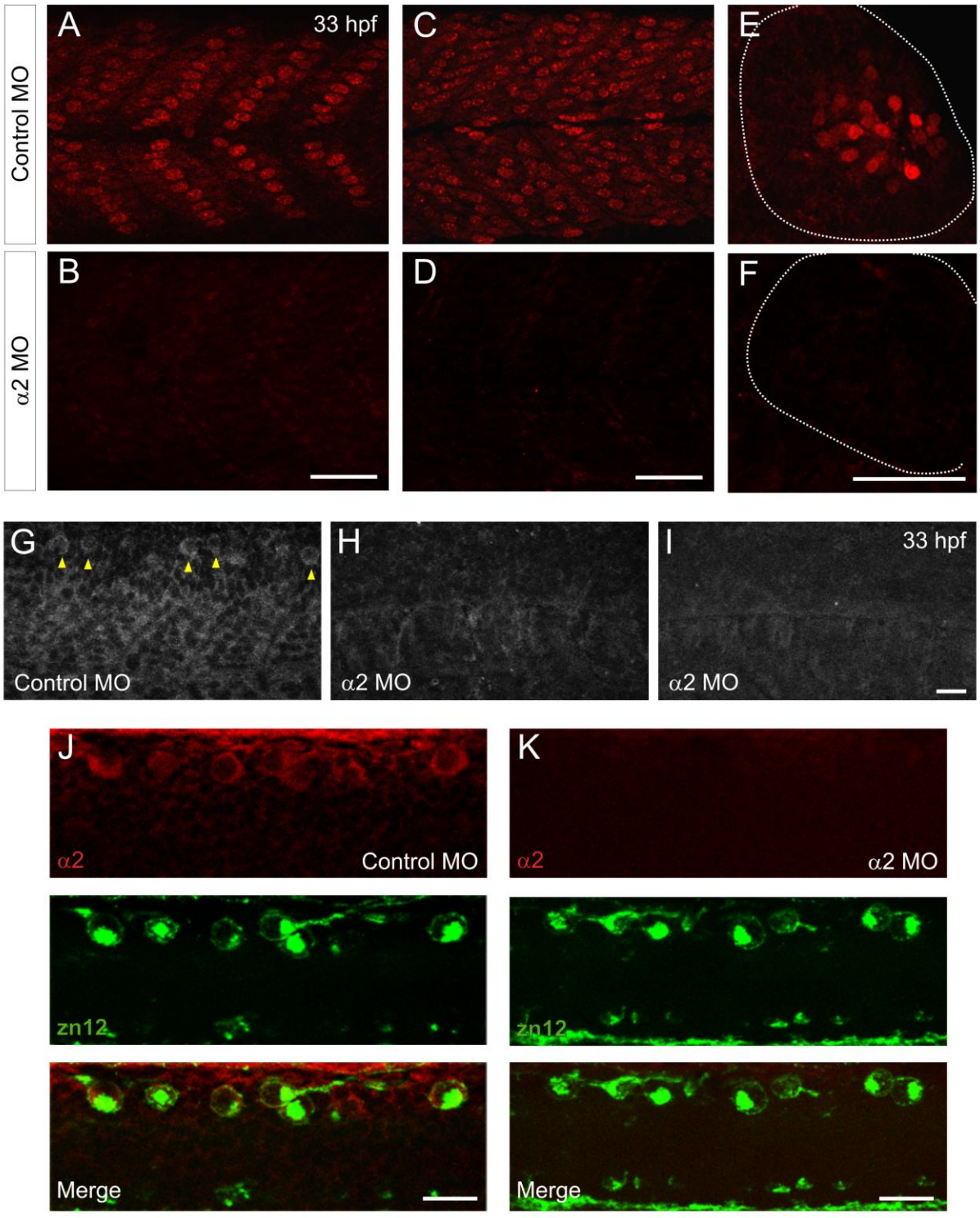
Control MO
α2 MO
A
33 hpf
C
E
B
D
F
G
Control MO
H
α2 MO
I
33 hpf
α2 MO
J
α2
Control MO
K
α2
α2 MO
zn12
zn12
Merge
Merge

videotaped between three and five minutes (Fig. 5.6A) and zebrafish bend rates were plotted across time points (Fig. 5.6B). The spontaneous bend rate of zebrafish embryos injected with the α2 MO peaked at ~20 hpf and steadily decreased by 28 hpf. Their baseline motor activity was hence similar to control MO-injected embryos (Fig. 5.6B) and are in accord with studies that have characterized the spontaneous activity in zebrafish (Thomas et al., 2009; Saint-Amant and Drapeau, 1998).

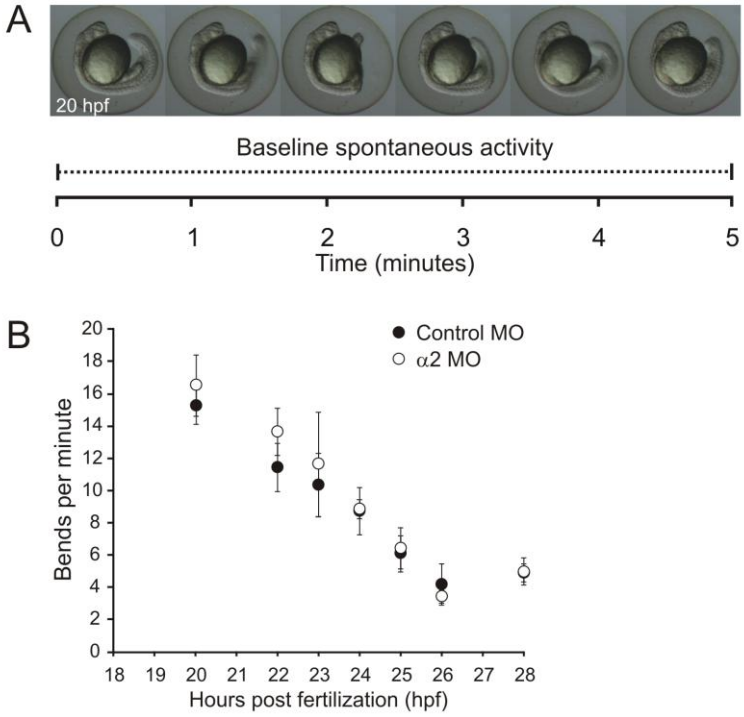

Figure 5.6. Embryonic motor behavior in zebrafish. A) Video stills of a 20 hpf embryo in the chorion demonstrating embryonic spontaneous motor activity. The spontaneous motor output (bends per minute) was quantified in a 3-5-minute epoch (dotted line, shown here for 5 minutes). B) Baseline spontaneous motor activity rates from control MO and α2 MO-injected embryos across developmental stages.

Since α2 MO injection did not affect the baseline spontaneous activity in zebrafish embryos, we were then in the position to examine whether α2-containing nAChRs could modulate embryonic motor behavior. To test this, we used nicotine which was previously shown to reliably increase the musculature bend rates in zebrafish (Thomas et al., 2009). The spontaneous activity of 25 hpf MO-injected embryos was first monitored for three minutes and

then transferred in embryo media containing 60 μM nicotine (Fig. 5.7A). Control MO-injected embryos exhibited increased bend rates when exposed to nicotine. In contrast, α2 MO-injected embryos displayed a much lower musculature bend rate when compared to stage matched controls (Fig.5.7B). When we plotted the bend rates of the individual control MO and α2 MO-injected embryos from the first minute of nicotine exposure (Fig. 5.7C, embryos from minute 4

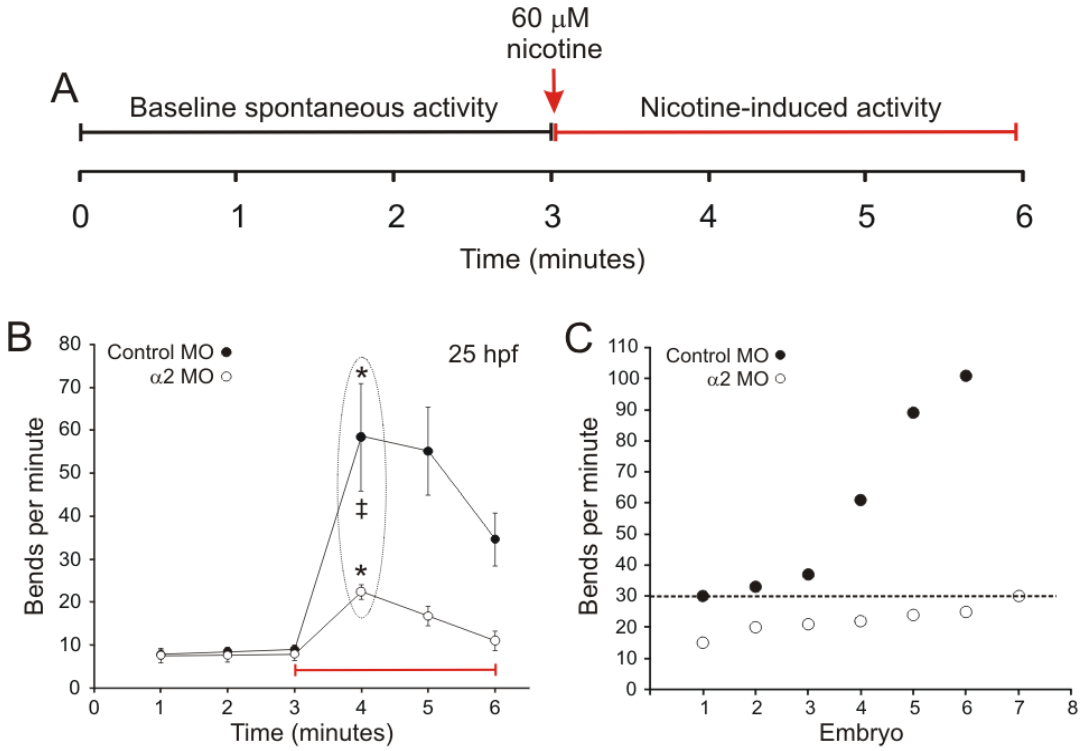

Figure 5.7. Nicotine-induced motor behavior in zebrafish. A) The baseline spontaneous motor activity of zebrafish embryos (in the chorion) was recorded for 3 minutes (black line) and at the end of minute 3, the embryos were transferred to embryo medium containing 60μM nicotine (red line) for another 3 minutes. B) Baseline spontaneous motor activity and nicotine-induced motor activity from 25 hpf embryos injected with a control MO (black circles, n=6) and the α2 MO (white circles, n=7). The black dashed circle indicates the embryos from minute 4 which were individually plotted in C. C) Bend rates from the individual embryos were taken from minute 4 as indicated by the dashed circle. Dashed line (threshold) marks the lowest bend rate produced by nicotine in control MO-injected embryos. Embryos injected with the α2 MO exhibited reduced bend rates in response to nicotine since most embryos had bend rates falling below the minimum, control threshold. Asterisks denote significant differences between baseline and nicotine-induced bend rates (control MO, $p<0.001$ and α2 MO, $p<0.05$; repeated measures ANOVA). ‡ denotes significance between control MO and α2 MO nicotine responses ($p<0.001$; repeated measures ANOVA).

in B), 6 out 7 α2 MO embryos had bend rates below the lowest control MO bend rate (Fig. 5.7C, red line indicates the lowest control MO bend rate). These results suggest that the nicotine-induced motor behavior in zebrafish is most likely mediated through the activation of α2-containing nAChRs.

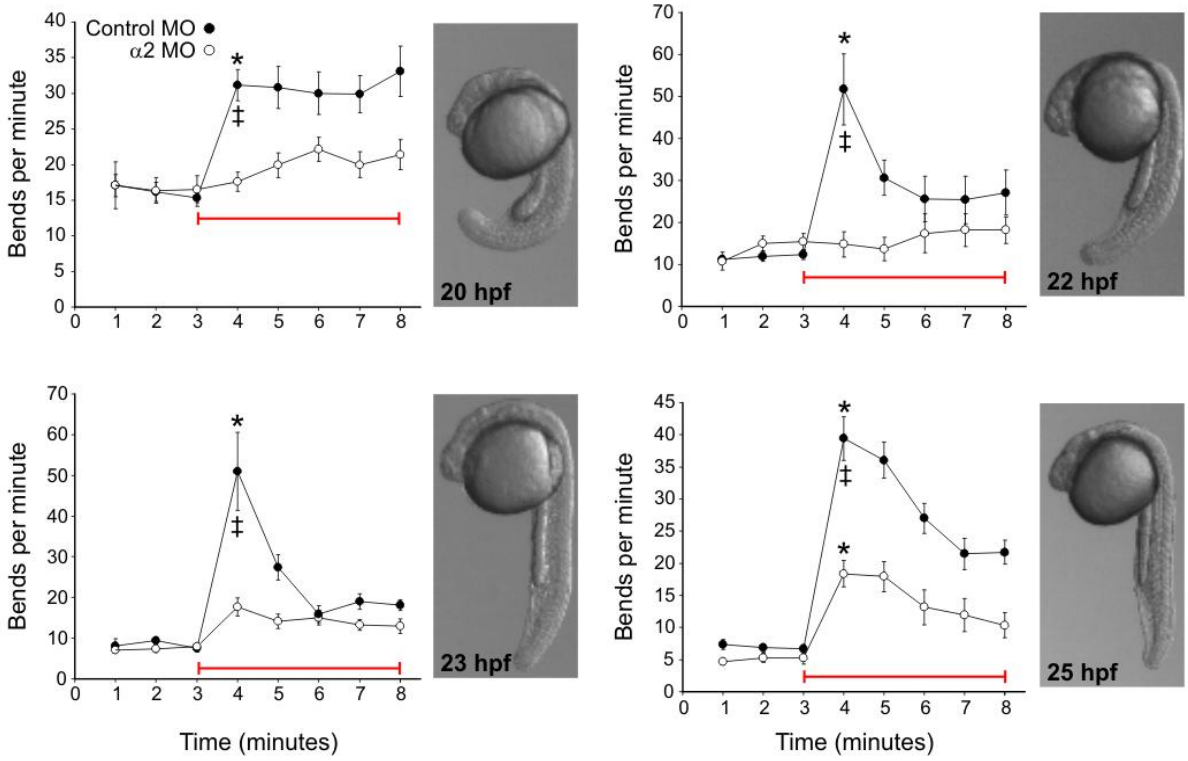

Figure 5.8. α2 MO injection reduces nicotine-induced motor output at various times in early embryogenesis. From top, baseline spontaneous motor activity (embryos in chorion) was recorded for 3 minutes and at the end of minute 3, embryos were quickly transferred into embryo medium containing 60μM nicotine. Between 20-22 hpf, the nicotine-induced motor behavior (red bar) was almost completely abolished in α2 MO-injected embryos when compared with their stage matched control MO counterparts. At later stages of development (>23 hpf), α2 MO-injected embryos respond to nicotine but their nicotine-induced motor output was still reduced when compared to control MOs. Asterisks denote significant differences between baseline and nicotine-induced bend rates ($p<0.001$; repeated measures ANOVA). ‡ denotes significance between control MO and α2 MO nicotine responses ($p<0.001$; repeated measures ANOVA).

The nicotine-induced swim-like behavior was examined at different developmental stages in MO-injected embryos since spinal neurons that are part of the embryonic spinal circuit producing locomotion in zebrafish are functional at a very young age (Downes and Granato,

2006). At 19-20 hpf, the nicotine-induced motor output was completely abolished in embryos injected with α2 MO. Motor activity in response to nicotine was also reduced to almost completely abolished in 21-22 hpf α2 MO-injected embryos (Fig. 5.8, 20 and 22 hpf). This nicotine-induced motor output was not completely abolished by the α2 MO at later stages of development (23 and 25 hpf, Fig. 5.8), but it was still greatly reduced at all the time points analyzed thereafter when compared to control MO-injected embryos (latest point analyzed was 28 hpf).

The Act of Dechorionation Increases the Musculature Bend Rates

Neural networks of the central pattern generator (CPG) produce the swim-like motor behaviors in zebrafish. These locomotive behaviors are governed by input/output elements (sensory neurons and interneurons/motoneurons and muscle) within the spinal circuitry (see Fig. 1.3 in Chapter 1). Therefore, it was necessary to determine whether the reduced nicotine-induced motor behaviors in α2 MO-injected embryos involved defects in the input or output elements of the spinal network. In order to explore these possibilities we used the act of dechorionation to unveil any potential defects on the output elements involved with the motor behavior. Zebrafish remain in their chorions during embryonic stages of development and when embryos are dechorionated, an increase in the musculature bend rate occurred (Saint-Amant and Drapeau, 1998; Thomas et al., 2009).

Zebrafish embryos injected with the α2 MO exhibited a reduced motor output in response to nicotine at 22 hpf (Fig. 5.9B, minute 4). When the same embryos were allowed to recover back to baseline and then manually dechorionated, they exhibited increased musculature bend rates similar to bend rates of controls (Fig. 5.9). The ability of the α2 MO-injected embryos to produce robust motor outputs following the act of dechorionation suggested that output elements

(motoneurons and/or muscle) associated with the swim-like motor behaviors were not contributing in the reduced nicotine-induced responses in the α2 MO-injected embryos.

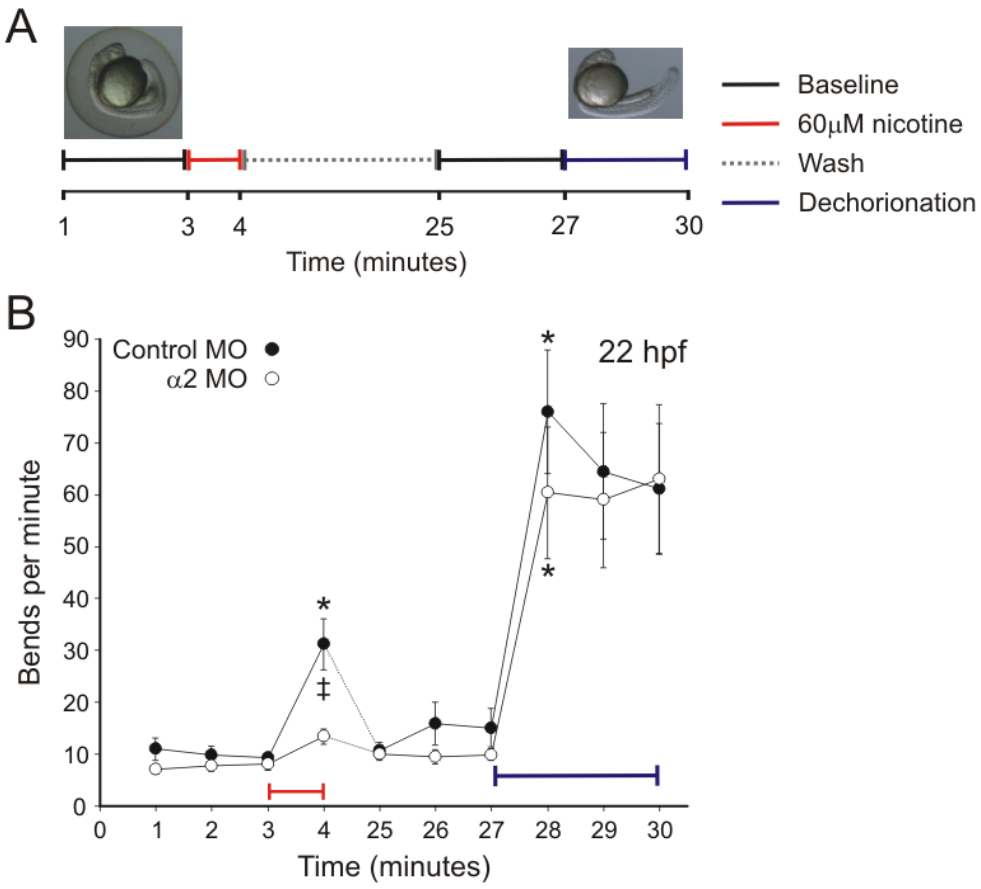

Figure 5.9. Blocking nAChR α2 subunit expression and its affect on non-nicotine-induced motor output produced by dechorionation. A) Experimental design for the dechorionation experiment. The spontaneous motor activity was first recorded while embryos were still in their chorions for 3 minutes (black). They were then transferred in embryo medium containing 60μM nicotine for 1 minute (red bar) and subsequently placed in fresh embryo media and allowed to wash for 20 minutes (dashed line). Following the 20-minute wash the spontaneous activity was recorder for 3 minutes and at minute 27, embryos were quickly dechorionated (blue bar). Their motor activity following dechorionation was recorded for 3 minutes. B) Quantification of motor behaviors as described in A. The nicotine-induced response of 22 hpf α2 MO-injected embryos (n=10) was reduced but dechorionation (blue bar) produced the same large increase in the bend rate when compared to their control counterparts (n=10). Asterisks denote significant differences between baseline and nicotine-induced bend rates (control MO, $p<0.001$ repeated measures ANOVA). ‡ denotes significance between control MO and α2 MO nicotine responses ($p<0.001$; repeated measures ANOVA).

Knocking Down nAChR α2 Subunit Expression Does Not Alter Motoneuron or Muscle Development

Our findings from the dechorionation experiment predicted that the components comprising the output side of the motor behavior would not be affected by α2 subunit knockdown. In order to test this, we closely examined the morphological development of motoneurons (PMN and SMN) and muscle. We also assessed the ability of motoneuron axons to properly recognize postsynaptic muscle targets using α-bungarotoxin. At 30 hpf, there were no differences in primary motoneuron axons and slow muscle fibers between control and α2 MO-injected embryos (Fig.5.10A-D, Table 5.1). When analyzed at 26 hpf, the postsynaptic targeting of motoneuron axons did not appear to be altered by injecting either control or α2 MO (Fig.5.10E and F). Since secondary motoneurons and their axons labeled with the α2 antibody (see Fig.5.2), we examined whether the injection of the α2 MO played a role in their development. At 72 hpf, α2 MO-injected zebrafish had no differences in their axonal morphologies when compared to their control MO-injected embryos (Fig.5.10G and H, Table 5.1). These findings suggest that reduction of the nicotine-induced motor output in α2 MOs is most likely mediated through upstream input elements of the spinal circuit associated with the swim-like behaviors (see Fig.1.3 in Chapter 1).

Table 5.1. Morphology of PMN and SMN axons in control and α2 MO-injected zebrafish.

	Normal (%)			Total hemisegments
	Dorsal	Ventral	Mediolateral	
Primary motoneurons (znp1)				
Control MO	93.96±1.99	88.88±5.57	-	247 (n=18)
α2 MO	96.86±1.20	96.36±1.38	-	258 (n=18)
Secondary motoneurons (zn5)				
Control MO	89.54±2.43	88.01±2.24	98.05±1.16	246 (n=16)
α2 MO	91.86±1.95	88.50±1.71	95.28±1.67	585 (n=36)

Values are means±SEM. The number (n) of fish analyzed is indicated in the parenthesis. There was no statistical difference between Control MO and α2 MO ($p>0.05$, Mann Whitney U test).

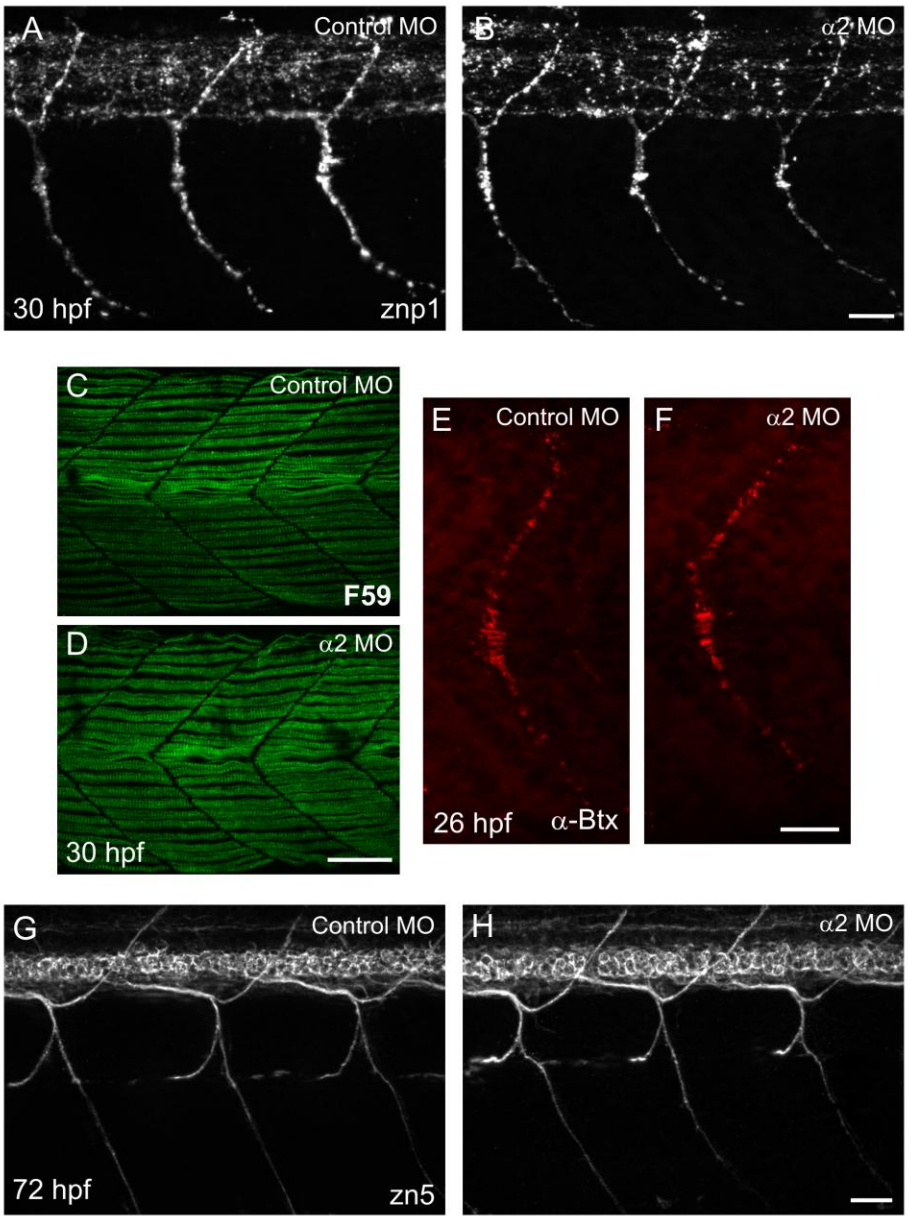

Figure 5.10. **Neuronal and muscle elements associated with motor output are not affected by knockdown of nAChR α2 subunit expression.** All panels are representative images of either control MO or α2 MO-injected embryos. A-B) Znp-1 immunoreactivity in 30 hpf control MO and α2 MO-injected embryos showing similar primary motoneurons axonal trajectories. C-D) Slow muscle fibers labeled with the antibody F59 have normal morphology with no signs of degeneration in control MO and α2 MO-injected embryos. E-F) At 26 hpf, neuromuscular junctions in control MO and α2 MO-injected embryos were stained with rhodamine-conjugated α-bungarotoxin (α-Btx). G-H) The antibody zn5 was used to label secondary motoneuron somata and axons in 72 hpf control MO and α2 MO-injected larvae. There were no obvious differences in SMN axon trajectories between the two groups of larvae. Quantitative results are shown in table 5.1 for primary and secondary motoneurons. Scale bars in C and D, 20 μm; A,B, E-H, 40 μm.

Knocking Down nAChR α2 Subunit Expression Does Not Alter Touch Response or RB Neuron Development

In addition to the swim-like motor behavior, zebrafish embryos possess a distinct behavioral response to tactile stimulation referred to as touch response. Mechanosensory Rohon-Beard neurons are thought to initiate and maintain the touch responses (Ribera and Nusslein-Volhard, 1998). RB neurons have peripheral processes that innervate the skin and are sensitive to mechanical stimulation through mechanosensory terminals. In response to touch, they can relay excitation from the skin to commissural interneurons that project into the contralateral spinal neurons of the CPG (Downes and Granato, 2006). This would in turn produce contralateral muscle contractions through the activation of motoneurons. Since zebrafish embryos expressed the nAChR α2 subunit on RB neurons (Fig. 5.1A-C), we assessed the role of RB neurons in mediating these behavioral responses by evaluating touch sensitivity in embryos injected with control and α2 MO. Any differences in their sensitivity to touch would indicate possible defects on RB neurons excitability, connectivity, or mechanosensation. Tactile stimulation to the trunk at 31 hpf induced a robust tail flip away from the stimulus site (Fig. 5.11A). Zebrafish embryos injected with α2 MO did not exhibit a reduction in touch responses when compared to control MO-injected embryos (Fig.5.11B).

We also examined aspects of RB neuron anatomy and development, focusing on RB neuron peripheral processes and RB neuron migration using antibodies for acetylated tubulin (aat) and anti-Hu, respectively. RB cells also extend peripheral processes into the skin in a stereotypical ventral projecting manner and can be easily visualized using aat immunoreactivity (Svoboda et al., 2001; Paulus et al., 2009). By 48 hpf, acetylated tubulin appears to fragment on the peripheral processes of RB neurons and this fragmentation process serves as an index of RB neurons entering programmed cell death (Svoboda et al., 2001). Embryos injected with α2 MO

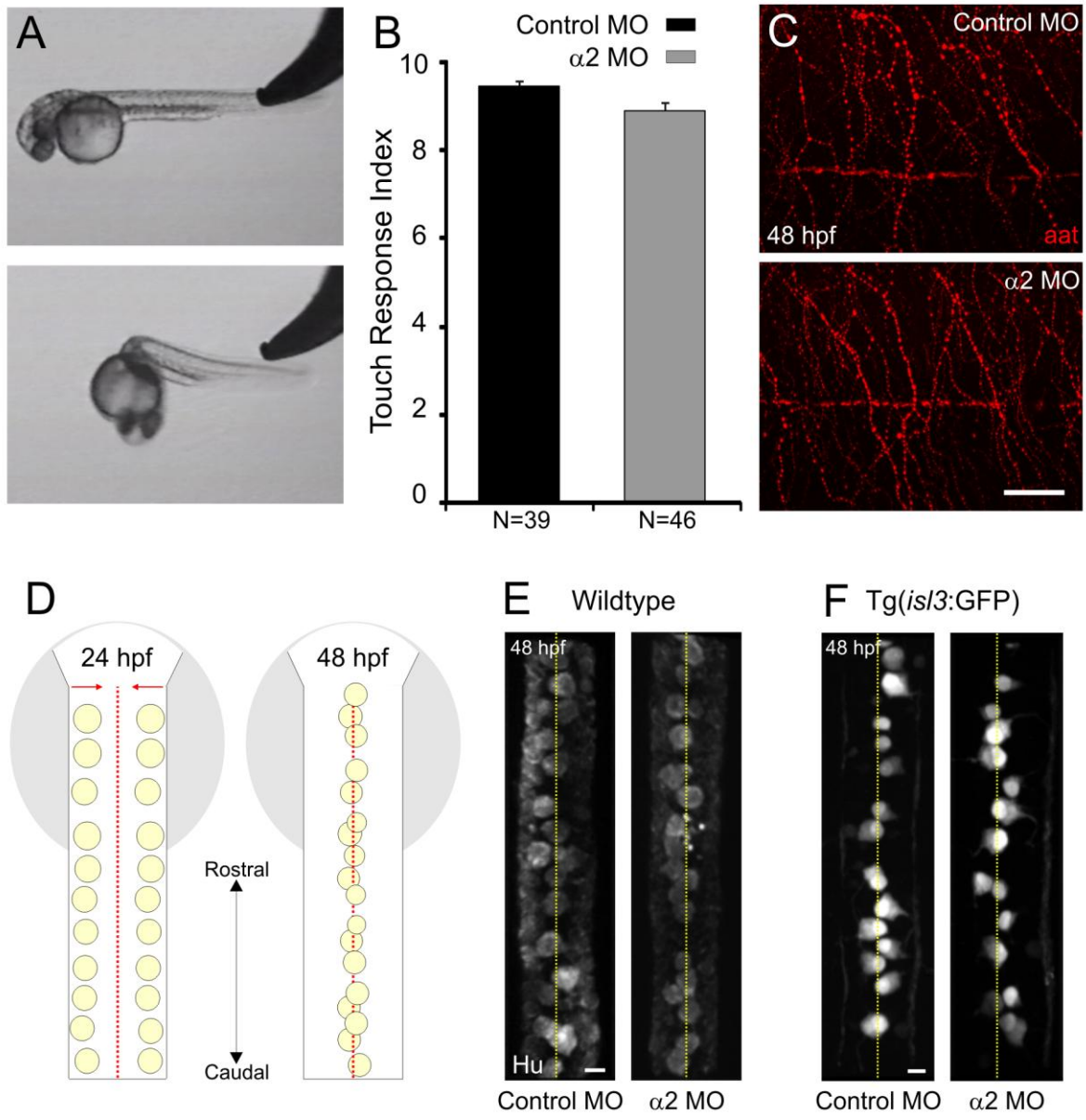

Figure 5.11. The effect of α2 MO injection on touch response and Rohon-Beard neuron development. A) Video stills from 31 hpf embryos that exhibit a touch response following tactile stimulation to their tails. B) Quantification of touch response from 31 hpf control and α2 MO-injected embryos. N indicates the number of embryos analyzed. C) Lateral view of anti-acetylated tubulin (aat) labeling reveals that Rohon-Beard processes are fragmented at 48 hpf in control MO (top, n=5) and α2 MO-injected embryos (bottom, n=3). D) Diagrammatic illustration reveals dorsal views of the migration of Rohon-Beard neurons (yellow circles). Early in development RB neurons are positioned bilaterally at the dorsolateral aspect of spinal cord (shown here at 24 hpf). Around 36 hpf they enter a migratory phase to the midline (indicated by red dashed line) forming an almost linear row of cells by 48 hpf. E) Dorsal views of RB neurons in 48 hpf wildtype zebrafish injected with a control and α2 MO. F) Dorsal views of RB neurons in 48 hpf Tg(*isl3*:GFP) zebrafish injected with a control and α2 MO. RB cells were labeled with the anti-Hu antibody and the midline is indicated by the dashed yellow line. Scale bars, 40 μm in C; 10 μm in E and F.

appear to have similar processes with fragmented tubulin projecting ventrally into the skin when compared to control MOs (Fig. 5.11C). During early stages of development (18-30 hpf), RB neurons can be seen in two bilateral rows in the dorsal and lateral-most aspect of spinal cord (Fig. 5.11D). RB neurons enter a migratory phase (~36 hpf) to the midline forming an almost single row of cells by 48 hpf (Paul and Svoboda, *submitted*). Therefore, by 48 hpf RB neurons should have reached the midline forming a single row of cells (Fig. 5.11D). In order to assess RB neuron migration, we labeled RB neurons with the anti-Hu antibody in wildtype embryos and also used the Tg(*isl3*:GFP) line of zebrafish which expresses GFP in RB neurons. When RB neuron migration to the midline was assessed in 48 hpf wildtype and Tg(*isl3*:GFP) embryos, there were no significant differences between α2 MO and control MO embryos (Table 5.2).

Table 5.2. Rohon-Beard cell migration to the midline in 48-hpf zebrafish.

		Fish (n)	RB cell (n)	Average RB cell distance from midline (μm)
Wildtype	Control MO	12	157	3.05±0.14
	α2 MO	16	193	2.95±0.13
Tg(*isl3*:GFP)	Control MO	7	67	2.73±0.19
	α2 MO	3	43	2.85±0.26

Values are means ± SEM. There was no statistical difference between control MO and α2 MO for wildtype and Tg(*isl3*:GFP) zebrafish ($p>0.05$, Student's *t*-test).

Discussion

The presence of nAChRs during early stages of embryogenesis suggests that they likely mediate nicotine-induced abnormalities in the developing nervous system. Since little is known about the specific nAChRs or the neuronal targets that mediate the nicotine-induced effects, it was thus important to characterize the expression profiles of these nAChRs in zebrafish. This

would provide insights on the underlying developmental responses to nicotine and also identify potential cellular substrates. In this chapter, we presented the expression profiles of the nAChR α2 subunit using α2 antibody labeling. Our findings revealed α2 expression on neuronal and non-neuronal structures in a developmentally regulated manner. Also, using an antisense modified oligonucleotide for the α2 subunit to knockdown α2 expression, we investigated the potential role(s) of α2-containing nAChRs during development. Our results indicate that functional nAChRs exist as early as 19-20 hpf in zebrafish based on the nicotine-induced activation of swim-like behaviors. We also provide great insight into possible neuronal substrates localized within the embryonic spinal cord that mediate the nicotine-induced behaviors through α2-containing nAChRs.

Differential Expression Patterns of the nAChR α2 Subunit

We detected the expression of α2 in a wide variety of neuronal and non-neuronal structures. The earliest developmental time point that neuronal α2 labeling was seen was at 22 hpf in RB neurons. Rohon-Beard neurons in the developing zebrafish and *Xenopus* are mainly thought to transmit mechanosensory information from the skin to spinal cord (Clarke et al., 1984). Dorsal root ganglia take over their role at later stages of development (>48 hpf). Therefore, the expression of the α2 subunit on RB neurons indicated that they could play a role during embryonic developmental processes. This is supported by the work of Paul and Svoboda (submitted manuscript), where embryonic nicotine exposure delayed RB cells from entering their normal programmed cell death pathway.

The α2 nAChR subunit was also detected on secondary motoneuron somata and their axons at later stages of development (>48 hpf). Embryonic nicotine exposure in zebrafish (see Chapter 2 and 3) caused secondary motoneuron axon pathfinding errors. These errors were mostly observed on dorsal projecting axons suggesting a different mechanism underlying the

nicotine effects for these axons. The presence of α2 subunit on dorsal projecting axons later in development may be associated with the formation of functional α2-containing receptors at these sites. If this were true, dorsal secondary motoneuron axons could be directly affected by nicotine exposures through activation of α2-containing nAChRs. This is supported by previous work in isolated embryonic spinal neurons, which showed that direct application of acetylcholine near growth cones mediates their guidance and turning and these responses were dependent upon nAChR activation (Zheng et al., 1994). Based on our findings, we support the idea that α2-containing AChRs are not required for normal motoneuron axon pathfinding but their sensitivity to cholinergic agonists makes them physiologically relevant in mediating nicotine-induced errors during axon pathfinding.

The α2 subunit was also expressed in structures of the lateral line system, specifically the sensory organs called neuromasts. The zebrafish lateral line system has been recently introduced as a model to study hair cell loss and regeneration. Hair cells and neuromasts share key sensory properties responsible for hearing and swimming behaviors, respectively (Ownes et al., 2009). It has been shown that acetylcholine is primarily released by efferent fibers onto outer hair cells of the cochlea and its actions are mediated via nAChRs in higher vertebrates (Elgoyhen et al., 2009).

We also showed that the α2 nAChR subunit, which is typically associated with neurons, localized to non-neuronal muscle fibers. Our findings are not unique in that aspect and are in agreement with similar results in the literature that demonstrated the expression of neuronal-type genes (α4, α5, α7, β4) in the skeletal muscle of the developing chick (Corriveau et al., 1995). The presence of α2-containing receptors in muscle fibers potentially implies a novel role for these channels. These ligand gated ion channels may be different from their conventional α1-containing muscle AChRs in that they have a greater permeability to calcium and sodium, thus

more efficiently elevating intracellular calcium levels. This is an intriguing possibility and this could suggest that their presence may facilitate specific developmental processes during a critical period of muscle development such as muscle differentiation and synaptogenesis.

Nicotine Modulation of Embryonic Motor Output

The nicotine-induced behavioral response has been previously established to serve as a diagnostic tool in identifying potential cell-specific targets and elucidating mechanisms underlying these locomotive behaviors (Thomas et al., 2009; Petzold et al., 2009). Zebrafish embryonic spontaneous activity and touch responses can occur in the absence of supraspinal inputs suggesting that these motor behaviors are intrinsic to neural networks within the spinal cord (Downes and Granato, 2006). This was also true in decapitated zebrafish embryos where nicotine was able to induce a swim-like behavior in the absence of brainstem inputs (Thomas et al., 2009).

In this chapter, we showed that nicotine-mediated responses appeared to be almost completely abolished in very young 19-22 hpf zebrafish embryos, whereas at later stages of development (23-28 hpf) α2 MO-injected embryos respond to nicotine but their nicotine-induced motor output was still reduced. These results indicate that early in development, activation of α2-containing nAChRs essentially mediates the nicotine-induced swim-like responses. However, as the embryo develops, additional spinals neurons develop which could potentially express different nAChR subunits that form other nAChR combinations, thus contributing to the nicotine responses at later stages of development. These findings altogether, provide evidence that α2-containing nAChRs are associated with modulating embryonic nicotine-induced motor behaviors. Importantly, α2-containing nAChRs do not seem necessary for normal non nicotine-induced motor output.

Candidate Spinal Neurons Modulating Swim-like Behaviors in Zebrafish

Our α2 morpholino knockdown experiments demonstrated that embryos exhibited normal spontaneous bursting activity but had reduced swim-like behaviors in response to nicotine. Motoneuron or muscle activation bypassing upstream elements of spinal cord would not be sufficient to produce alternating motor behaviors similar to the ones observed in response to nicotine. Therefore, candidate spinal neurons emerged involved in initiating and modulating swim-like behaviors in embryonic zebrafish. In this chapter, we provided evidence that RB neurons expressed the nAChR α2 subunit as early as 22 hpf (Fig.5.1E). During the normal course of development, RB cells may have functional α2-containing AChRs but may not be activated by endogenous acetylcholine. However, when they are presented with a robust excitation, in this case nicotine, all RB neurons could be potentially excited and result in generation of rhythmic motor activity. Our findings further support the above statements in that α2 MO injection did not affect the spontaneous bursting activity, yet dramatically reduced the nicotine-induced motor output. In figure 5.12C, we proposed a pathway for nicotine-induced motor output that involves RB neurons. Under this scenario, RB cells provide excitatory drive to CoPA interneurons which send their axons to contralateral excitatory cells of the CPG (EINs) which then drive motoneurons to release acetylcholine onto muscle fibers, thus producing muscle contractions. If α2 subunit expression is blocked, RB neurons may not be able to form functional receptors. This will render them unable to respond to cholinergic excitation and diminish the motor output produced by nicotine.

Other candidate cells that could be activated by nicotine include interneurons within the CPG. In mouse and *Xenopus*, motoneurons provide cholinergic excitatory feedback to interneurons within the CPG which helps sustain the motor output (Perrins and Roberts, 1995). Therefore, in order for these interneurons to mediate cholinergic signaling, they should possess

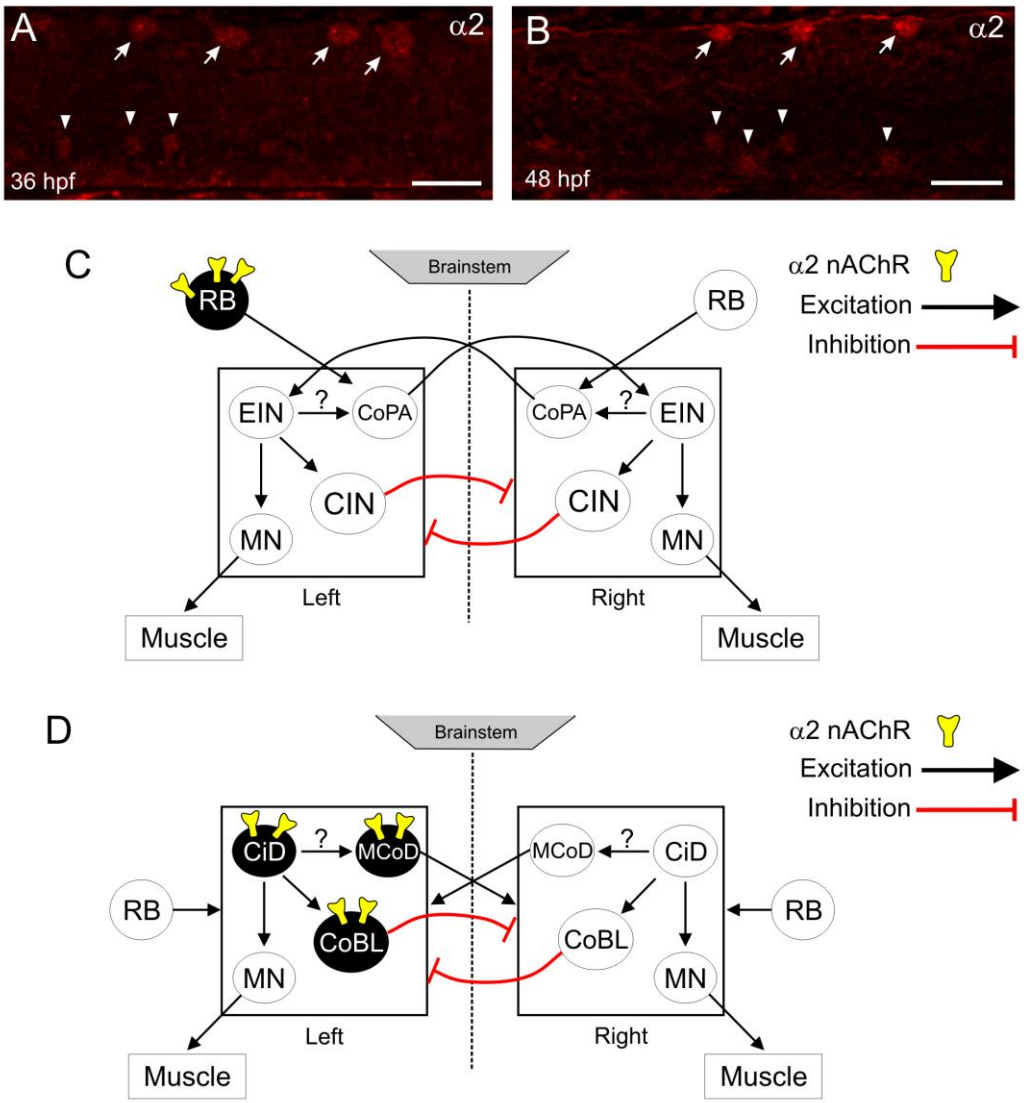

Figure 5.12. Candidate spinal neurons involved in nicotine-induced motor behavior. Photomicrographs of 36 (A) and 48 hpf (B) wildtype embryos labeled with the α2 antibody revealed Rohon-Beard neurons located in dorsal spinal cord (arrows) and spinal neurons located in ventral spinal cord (arrowheads). Scale bar, 20 μm. (C and D) Two proposed cellular models show possible interactions between the cells of the CPG that produce locomotor behaviors in zebrafish. Candidate cells are highlighted in black. C) Nicotinic activation of α2-containing nAChRs located on RB neurons can activate glutamatergic excitatory CoPA cells. CoPAs provide excitation to contralateral EINs of the CPG which then drive motoneurons to activate muscle. D) Based on the ventral position of the cells labeled with the α2 antibody in A and B, α2-containing nAChRs could also localize on either CiDs (EINs), MCoDs (CENs), or CoBLs (CINs). Question marks indicate synaptic connections that have not yet been identified. Dashed line indicates the midline of spinal cord. Abbreviations: EIN: excitatory interneuron; CEN: commissural excitatory interneuron; CIN: commissural inhibitory interneuron; CoPA: commissural primary ascending; CiD: commissural ipsilateral descending; MCoD: multipolar commissural descending; CoBL: commissural bifurcating longitudinal; MN: motoneuron; RB: Rohon-Beard neuron.

nAChRs. Based on our α2 expression profiles, ventrally located spinal neurons, presumably interneurons, also express the α2 subunit (Fig.5.12A and B, arrowheads). Based on the α2 expression profiles, there are likely three candidate interneurons in zebrafish that can be activated by nicotine to produce swimming. These include the excitatory interneurons, MCoDs and CiDs, and inhibitory interneurons, CoBLs (Hale et al., 2001; McLean et al., 2007). Our proposed pathway for nicotine-induced motor output that involves interneurons is shown in figure 5.12D. In this scenario, excitatory interneurons within the CPG can potentially assemble functional receptors containing the α2 subunit and hence by blocking the α2 expression, the nicotine-induced motor output can be disrupted.

In this chapter, we combined information from spatiotemporal expression profiles of the α2 subunit and behavioral responses to identify cell types targeted by nicotine. We provided evidence that cholinergic signaling through the activation of α2-containing nAChRs can modulate embryonic motor output in zebrafish. We also proposed that sensory RB neurons and interneurons within the CPG could likely mediate the actions of nicotine.

CHAPTER 6

SUMMARY AND CONCLUSIONS

Maternal smoking during pregnancy has been associated with cognitive and behavioral abnormalities in childhood and adolescence. Nicotine, one of the main ingredients of tobacco smoke has gained much attention because of its ability to mimic acetylcholine, the endogenous agonist of nicotinic receptors in developing systems. However, nicotine is a drug of abuse and fetal exposures involves levels of stimulation beyond those experienced during the normal course of development that can result in permanent alterations at later stages in life. However, the exact mechanisms by which nicotine exerts its effects during critical stages of development are not yet well understood. In this work, we took advantage of the zebrafish model to examine the effects of embryonic nicotine exposure on nervous system anatomy and function.

The first objective of this work focused on assessing neural specific effects following nicotine exposure. We specifically focused on the process of axon pathfinding of secondary motoneurons. Pathfinding errors in secondary motoneuron axons caused by nicotine exposure were first reported in 2002 in zebrafish (Svoboda et al., 2002) and these nicotine-induced effects were thought to directly act upon secondary motoneurons (SMNs) through the activation of nicotinic receptors. It was later discovered that during those exposure experiments, pathfinding errors coincided with degenerated muscle fibers (Welsh et al., 2009). This raised the possibility that nicotine exposure could directly activate muscle AChRs to cause muscle degeneration which then in turn, could lead to axonal pathfinding errors.

Therefore, the experiments in chapter 2 were geared towards addressing this issue, where we examined whether nicotine exposure can bypass muscle effects and directly affect motoneuron axon pathfinding. We performed experiments where zebrafish embryos were exposed to varying concentrations of nicotine at different exposure windows. We demonstrated that the motoneuron and muscle effects uncoupled in a dose-dependent manner following a long nicotine exposure window (same exposure at which motoneuron and muscle alterations

coincided). Exposure to high nicotine concentrations for a shorter period exhibited SMN axon pathfinding errors similar to the ones observed in zebrafish exposed to low concentrations for a longer period. In these experiments, 4 unique, abnormal axonal pathfinding errors that were caused by the exposure were identified which allowed us to demonstrate that different mechanisms most likely underlie the effects of nicotine exposure. For example, stalled axons were usually associated with an exposure paradigm that often resulted in muscle fiber degeneration. This was most likely the effect of high frequency Ca^{2+} transients at the growth cone due to over-activation of neuronal and muscle nAChRs. In contrast to stalls, trajectory errors were most likely associated with SMN axons following the incorrect paths, possibly established by PMN axons. This diversity of axonal pathfinding errors clearly demonstrated that different mechanisms likely underlie the nicotine-induced SMN axonal pathfinding errors.

Once it was evident that embryonic nicotine exposure could directly alter SMN axon pathfinding, we hypothesized that these nicotine-induced effects would persist into later stages of life. In order to address this, we developed a method allowing for consistent and efficient monitoring of motoneuron axon pathfinding in live juvenile and adult zebrafish. First, we selected and characterized a GFP-reporter fish [Tg(*isl1*:(GFP)] that expresses GFP in a subpopulation of SMNs and their axons to establish a working model for addressing long-term effects of embryonic nicotine exposure. Then we confirmed that nicotine exposure reliably produced similar effects on SMN axon pathfinding in Tg(*isl1*:(GFP) transgenic zebrafish similar to those observed in wildtype. We then developed a live imaging preparation where GFP could be visualized in the same transgenic animals over the course of several weeks. Using this approach, we demonstrated that zebrafish exposed to nicotine as embryos exhibited SMN axon pathfinding errors that persisted into adulthood.

If anatomical changes caused by nicotine exposure persisted into adult stages of life, these changes could potentially lead to physiological and/or behavioral alterations in the adult animal. In order to address this issue, we used the swimming behavior of zebrafish as an assessable endpoint for adult function. We demonstrated that adult zebrafish exposed to nicotine as embryos exhibited altered patterns of locomotor behavior without affecting the general properties of motoneuron activity. Several features that are indicative of swimming behavior in zebrafish were affected such as the overall swimming frequency, the relationship between burst duration over cycle time, and the alternating pattern of activity (contralateral phase). These results indicate that embryonic nicotine exposure may have caused alterations in the physiological properties of interneurons within the spinal circuitry that govern these distinct locomotor outputs, thus leading to altered patterns of swimming activity in adult zebrafish.

It is widely accepted that the actions of nicotine are mediated through the activation of nAChRs. In order to better understand the underlying effects of nicotine reported in this work, defining the spatiotemporal repertoire of nAChR's assembly and function is thus necessary. Therefore, we set out to investigate the spatial and temporal expression pattern of the nAChR α2 subunit using a zebrafish-specific antibody. We demonstrated that the expression pattern of α2 subunit was diverse and developmentally regulated. Rohon-Beard neurons were among the first neuronal structures that expressed the α2 subunit (~22 hpf, earliest time point detected). At later stages of development an up-regulation of the α2 subunit expression was evident and it appeared to mostly localize on secondary motoneurons and their axons. Then, we examined the potential role for α2-containing nAChRs during embryonic development in zebrafish. Blocking the expression of the α2 subunit altered the nicotine-induced swim-like behavior without affecting neuronal and muscle elements associated with this motor output (motoneurons and muscle).

Nicotine activates swimming in zebrafish via the activation of nAChRs located either in brainstem structures or spinal neurons. It was previously shown that nicotine could still activate swimming even in the absence of brainstem inputs (decapitated embryos). This indicated that functional nAChRs expressed by specific neurons in spinal cord were most likely mediating the nicotine-induced motor output. In addition to this, the expression of α2 nAChRs subunits on RB neurons and/or other spinal neurons as presented in Chapter 5, further suggests that α2-containing nAChRs are involved in initiating and maintaining nicotine-induced motor output.

Nicotinic AChRs play a fundamental role in the development of spatially and temporally complex neuronal signals. In developing systems, rich cholinergic inputs from different regions of the brain make synaptic contacts onto other neurons to modulate a wide range of cellular responses, such as neurotransmitter release, dendritic outgrowth, circuit excitability and other downstream signaling interactions. Perturbations that inappropriately alter cholinergic signaling in areas of the brain during critical stages of development can influence these responses and have associated with long-term behavioral consequences expressed later in life such as ADHD (Thapar et al., 2003).

People suffering from ADHD have altered dopaminergic transmission in the striatum and exhibit increased response inhibition, essential in all behavioral responses and executive functions (Levin et al., 2006). Response inhibition is a neural response governed by interneurons and in ADHD synaptic connections between these interneurons that modulate dopamine release are most likely altered following fetal exposure to nicotine. These alterations most likely underlie the behavioral attention deficits observed (Castellanos and Tannock, 2002). In this context, adult zebrafish exposed to nicotine as embryos exhibited altered locomotor activity and these effects suggested that changes in the spinal circuitry most likely underlie the alteration in locomotor behaviors. We also demonstrated that transient nicotine exposure can induce circuit excitability

in embryonic zebrafish and following a prolonged exposure, nicotine causes altered axonal projections of spinal neurons. Taken together, these findings strongly suggest that inappropriate activation of nAChRs in developing neurons during axon extension and outgrowth could lead to long-term alterations in synaptic connectivity and neural excitability and thus adult function. Therefore, perturbations of cholinergic signaling within neural networks that generate rhythmic patterns activity could result in altered adult behaviors including learning, memory or attention in humans, as well as swimming in fish.

How does nicotine exposure affect the synaptic connectivity and physiological properties of spinal interneurons? Which interneurons express nAChRs and how can they modulate neuronal excitability? In order to address these questions and better understand the underlying mechanisms of embryonic nicotine exposure, two approaches are necessary. First, a comprehensive characterization of the different nAChR subunits expressed in zebrafish is necessary. Current ongoing collaborative work between the Svoboda lab and Tanguay lab (Oregon State University) will fill this informational gap. We have evidence that Rohon-Beard neurons express both the $\alpha 2$ and $\beta 2$ nAChR subunits (Fig. 6.1). This implies that functional nAChRs are present in these neurons and are involved in the nicotine-induced behaviors. Second, whole-cell intracellular recordings from identified spinal interneurons and motor nerve recordings would provide evidence of nAChRs function *in vivo* and also provide information on the significance of cholinergic signaling in rhythmic patterns of behavior. Consequently, defining the varying combinations of nAChRs subunits, their spatial and temporal distribution, along with electrophysiological recordings from candidate cells will help understand the underlying mechanisms of nicotine exposure in the developing zebrafish.

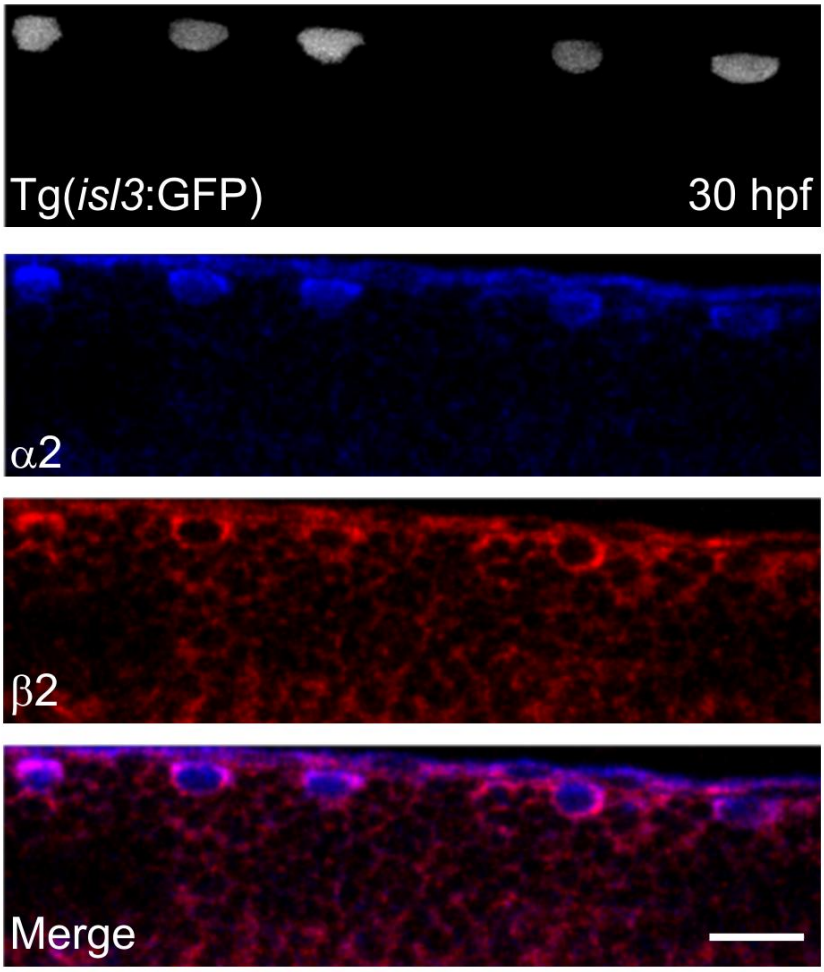

Figure 6.1. Rohon-Beard neurons express α2 and β2 nAChR subunits. Confocal images from a 30 hpf Tg(*isl3*:GFP) embryo showing GFP expression, labeling with the polyclonal α2 antibody (blue), and with a monoclonal β2 antibody (red) from the same embryo. Merged image shows that both the α2 and β2 antibody labeled GFP-positive RB neurons. Scale bar, 20 μm.

REFERENCES

Abreu-Villaça Y, Seidler F, Tate C, Slotkin T. 2003. Nicotine is a neurotoxin in the adolescent brain: critical periods, patterns of exposure, regional selectivity, and dose thresholds for macromolecular alterations. Brain Res 979:114-128.

Abreu-Villaça Y, Seidler FJ, Tate CA, Cousins MM, Slotkin TA. 2004. Prenatal nicotine exposure alters the response to nicotine administration in adolescence: effects on cholinergic systems during exposure and withdrawal. Neuropsychopharmacology 29(5):879-890.

Ackerman KM, Nakkula R, Zirger JM, Beattie CE, Boyd RT. 2009. Cloning and spatiotemporal expression of zebrafish neuronal nicotinic acetylcholine receptor alpha 6 and alpha 4 subunit RNAs. Dev Dyn 238(4):980-992.

Altringham JD, Ellerby DJ. 1999. Fish swimming: patterns in muscle function. J Exp Biol 202:3397-3403.

An M, Luo R, Henion PD. 2002. Differentiation and maturation of zebrafish dorsal root and sympathetic ganglion neurons. J Comp Neurol 446(3):267-275.

Appel B, Korzh V, Glasgow E, Thor S, Edlund T, Dawid IB, Eisen JS. 1995. Motoneuron fate specification revealed by patterned LIM homeobox gene expression in embryonic zebrafish. Development 121(12):4117-4125.

Atluri P, Fleck MW, Shen Q, Mah SJ, Stadfelt D, Barnes W, Goderie SK, Temple S, Schneider AS. 2001. Functional nicotinic acetylcholine receptor expression in stem and progenitor cells of the early embryonic mouse cerebral cortex. Dev Biol 240(1):143-156.

Baker ER, Zwart R, Sher E, Millar NS. 2004. Pharmacological properties of alpha 9 alpha 10 nicotinic acetylcholine receptors revealed by heterologous expression of subunit chimeras. Mol Pharmacol 65(2):453-460.

Beattie CE, Hatta K, Halpern ME, Liu H, Eisen JS, Kimmel CB. 1997. Temporal separation in the specification of primary and secondary motoneurons in zebrafish. Dev Biol 187(2):171-182.

Beattie CE, Melancon E, Eisen JS. 2000. Mutations in the stumpy gene reveal intermediate targets for zebrafish motor axons. Development 127(12):2653-2662.

Becker T, Becker CG, Schachner M, Bernhardt RR. 2001. Antibody to the HNK-1 glycoepitope affects fasciculation and axonal pathfinding in the developing posterior lateral line nerve of embryonic zebrafish. Mech Dev 109(1):37-49.

Behra M, Cousin X, Bertrand C, Vonesch J-L, Biellmann D, Chatonnet A, Strähle U. 2002. Acetylcholinesterase is required for neuronal and muscular development in the zebrafish embryo. Nat Neurosci 5(2):111-118.

Berger F, Gage FH, Vijayaraghavan S. 1998. Nicotinic receptor-induced apoptotic cell death of hippocampal progenitor cells. J Neurosci 18(17):6871-6881.

Bernhardt RR, Chitnis AB, Lindamer L, Kuwada JY. 1990. Identification of spinal neurons in the embryonic and larval zebrafish. J Comp Neurol 302(3):603-616.

Bernhardt RR, Schachner M. 2000. Chondroitin sulfates affect the formation of the segmental motor nerves in zebrafish embryos. Dev Biol 221(1):206-219.

Bhatt DH, McLean DL, Hale ME, Fetcho JR. 2007. Grading movement strength by changes in firing intensity versus recruitment of spinal interneurons. Neuron 53(1):91-102.

Bhatt DH, Otto SJ, Depoister B, Fetcho JR. 2004. Cyclic AMP-induced repair of zebrafish spinal circuits. Science 305(5681):254-258.

Boyd MR, McClellan AD. 2002. Changes in locomotor activity parameters with variations in cycle time in larval lamprey. J Exp Biol 205:3707-3716.

Brennan C, Mangoli M, Dyer CEF, Ashworth R. 2005. Acetylcholine and calcium signalling regulates muscle fibre formation in the zebrafish embryo. J Cell Sci 118:5181-5190.

Burns FR, von Kannen S, Guy L, Raper JA, Kamholz J, Chang S. 1991. DM-GRASP, a novel immunoglobulin superfamily axonal surface protein that supports neurite extension. Neuron 7(2):209-220.

Cangiano L, Grillner S. 2005. Mechanisms of rhythm generation in a spinal locomotor network deprived of crossed connections: the lamprey hemicord. J Neurosci 25(4):923-935.

Castellanos FX, Tannock R. 2002. Neuroscience of attention-deficit/hyperactivity disorder: the search for endophenotypes. Nat Rev Neurosci 3(8):617-628.

Cheesman SE, Layden MJ, Von Ohlen T, Doe CQ, Eisen JS. 2004. Zebrafish and fly Nkx6 proteins have similar CNS expression patterns and regulate motoneuron formation. Development 131(21):5221-5232.

Clarke JD, Hayes BP, Hunt SP, Roberts A. 1984. Sensory physiology, anatomy and immunohistochemistry of Rohon-Beard neurones in embryos of Xenopus laevis. J Physiol (Lond) 348:511-525.

Cohen G, Roux J-C, Grailhe R, Malcolm G, Changeux J-P, Lagercrantz H. 2005. Perinatal exposure to nicotine causes deficits associated with a loss of nicotinic receptor function. Proc Natl Acad Sci USA 102(10):3817-3821.

Cordero-Erausquin M, Pons S, Faure P, Changeux J-P. 2004. Nicotine differentially activates inhibitory and excitatory neurons in the dorsal spinal cord. Pain 109(3):308-318.

Cornelius MD, Day NL. 2009. Developmental consequences of prenatal tobacco exposure. Curr Opin Neurol 22(2):121-125.

Corriveau RA, Romano SJ, Conroy WG, Oliva L, Berg DK. 1995. Expression of neuronal acetylcholine receptor genes in vertebrate skeletal muscle during development. J Neurosci 15(2):1372-1383.

Crow MT, Stockdale FE. 1986. Myosin expression and specialization among the earliest muscle fibers of the developing avian limb. Dev Biol 113(1):238-254.

Dajas-Bailador F, Wonnacott S. 2004. Nicotinic acetylcholine receptors and the regulation of neuronal signalling. Trends Pharmacol Sci 25(6):317-324.

Dale N. 1995. Experimentally derived model for the locomotor pattern generator in the Xenopus embryo. J Physiol (Lond) 489:489-510.

Dani JA, Bertrand D. 2007. Nicotinic acetylcholine receptors and nicotinic cholinergic mechanisms of the central nervous system. Annu Rev Pharmacol Toxicol 47:699-729.

Dessaud E, McMahon AP, Briscoe J. 2008. Pattern formation in the vertebrate neural tube: a sonic hedgehog morphogen-regulated transcriptional network. Development 135(15):2489-2503.

Devay P, Qu X, Role L. 1994. Regulation of nAChR subunit gene expression relative to the development of pre- and postsynaptic projections of embryonic chick sympathetic neurons. Dev Biol 162(1):56-70.

Devoto SH, Melançon E, Eisen JS, Westerfield M. 1996. Identification of separate slow and fast muscle precursor cells in vivo, prior to somite formation. Development 122(11):3371-3380.

DiFranza JR, Lew RA. 1995. Effect of maternal cigarette smoking on pregnancy complications and sudden infant death syndrome. J Fam Pract 40(4):385-394.

Distel M, Babaryka A, Köster RW. 2006. Multicolor in vivo time-lapse imaging at cellular resolution by stereomicroscopy. Dev Dyn 235(4):1100-1106.

Dolmetsch RE, Lewis RS, Goodnow CC, Healy JI. 1997. Differential activation of transcription factors induced by Ca2+ response amplitude and duration. Nature 386(6627):855-858.

Downes GB, Granato M. 2006. Supraspinal input is dispensable to generate glycine-mediated locomotive behaviors in the zebrafish embryo. J Neurobiol 66(5):437-451.

Draper BW, Morcos PA, Kimmel CB. 2001. Inhibition of zebrafish fgf8 pre-mRNA splicing with morpholino oligos: a quantifiable method for gene knockdown. Genesis 30(3):154-156.

Eisen JS, Myers PZ, Westerfield M. 1986. Pathway selection by growth cones of identified motoneurones in live zebra fish embryos. Nature 320(6059):269-271.

Eisen JS, Pike SH, Romancier B. 1990. An identified motoneuron with variable fates in embryonic zebrafish. J Neurosci 10(1):34-43.

Elgoyhen AB, Katz E, Fuchs PA. 2009. The nicotinic receptor of cochlear hair cells: a possible pharmacotherapeutic target? Biochem Pharmacol 78(7):712-719.

Engel AG, Lambert EH, Mulder DM, Torres CF, Sahashi K, Bertorini TE, Whitaker JN. 1982. A newly recognized congenital myasthenic syndrome attributed to a prolonged open time of the acetylcholine-induced ion channel. Ann Neurol 11(6):553-569.

Falk L, Nordberg A, Seiger A, Kjaldgaard A, Hellstromlindahl E. 2005. Smoking during early pregnancy affects the expression pattern of both nicotinic and muscarinic acetylcholine receptors in human first trimester brainstem and cerebellum. Neuroscience 132(2):389-397.

Fashena D, Westerfield M. 1999. Secondary motoneuron axons localize DM-GRASP on their fasciculated segments. J Comp Neurol 406(3):415-424.

Feldner J, Becker T, Goishi K, Schweitzer J, Lee P, Schachner M, Klagsbrun M, Becker CG. 2005. Neuropilin-1a is involved in trunk motor axon outgrowth in embryonic zebrafish. Dev Dyn 234(3):535-549.

Feng G, Mellor RH, Bernstein M, Keller-Peck C, Nguyen QT, Wallace M, Nerbonne JM, Lichtman JW, Sanes JR. 2000. Imaging neuronal subsets in transgenic mice expressing multiple spectral variants of GFP. Neuron 28(1):41-51.

Fetcho JR. 1986. The organization of the motoneurons innervating the axial musculature of vertebrates. I. Goldfish (Carassius auratus) and mudpuppies (Necturus maculosus). J Comp Neurol 249(4):521-550.

Fetcho JR. 2007. The utility of zebrafish for studies of the comparative biology of motor systems. J Exp Zool B Mol Dev Evol 308(5):550-562.

Fetcho JR, Higashijima S, McLean DL. 2008. Zebrafish and motor control over the last decade. Brain Res Rev 57(1):86-93.

Fetcho JR, O'Malley DM. 1995. Visualization of active neural circuitry in the spinal cord of intact zebrafish. J Neurophysiol 73(1):399-406.

Fetcho JR, Svoboda KR. 1993. Fictive swimming elicited by electrical stimulation of the midbrain in goldfish. J Neurophysiol 70(2):765-780.

Funakoshi H, Belluardo N, Arenas E, Yamamoto Y, Casabona A, Persson H, Ibáñez CF. 1995. Muscle-derived neurotrophin-4 as an activity-dependent trophic signal for adult motor neurons. Science 268(5216):1495-1499.

Gabriel JP, Mahmood R, Walter AM, Kyriakatos A, Hauptmann G, Calabrese RL, El Manira A. 2008. Locomotor pattern in the adult zebrafish spinal cord in vitro. J Neurophysiol 99(1):37-48.

Gan WB, Bishop DL, Turney SG, Lichtman JW. 1999. Vital imaging and ultrastructural analysis of individual axon terminals labeled by iontophoretic application of lipophilic dye. J Neurosci Methods 93(1):13-20.

Ge S, Dani JA. 2005. Nicotinic acetylcholine receptors at glutamate synapses facilitate long-term depression or potentiation. J Neurosci 25(26):6084-6091.

Gilbert S. 2003. Developmental Biology: Sinauer Associates Inc., Sunderland, Massachussetts.

Ginzel KH, Maritz GS, Marks DF, Neuberger M, Pauly JR, Polito JR, Schulte-Hermann R, Slotkin TA. 2007. Critical review: nicotine for the fetus, the infant and the adolescent? J Health Psychol 12(2):215-224.

Gleason MR, Higashijima S, Dallman J, Liu K, Mandel G, Fetcho JR. 2003. Translocation of CaM kinase II to synaptic sites in vivo. Nat Neurosci 6(3):217-218.

Gomez CM, Maselli RA, Groshong J, Zayas R, Wollmann RL, Cens T, Charnet P. 2002. Active calcium accumulation underlies severe weakness in a panel of mice with slow-channel syndrome. J Neurosci 22(15):6447-6457.

Gomez TM, Spitzer NC. 1999. In vivo regulation of axon extension and pathfinding by growth-cone calcium transients. Nature 397(6717):350-355.

Goulding M. 2009. Circuits controlling vertebrate locomotion: moving in a new direction. Nat Rev Neurosci 10(7):507-518.

Granato M, van Eeden FJ, Schach U, Trowe T, Brand M, Furutani-Seiki M, Haffter P, Hammerschmidt M, Heisenberg CP, Jiang YJ, Kane DA, Kelsh RN, Mullins MC, Odenthal J, Nüsslein-Volhard C. 1996. Genes controlling and mediating locomotion behavior of the zebrafish embryo and larva. Development 123:399-413.

Greenberg ME, Ziff EB, Greene LA. 1986. Stimulation of neuronal acetylcholine receptors induces rapid gene transcription. Science 234(4772):80-83.

Greer PL, Greenberg ME. 2008. From synapse to nucleus: calcium-dependent gene transcription in the control of synapse development and function. Neuron 59(6):846-860.

Grillner S, Ekeberg, El Manira A, Lansner A, Parker D, Tegnér J, Wallén P. 1998. Intrinsic function of a neuronal network - a vertebrate central pattern generator. Brain Res Brain Res Rev 26(2-3):184-197.

Guthrie S. 2007. Patterning and axon guidance of cranial motor neurons. Nat Rev Neurosci 8(11):859-871.

Hale ME, Ritter DA, Fetcho JR. 2001. A confocal study of spinal interneurons in living larval zebrafish. J Comp Neurol 437(1):1-16.

Hansen A, Zeiske E. 1993. Development of the olfactory organ in the zebrafish, Brachydanio rerio. J Comp Neurol 333(2):289-300.

Hanson MG, Landmesser LT. 2003. Characterization of the circuits that generate spontaneous episodes of activity in the early embryonic mouse spinal cord. J Neurosci 23(2):587-600.

Hanson MG, Landmesser LT. 2004. Normal patterns of spontaneous activity are required for correct motor axon guidance and the expression of specific guidance molecules. Neuron 43(5):687-701.

Hanson MG, Landmesser LT. 2006. Increasing the frequency of spontaneous rhythmic activity disrupts pool-specific axon fasciculation and pathfinding of embryonic spinal motoneurons. J Neurosci 26(49):12769-12780.

Higashijima S, Hotta Y, Okamoto H. 2000. Visualization of cranial motor neurons in live transgenic zebrafish expressing green fluorescent protein under the control of the islet-1 promoter/enhancer. J Neurosci 20(1):206-218.

Higashijima S. 2008. Transgenic zebrafish expressing fluorescent proteins in central nervous system neurons. Dev Growth Differ 50(6):407-413.

Higashijima S, Mandel G, Fetcho JR. 2004a. Distribution of prospective glutamatergic, glycinergic, and GABAergic neurons in embryonic and larval zebrafish. J Comp Neurol 480(1):1-18.

Higashijima S, Masino MA, Mandel G, Fetcho JR. 2004b. Engrailed-1 expression marks a primitive class of inhibitory spinal interneuron. J Neurosci 24(25):5827-5839.

Hory-Lee F, Frank E. 1995. The nicotinic blocking agents d-tubocurare and alpha-bungarotoxin save motoneurons from naturally occurring death in the absence of neuromuscular blockade. J Neurosci 15(10):6453-6460.

Howard MJ, Gershon MD, Margiotta JF. 1995. Expression of nicotinic acetylcholine receptors and subunit mRNA transcripts in cultures of neural crest cells. Dev Biol 170(2):479-495.

Hutchinson SA, Eisen JS. 2006. Islet1 and Islet2 have equivalent abilities to promote motoneuron formation and to specify motoneuron subtype identity. Development 133(11):2137-2147.

Ishii K, Wong JK, Sumikawa K. 2005. Comparison of alpha2 nicotinic acetylcholine receptor subunit mRNA expression in the central nervous system of rats and mice. J Comp Neurol 493(2):241-260.

Kalamida D, Poulas K, Avramopoulou V, Fostieri E, Lagoumintzis G, Lazaridis K, Sideri A, Zouridakis M, Tzartos SJ. 2007. Muscle and neuronal nicotinic acetylcholine receptors. Structure, function and pathogenicity. FEBS J 274(15):3799-3845.

Karlin A. 2002. Emerging structure of the nicotinic acetylcholine receptors. Nat Rev Neurosci 3(2):102-114.

Katz B, Thessleff S. 1957. A study of the desensitization produced by acetylcholine at the motor end-plate. J Physiol (Lond) 138(1):63-80.

Kawahara A, Chien C-B, Dawid IB. 2002. The homeobox gene mbx is involved in eye and tectum development. Dev Biol 248(1):107-117.

Keiger CJH, Prevette D, Conroy WG, Oppenheim RW. 2003. Developmental expression of nicotinic receptors in the chick and human spinal cord. J Comp Neurol 455(1):86-99.

Kerschensteiner M, Schwab ME, Lichtman JW, Misgeld T. 2005. In vivo imaging of axonal degeneration and regeneration in the injured spinal cord. Nat Med 11(5):572-577.

Kimura Y, Okamura Y, Higashijima S. 2006. alx, a zebrafish homolog of Chx10, marks ipsilateral descending excitatory interneurons that participate in the regulation of spinal locomotor circuits. J Neurosci 26(21):5684-5697.

Knobel KM, Jorgensen EM, Bastiani MJ. 1999. Growth cones stall and collapse during axon outgrowth in Caenorhabditis elegans. Development 126(20):4489-4498.

Langley JN. 1905. On the reaction of cells and of nerve-endings to certain poisons, chiefly as regards the reaction of striated muscle to nicotine and to curari. J Physiol (Lond) 33(4-5):374-413.

Lawson ND, Weinstein BM. 2002. In vivo imaging of embryonic vascular development using transgenic zebrafish. Dev Biol 248(2):307-318.

Lefebvre JL, Ono F, Puglielli C, Seidner G, Franzini-Armstrong C, Brehm P, Granato M. 2004. Increased neuromuscular activity causes axonal defects and muscular degeneration. Development 131(11):2605-2618.

Léna C, Changeux JP, Mulle C. 1993. Evidence for "preterminal" nicotinic receptors on GABAergic axons in the rat interpeduncular nucleus. J Neurosci 13(6):2680-2688.

Leonard JP, Salpeter MM. 1979. Agonist-induced myopathy at the neuromuscular junction is mediated by calcium. J Cell Biol 82(3):811-819.

Levin ED, Chen E. 2004. Nicotinic involvement in memory function in zebrafish. Neurotoxicology and teratology 26(6):731-735.

Levin ED, Mcclernon FJ, Rezvani AH. 2006. Nicotinic effects on cognitive function: behavioral characterization, pharmacological specification, and anatomic localization. Psychopharmacology 184(3-4):523-539.

Lewis KE, Eisen JS. 2003. From cells to circuits: development of the zebrafish spinal cord. Prog Neurobiol 69(6):419-449.

Liu DW, Westerfield M. 1988. Function of identified motoneurones and co-ordination of primary and secondary motor systems during zebra fish swimming. J Physiol (Lond) 403:73-89.

Martin JA, Hamilton BE, Sutton PD, Ventura SJ, Menacker F, Kirmeyer S, Munson ML. 2007. Births: final data for 2005. Natl Vital Stat Rep 56(6):1-103.

Masino MA, Fetcho JR. 2005. Fictive swimming motor patterns in wild type and mutant larval zebrafish. J Neurophysiol 93(6):3177-3188.

McLean DL, Fan J, Higashijima S, Hale ME, Fetcho JR. 2007. A topographic map of recruitment in spinal cord. Nature 446(7131):71-75.

McLean DL, Fetcho JR. 2009. Spinal interneurons differentiate sequentially from those driving the fastest swimming movements in larval zebrafish to those driving the slowest ones. J Neurosci 29(43):13566-13577.

McLean DL, Masino MA, Koh IYY, Lindquist WB, Fetcho JR. 2008. Continuous shifts in the active set of spinal interneurons during changes in locomotor speed. Nat Neurosci 11(12):1419-1429.

Melançon E, Liu DW, Westerfield M, Eisen JS. 1997. Pathfinding by identified zebrafish motoneurons in the absence of muscle pioneers. J Neurosci 17(20):7796-7804.

Menelaou E, Svoboda KR. 2009. Secondary motoneurons in juvenile and adult zebrafish: axonal pathfinding errors caused by embryonic nicotine exposure. J Comp Neurol 512(3):305-322.

Meng A, Tang H, Ong BA, Farrell MJ, Lin S. 1997. Promoter analysis in living zebrafish embryos identifies a cis-acting motif required for neuronal expression of GATA-2. Proc Natl Acad Sci USA 94(12):6267-6272.

Metcalfe WK, Myers PZ, Trevarrow B, Bass MB, Kimmel CB. 1990. Primary neurons that express the L2/HNK-1 carbohydrate during early development in the zebrafish. Development 110(2):491-504.

Miao H, Liu C, Bishop K, Gong ZH, Nordberg A, Zhang X. 1998. Nicotine exposure during a critical period of development leads to persistent changes in nicotinic acetylcholine receptors of adult rat brain. J Neurochem 70(2):752-762.

Missias AC, Chu GC, Klocke BJ, Sanes JR, Merlie JP. 1996. Maturation of the acetylcholine receptor in skeletal muscle: regulation of the AChR gamma-to-epsilon switch. Dev Biol 179(1):223-238.

Moore KL and Persaud TVN, 2003. The Developing Human: Clinically Oriented Embryology. Saunders, Philadelphia, PA.

Miyazawa A, Fujiyoshi Y, Unwin N. 2003. Structure and gating mechanism of the acetylcholine receptor pore. Nature 423(6943):949-955.

Müller UK, Stamhuis EJ, Videler JJ. 2000. Hydrodynamics of unsteady fish swimming and the effects of body size: comparing the flow fields of fish larvae and adults. J Exp Biol 203:193-206.

Müller UK, van Leeuwen JL. 2004. Swimming of larval zebrafish: ontogeny of body waves and implications for locomotory development. J Exp Biol 207:853-868.

Myers CP, Lewcock JW, Hanson MG, Gosgnach S, Aimone JB, Gage FH, Lee K-F, Landmesser LT, Pfaff SL. 2005. Cholinergic input is required during embryonic development to mediate proper assembly of spinal locomotor circuits. Neuron 46(1):37-49.

Myers PZ. 1985. Spinal motoneurons of the larval zebrafish. J Comp Neurol 236(4):555-561.

Myers PZ, Eisen JS, Westerfield M. 1986. Development and axonal outgrowth of identified motoneurons in the zebrafish. J Neurosci 6(8):2278-2289.

Nasevicius A, Ekker SC. 2000. Effective targeted gene 'knockdown' in zebrafish. Nat Genet 26(2):216-220.

Ono F, Higashijima S, Shcherbatko A, Fetcho JR, Brehm P. 2001. Paralytic zebrafish lacking acetylcholine receptors fail to localize rapsyn clusters to the synapse. J Neurosci 21(15):5439-5448.

Ott H, Diekmann H, Stuermer CA, Bastmeyer M. 2001. Function of Neurolin (DM-GRASP/SC-1) in guidance of motor axons during zebrafish development. Dev Biol 235(1):86-97.

Owens KN, Coffin AB, Hong LS, Bennett KOC, Rubel EW, Raible DW. 2009. Response of mechanosensory hair cells of the zebrafish lateral line to aminoglycosides reveals distinct cell death pathways. Hearing Res 253(1-2):32-41.

Palaisa KA, Granato M. 2007. Analysis of zebrafish sidetracked mutants reveals a novel role for Plexin A3 in intraspinal motor axon guidance. Development 134(18):3251-3257.

Panzer J, Gibbs S, Dosch R, Wagner D, Mullins M, Granato M, Balicegordon R. 2005. Neuromuscular synaptogenesis in wild-type and mutant zebrafish. Dev Biol 285(2):340-357.

Paulus JD, Willer GB, Willer JR, Gregg RG, Halloran MC. 2009. Muscle Contractions Guide Rohon-Beard Peripheral Sensory Axons. J Neurosci 29(42):13190-13201.

Paz R, Barsness B, Martenson T, Tanner D, Allan AM. 2007. Behavioral teratogenicity induced by nonforced maternal nicotine consumption. Neuropsychopharmacology 32(3):693-699.

Perrins R, Roberts A. 1995. Cholinergic and electrical synapses between synergistic spinal motoneurones in the Xenopus laevis embryo. J Physiol (Lond) 485:135-144.

Petzold A, Balciunas D, Sivasubbu S, Clark K, Bedell V, Westcot S, Myers S, Moulder G, Thomas M, Ekker S. 2009. Nicotine response genetics in the zebrafish. Proc Natl Acad Sci USA 106(44):18662-18667.

Pike SH, Melancon EF, Eisen JS. 1992. Pathfinding by zebrafish motoneurons in the absence of normal pioneer axons. Development 114(4):825-831.

Pineda RH, Svoboda KR, Wright MA, Taylor AD, Novak AE, Gamse JT, Eisen JS, Ribera AB. 2006. Knockdown of Nav1.6a Na+ channels affects zebrafish motoneuron development. Development 133(19):3827-3836.

Potter AS, Newhouse PA, Bucci DJ. 2006. Central nicotinic cholinergic systems: a role in the cognitive dysfunction in attention-deficit/hyperactivity disorder? Behav Brain Res 175(2):201-211.

Pugh PC, Berg DK. 1994. Neuronal acetylcholine receptors that bind alpha-bungarotoxin mediate neurite retraction in a calcium-dependent manner. J Neurosci 14(2):889-896.

Ribera AB, Nüsslein-Volhard C. 1998. Zebrafish touch-insensitive mutants reveal an essential role for the developmental regulation of sodium current. J Neurosci 18(22):9181-9191.

Roberts A, Li W, Soffe S, Wolf E. 2008. Origin of excitatory drive to a spinal locomotor network. Brain Res Rev 57(1):22-28.

Roy TS, Andrews JE, Seidler FJ, Slotkin TA. 1998. Nicotine evokes cell death in embryonic rat brain during neurulation. J Pharmacol Exp Ther 287(3):1136-1144.

Saint-Amant L, Drapeau P. 1998. Time course of the development of motor behaviors in the zebrafish embryo. J Neurobiol 37(4):622-632.

Sato Y, Miyasaka N, Yoshihara Y. 2005. Mutually exclusive glomerular innervation by two distinct types of olfactory sensory neurons revealed in transgenic zebrafish. J Neurosci 25(20):4889-4897.

Schneider VA, Granato M. 2006. The myotomal diwanka (lh3) glycosyltransferase and type XVIII collagen are critical for motor growth cone migration. Neuron 50(5):683-695.

Schweitzer J, Becker T, Lefebvre J, Granato M, Schachner M, Becker CG. 2005. Tenascin-C is involved in motor axon outgrowth in the trunk of developing zebrafish. Dev Dyn 234(3):550-566.

Shadwick R SJ, Katz SL, Knower T. 1998. Muscle dynamics during steady swimming. Amer Zool 38:755-770.

Sharma K, Leonard AE, Lettieri K, Pfaff SL. 2000. Genetic and epigenetic mechanisms contribute to motor neuron pathfinding. Nature 406(6795):515-519.

Sillar KT, McLean DL, Fischer H, Merrywest SD. 2002. Fast inhibitory synapses: targets for neuromodulation and development of vertebrate motor behaviour. Brain Res Brain Res Rev 40(1-3):130-140.

Skromne I, Prince VE. 2008. Current perspectives in zebrafish reverse genetics: Moving forward. Dev Dyn 237(4):861-882.

Slikker W, Xu ZA, Levin ED, Slotkin TA. 2005. Mode of action: disruption of brain cell replication, second messenger, and neurotransmitter systems during development leading to cognitive dysfunction--developmental neurotoxicity of nicotine. Crit Rev Toxicol 35(8-9):703-711.

Slotkin TA. 1998. Fetal nicotine or cocaine exposure: which one is worse? J Pharmacol Exp Ther 285(3):931-945.

Slotkin TA. 2004. Cholinergic systems in brain development and disruption by neurotoxicants: nicotine, environmental tobacco smoke, organophosphates. Toxicol Appl Pharmacol 198(2):132-151.

Slotkin TA, Orband-Miller L, Queen KL. 1987a. Development of [3H]nicotine binding sites in brain regions of rats exposed to nicotine prenatally via maternal injections or infusions. J Pharmacol Exp Ther 242(1):232-237.

Slotkin TA, Orband-Miller L, Queen KL, Whitmore WL, Seidler FJ. 1987b. Effects of prenatal nicotine exposure on biochemical development of rat brain regions: maternal drug infusions via osmotic minipumps. J Pharmacol Exp Ther 240(2):602-611.

Smith J, Fauquet M, Ziller C, Le Douarin NM. 1979. Acetylcholine synthesis by mesencephalic neural crest cells in the process of migration in vivo. Nature 282(5741):853-855.

Summerton JE. 2007. Morpholino, siRNA, and S-DNA compared: impact of structure and mechanism of action on off-target effects and sequence specificity. Cur Top Med Chem 7(7):651-660.

Svoboda KR, Linares AE, Ribera AB. 2001. Activity regulates programmed cell death of zebrafish Rohon-Beard neurons. Development 128(18):3511-3520.

Svoboda KR, Vijayaraghavan S, Tanguay RL. 2002. Nicotinic receptors mediate changes in spinal motoneuron development and axonal pathfinding in embryonic zebrafish exposed to nicotine. J Neurosci 22(24):10731-10741.

Tanguay RL, Abnet CC, Heideman W, Peterson RE. 1999. Cloning and characterization of the zebrafish (Danio rerio) aryl hydrocarbon receptor. Biochim Biophys Acta 1444(1):35-48.

te Kronnié G. 2000. Axial Muscle Development in Fish. Basic Appl Myol 10(6):261-267.

Thapar A, Fowler T, Rice F, Scourfield J, van den Bree M, Thomas H, Harold G, Hay D. 2003. Maternal smoking during pregnancy and attention deficit hyperactivity disorder symptoms in offspring. Am J Psychiat 160(11):1985-1989.

Thomas LT, Welsh L, Galvez F, Svoboda KR. 2009. Acute nicotine exposure and modulation of a spinal motor circuit in embryonic zebrafish. Toxicol Appl Pharmacol 239(1):1-12.

Thompson BL, Levitt P, Stanwood GD. 2009. Prenatal exposure to drugs: effects on brain development and implications for policy and education. Nat Rev Neurosci 10(4):303-312.

Thorsen DH, Hale ME. 2007. Neural development of the zebrafish (Danio rerio) pectoral fin. J Comp Neurol 504(2):168-184.

Tizabi Y, Popke EJ, Rahman MA, Nespor SM, Grunberg NE. 1997. Hyperactivity induced by prenatal nicotine exposure is associated with an increase in cortical nicotinic receptors. Pharmacol Biochem Behav 58(1):141-146.

Torrão AS, Lindstrom JM, Britto LRG. 2003. Nicotine and alpha-bungarotoxin modify the dendritic growth of cholinoceptive neurons in the developing chick tectum. Brain Res Dev Brain Res 143(1):115-118.

van Eeden FJ, Granato M, Schach U, Brand M, Furutani-Seiki M, Haffter P, Hammerschmidt M, Heisenberg CP, Jiang YJ, Kane DA, Kelsh RN, Mullins MC, Odenthal J, Warga RM, Allende ML, Weinberg ES, Nüsslein-Volhard C. 1996. Mutations affecting somite formation and patterning in the zebrafish, Danio rerio. Development 123:153-164.

Vitebsky A, Reyes R, Sanderson MJ, Michel WC, Whitlock KE. 2005. Isolation and characterization of the laure olfactory behavioral mutant in the zebrafish, Danio rerio. Dev Dyn 234(1):229-242.

Wallén P, Williams TL. 1984. Fictive locomotion in the lamprey spinal cord in vitro compared with swimming in the intact and spinal animal. J Physiol (Lond) 347:225-239.

Wang S, Polo-Parada L, Landmesser LT. 2009. Characterization of rhythmic Ca2+ transients in early embryonic chick motoneurons: Ca2+ sources and effects of altered activation of transmitter receptors. J Neurosci 29(48):15232-15244.

Welsh L, Tanguay RL, Svoboda KR. 2009. Uncoupling nicotine mediated motoneuron axonal pathfinding errors and muscle degeneration in zebrafish. Toxicol Appl Pharmacol 237(1):29-40.

Westerfield M. 1995. The Zebrafish Book: A Guide for the Laboratory Use of Zebrafish (Danio Rerio).

Westerfield M, McMurray JV, Eisen JS. 1986. Identified motoneurons and their innervation of axial muscles in the zebrafish. J Neurosci 6(8):2267-2277.

Whitfield TT. 2005. Lateral line: precocious phenotypes and planar polarity. Curr Biol 15(2):R67-70.

Yaniv K, Isogai S, Castranova D, Dye L, Hitomi J, Weinstein BM. 2006. Live imaging of lymphatic development in the zebrafish. Nat Med 12(6):711-716.

Zagoraiou L, Akay T, Martin JF, Brownstone RM, Jessell TM, Miles GB. 2009. A cluster of cholinergic premotor interneurons modulates mouse locomotor activity. Neuron 64(5):645-662.

Zarei MM, Radcliffe KA, Chen D, Patrick JW, Dani JA. 1999. Distributions of nicotinic acetylcholine receptor alpha7 and beta2 subunits on cultured hippocampal neurons. Neuroscience 88(3):755-764.

Zeller J, Schneider V, Malayaman S, Higashijima S, Okamoto H, Gui J, Lin S, Granato M. 2002. Migration of zebrafish spinal motor nerves into the periphery requires multiple myotome-derived cues. Dev Biol 252(2):241-256.

Zhang G, Jin L-Q, Sul J-Y, Haydon PG, Selzer ME. 2005. Live imaging of regenerating lamprey spinal axons. Neurorehabil Neural Repair 19(1):46-57.

Zhao Z, Reece EA. 2005. Nicotine-induced embryonic malformations mediated by apoptosis from increasing intracellular calcium and oxidative stress. Birth Defects Res B Dev Reprod Toxicol 74(5):383-391.

Zheng JQ, Felder M, Connor JA, Poo MM. 1994. Turning of nerve growth cones induced by neurotransmitters. Nature 368(6467):140-144.

Zirger J, Beattie C, McKay D, Thomas Boyd R. 2003. Cloning and expression of zebrafish neuronal nicotinic acetylcholine receptors. Gene Expression Patterns 3:747-754.

Zoli M, Le Novère N, Hill JA, Changeux JP. 1995. Developmental regulation of nicotinic ACh receptor subunit mRNAs in the rat central and peripheral nervous systems. J Neurosci 15:1912-1939.

APPENDIX

PERMISSION TO REPRINT CHAPTER 3

JOHN WILEY AND SONS LICENSE TERMS AND CONDITIONS

Apr 26, 2010

This is a License Agreement between Evdokia Menelaou ("You") and John Wiley and Sons ("John Wiley and Sons") provided by Copyright Clearance Center ("CCC"). The license consists of your order details, the terms and conditions provided by John Wiley and Sons, and the payment terms and conditions.

All payments must be made in full to CCC. For payment instructions, please see information listed at the bottom of this form.

License Number: 2416550565886

License date: Apr 26, 2010

Licensed content publisher: John Wiley and Sons

Licensed content publication: Journal of Comparative Neurology

Licensed content title: Secondary motoneurons in juvenile and adult zebrafish: Axonal pathfinding errors caused by embryonic nicotine exposure

Licensed content author: Menelaou Evdokia, Svoboda Kurt R.

Licensed content date: Nov 12, 2008

Start page: 305

End page: 322

Type of use: Dissertation/Thesis

Requestor type: Author of this Wiley article

Format: Print and electronic

Portion: Full article

Will you be translating? No

Order reference number

Total 0.00 USD

TERMS AND CONDITIONS

This copyrighted material is owned by or exclusively licensed to John Wiley & Sons, Inc. or one if its group companies (each a "Wiley Company") or a society for whom a Wiley Company has exclusive publishing rights in relation to a particular journal (collectively "WILEY"). By clicking "accept" in connection with completing this licensing transaction, you agree that the following terms and conditions apply to this transaction (along with the billing and payment terms and conditions established by the Copyright Clearance Center Inc., ("CCC's Billing and Payment terms and conditions"), at the time that you opened your Rightslink account (these are available at any time at http://myaccount.copyright.com).

Terms and Conditions
1. The materials you have requested permission to reproduce (the "Materials") are protected by copyright.

2. You are hereby granted a personal, non-exclusive, non-sublicensable, non-transferable, worldwide, limited license to reproduce the Materials for the purpose specified in the licensing process. This license is for a one-time use only with a maximum distribution equal to the number that you identified in the licensing process. Any form of republication granted by this licence must be completed within two years of the date of the grant of this licence (although copies prepared before may be distributed thereafter). Any electronic posting of the Materials is limited to one year from the date permission is granted and is on the condition that a link is placed to the journal homepage on Wiley's online journals publication platform at www.interscience.wiley.com. The Materials shall not be used in any other manner or for any other purpose. Permission is granted subject to an appropriate acknowledgement given to the author, title of the material/book /journal and the publisher and on the understanding that nowhere in the text is a previously published source acknowledged for all or part of this Material. Any third party material is expressly excluded from this permission.

3. With respect to the Materials, all rights are reserved. No part of the Materials may be copied, modified, adapted, translated, reproduced, transferred or distributed, in any form or by any means, and no derivative works may be made based on the Materials without the prior permission of the respective copyright owner. You may not alter, remove or suppress in any manner any copyright, trademark or other notices displayed by the Materials. You may not license, rent, sell, loan, lease, pledge, offer as security, transfer or assign the Materials, or any of the rights granted to you hereunder to any other person.

4. The Materials and all of the intellectual property rights therein shall at all times remain the exclusive property of John Wiley & Sons Inc or one of its related companies (WILEY) or their respective licensors, and your interest therein is only that of having possession of and the right to reproduce the Materials pursuant to Section 2 herein during the continuance of this Agreement. You agree that you own no right, title or interest in or to the Materials or any of the intellectual property rights therein. You shall have no rights hereunder other than the license as provided for above in Section 2. No right, license or interest to any trademark, trade name, service mark or other branding ("Marks") of WILEY or its licensors is granted hereunder, and you agree that you shall not assert any such right, license or interest with respect thereto.

5. WILEY DOES NOT MAKE ANY WARRANTY OR REPRESENTATION OF ANY KIND TO YOU OR ANY THIRD PARTY, EXPRESS, IMPLIED OR STATUTORY, WITH RESPECT TO THE MATERIALS OR THE ACCURACY OF ANY INFORMATION CONTAINED IN THE MATERIALS, INCLUDING, WITHOUT LIMITATION, ANY IMPLIED WARRANTY OF MERCHANTABILITY, ACCURACY, SATISFACTORY QUALITY, FITNESS FOR A PARTICULAR PURPOSE, USABILITY, INTEGRATION OR NON-INFRINGEMENT AND ALL SUCH WARRANTIES ARE HEREBY EXCLUDED BY WILEY AND WAIVED BY YOU.

6. WILEY shall have the right to terminate this Agreement immediately upon breach of this Agreement by you.

7. You shall indemnify, defend and hold harmless WILEY, its directors, officers, agents and employees, from and against any actual or threatened claims, demands, causes of action or proceedings arising from any breach of this Agreement by you.

8. IN NO EVENT SHALL WILEY BE LIABLE TO YOU OR ANY OTHER PARTY OR ANY OTHER PERSON OR ENTITY FOR ANY SPECIAL, CONSEQUENTIAL, INCIDENTAL, INDIRECT, EXEMPLARY OR PUNITIVE DAMAGES, HOWEVER CAUSED, ARISING OUT OF OR IN CONNECTION WITH THE DOWNLOADING, PROVISIONING, VIEWING OR USE OF THE MATERIALS REGARDLESS OF THE FORM OF ACTION, WHETHER FOR BREACH OF CONTRACT, BREACH OF WARRANTY, TORT, NEGLIGENCE, INFRINGEMENT OR OTHERWISE (INCLUDING, WITHOUT LIMITATION, DAMAGES BASED ON LOSS OF PROFITS, DATA, FILES, USE, BUSINESS OPPORTUNITY OR CLAIMS OF THIRD PARTIES), AND WHETHER OR NOT THE PARTY HAS BEEN ADVISED OF THE POSSIBILITY OF SUCH

DAMAGES. THIS LIMITATION SHALL APPLY NOTWITHSTANDING ANY FAILURE OF ESSENTIAL PURPOSE OF ANY LIMITED REMEDY PROVIDED HEREIN.

9. Should any provision of this Agreement be held by a court of competent jurisdiction to be illegal, invalid, or unenforceable, that provision shall be deemed amended to achieve as nearly as possible the same economic effect as the original provision, and the legality, validity and enforceability of the remaining provisions of this Agreement shall not be affected or impaired thereby.

10. The failure of either party to enforce any term or condition of this Agreement shall not constitute a waiver of either party's right to enforce each and every term and condition of this Agreement. No breach under this agreement shall be deemed waived or excused by either party unless such waiver or consent is in writing signed by the party granting such waiver or consent. The waiver by or consent of a party to a breach of any provision of this Agreement shall not operate or be construed as a waiver of or consent to any other or subsequent breach by such other party.

11. This Agreement may not be assigned (including by operation of law or otherwise) by you without WILEY's prior written consent.

12. These terms and conditions together with CCC's Billing and Payment terms and conditions (which are incorporated herein) form the entire agreement between you and WILEY concerning this licensing transaction and (in the absence of fraud) supersedes all prior agreements and representations of the parties, oral or written. This Agreement may not be amended except in a writing signed by both parties. This Agreement shall be binding upon and inure to the benefit of the parties' successors, legal representatives, and authorized assigns.

13. In the event of any conflict between your obligations established by these terms and conditions and those established by CCC's Billing and Payment terms and conditions, these terms and conditions shall prevail.

14. WILEY expressly reserves all rights not specifically granted in the combination of (i) the license details provided by you and accepted in the course of this licensing transaction, (ii) these terms and conditions and (iii) CCC's Billing and Payment terms and conditions.

15. This Agreement shall be governed by and construed in accordance with the laws of England and you agree to submit to the exclusive jurisdiction of the English courts.
BY CLICKING ON THE "I ACCEPT" BUTTON, YOU ACKNOWLEDGE THAT YOU HAVE READ AND FULLY UNDERSTAND EACH OF THE SECTIONS OF AND PROVISIONS SET FORTH IN THIS AGREEMENT AND THAT YOU ARE IN AGREEMENT WITH AND ARE WILLING TO ACCEPT ALL OF YOUR OBLIGATIONS AS SET FORTH IN THIS AGREEMENT.V1.2
Gratis licenses (referencing $0 in the Total field) are free. Please retain this printable license for your reference. No payment is required.
If you would like to pay for this license now, please remit this license along with your payment made payable to "COPYRIGHT CLEARANCE CENTER" otherwise you will be invoiced within 48 hours of the license date. Payment should be in the form of a check or money order referencing your account number and this invoice number RLNK10773928. Once you receive your invoice for this order, you may pay your invoice by credit card.Please follow instructions provided at that time.

Make Payment To:
Copyright Clearance Center
Dept 001
P.O. Box 843006
Boston, MA 02284-3006
If you find copyrighted material related to this license will not be used and wish to cancel, please contact us referencing this license number 2416550565886 and noting the reason for cancellation.
Questions? customercare@copyright.com or +1-877-622-5543 (toll free in the US) or +1-978-646-2777

VITA

Evdokia Menelaou was born to Charita and Marios Menelaou in Limassol, Cyprus, in 1981. She received her primary and secondary education in Limassol and graduated from St.Peter & Paul Lyceum in June of 1999. Two months later she moved to Louisiana where she enrolled as an undergraduate at the University of Louisiana at Monroe. She graduated with a Bachelor of Science in December 2002. She then moved to Baton Rouge in January 2003 where she obtained her Master of Science in August of 2004. She began working toward her doctorate degree in August 2006 in Dr. Kurt Svoboda's laboratory. She successfully defended her dissertation in June 2010 and will be awarded the degree of Doctor of Philosophy in August 2010.